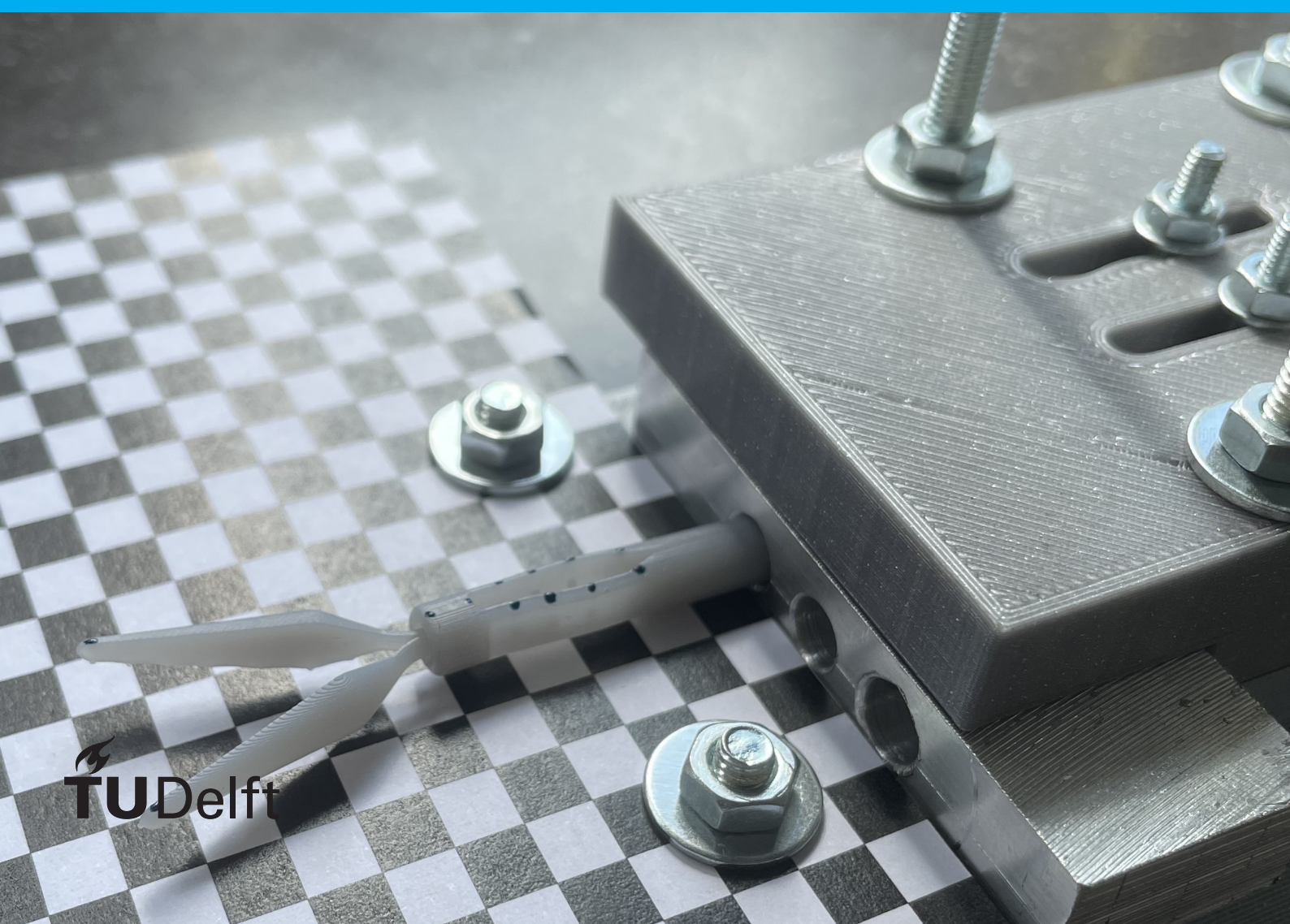


Design of a Non-Assembly Articulating Neuroendoscopic Forceps

S.J. van Schoor

Master Thesis



Design of a Non-Assembly Articulating Neuroendoscopic Forceps

by

S.J. van Schoor

to obtain the degree of Master of Science
in Mechanical Engineering
at the Delft University of Technology,
to be defended publicly on Friday December 3, 2021 at 2:00 PM.

Student number: 4378520
Thesis committee: Ir. K. Lussenburg, TU Delft, daily supervisor
Prof. dr. ir. P. Breedveld, TU Delft, supervisor
Dr. ir. A. Sakes, TU Delft

An electronic version of this thesis is available at <http://repository.tudelft.nl/>.

Preface

Before you is the culmination of my master Mechanical Engineering – BioMechanical Design. In my bachelor studies I developed an interest for devices to heal, support, or improve the human body. A minor in Technical Medicine, especially tailored for the peculiar TU Delft student, confirmed and even reinforced this interest. This thesis report is an apt example of what could be possible when the bridge between engineering and medicine is made.

During my graduation year I have had many meetings with my supervisor Kirsten, and—in the first months—Costanza. I did not always make it easy for them, but their feedback and patience enabled this report, for which I am very grateful. Furthermore, I could always rely on my friends and family for support, help, or just some friendly banter when I needed it. In particular, I would like to thank my neighbour Veronique, for her unexpected help during challenging times.

Hopefully you will enjoy reading this report, and may it inspire as much as its writing inspired me.

*S.J. van Schoor
Delft, December 2021*

Contents

1	Introduction	1
1.1	Minimally invasive surgery	1
1.1.1	General procedure	1
1.1.2	Endoscopic neurosurgery	1
1.1.3	Traditional manipulators for minimally invasive surgery	2
1.1.4	Articulating manipulators for minimally invasive surgery	2
1.2	Additive manufacturing	3
1.3	Problem statement	3
1.4	Project goal	4
1.5	Report outline	4
2	State of the art	4
2.1	Neuroendoscopic trocars	4
2.2	Surgical articulation	4
2.2.1	Concentrated planar bending (I)	5
2.2.2	Distributed planar bending (II)	6
2.2.3	Concentrated spatial bending (III)	6
2.2.4	Distributed spatial bending (IV)	8
2.3	Non-assembly additive manufacturing	8
3	Problem analysis	8
3.1	Function analysis	8
3.2	Small-scale challenges	9
3.3	3D printer selection	9
3.4	Challenges and opportunities of AM	10
3.5	Challenges and opportunities of compliant mechanisms	11
4	Design criteria	11
5	Working principles concept	13
5.1	Concept generation	13
5.1.1	Methodology	13
5.1.2	Morphological overviews	13
5.2	Sub-solutions	15
5.2.1	Bending mechanism	15
5.2.2	Grasping mechanism	15
5.2.3	Transmission mechanism	16
5.3	Combination of sub-solutions	16
5.3.1	Parallel flexure concept	16
5.3.2	Cross-flexure concept	16
5.4	Concept selection	16
5.4.1	Concept comparison	16
5.4.2	Stiffness related risks	18
5.4.3	Final concept choice	18
6	Planar bending designs	18
6.1	Conceptual designs	18
6.1.1	Concept I – Concentrated planar bending	18
6.1.2	Concept II – Distributed planar bending	20
6.2	Bending flexure design	20
6.2.1	Cross-section geometry	20
6.2.2	Bending flexure length: stiffness approach	20
6.2.3	Bending flexure length: deformation approach	21
6.2.4	Leaf flexure geometry	21
6.3	Grasper design	22
6.3.1	Grasper principles	22
6.3.2	Grasping bearing	22

6.3.3	Flexible grasping rod	22
6.4	Shaft design	23
6.4.1	Shaft functions	23
6.4.2	Shaft cross-section	23
6.4.3	Printing rods further apart	23
6.5	Prototyping	24
6.5.1	Prototype designs	24
6.5.2	Print orientation	24
6.5.3	Design iterations	25
6.5.4	Print settings	25
7	Experimental validation of planar bending designs	25
7.1	Experiments	25
7.1.1	Test setup	25
7.1.2	Bending test	26
7.1.3	Stiffness test	26
7.2	Results and discussion	28
7.2.1	General measurements	28
7.2.2	Bending test results	28
7.2.3	Stiffness test results	29
7.3	Evaluation of experimental validation	29
8	Spatial bending design exploration	30
8.1	Conceptual designs	30
8.1.1	Concept III – Concentrated spatial bending	30
8.1.2	Concept IV – Distributed spatial bending	31
8.2	Final designs	31
8.2.1	Elliptical flexure dimensions	31
8.2.2	Shaft design	31
8.2.3	Prototyping	32
8.3	Experimental validation of spatial bending designs	34
9	Discussion	34
9.1	Handle design	34
9.2	Main findings	35
9.2.1	Project goal	35
9.2.2	Expected functioning Category IV	37
9.2.3	Design improvements	37
9.2.4	3D printing opportunities used	38
9.3	Study limitations	39
9.3.1	Categorisation	39
9.3.2	Experimental validation	39
9.4	Future recommendations	40
10	Conclusion	40
	Appendix A Morphological schemes	47
	Appendix B Comparison with compliant grasper	48
	Appendix C Bending calculations	49
	Appendix D Alternative bending concepts	50
	Appendix E Design of a spacing flexure	53
	Appendix F Matlab scripts	58

List of Figures

1	Schematic drawing of the brain’s ventricular system.	2
2	Workspace and DOF for general MIS manipulators.	2
3	Schematic drawing of neuroendoscopic system.	3
4	Example of neuroendoscopic system.	5
5	’Oriceps’ surgical grasper by the Compliant Mechanisms Research Group from BYU.	5
6	Schematic representation of four bending categories, using the Cans in series system.	6
7	Overview of state-of-the-art articulating surgical devices.	7
8	Visualisation of 0.3 mm clearance proportions in a 2 mm revolute joint.	11
9	Schematic representation of functional requirements.	13
10	Morphological bending scheme.	14
11	Morphological grasping scheme.	14
12	Morphological transmission scheme.	15
13	Hand drawings of parallel flexure concept and cross-flexure concept.	17
14	Concept comparison.	19
15	Conceptual planar bending designs.	20
16	Free Body Diagrams of bending mechanism during bending.	21
17	Close-up of grasper bearing.	22
18	Cross-sections planar bending designs.	23
19	Printing rods further apart	24
20	Printing upright vs. printing flat.	25
21	Photo of printed prototypes	26
22	Experimental setup	27
23	Concept overview of four categories.	31
24	Cross-sections of bending mechanisms.	32
25	Cross-sections of shafts.	32
26	CAD model close-ups of the tip.	33
27	Bar graph with mean deflection values from stiffness experiments.	35
28	Schematic handle drawing	36
29	Photos of 2 mm 3D printed tips	38
30	Improved grasper design.	38
A.1	Morphological overviews including chosen solutions.	47
C.1	Schematic representation of flexures during bending.	49
D.1	Equivalents of Cans in series models	50
D.2	Hand sketches of zero-radius bending concept.	51
D.3	Hand sketches of alternative concepts.	52
E.1	Bending behaviour of the tip.	53

List of Tables

1	Challenges and opportunities of 3D printing.	10
2	Overview of design criteria	12
3	Overview of scaled design criteria for 5 mm prototypes	28
4	Bending radius at 60° bending – Planar bending	28
5	Input displacement at 60° bending – Planar bending	29
6	Deflection upon external 0.68 N force – Planar bending	30
7	Bending radius at 60° bending – Spatial bending	34
8	Input displacement at 60° bending – Spatial bending	34
9	Deflection upon external 0.68 N force – Spatial bending	35
10	Overview of design criteria fulfilment (expected outcomes in black)	37
B.1	Comparison with the compliant grasper by Herder and Van den Berg.	48
E.1	Spacing flexure design, approach 1: Flexure equivalent of a cable	55
E.2	Spacing flexure design, approach 2: Geometrical reasoning starting from a simple leaf flexure	56
E.3	Spacing flexure design, approach 3: Geometrical reasoning starting from a compliant slider	57

Design of a Non-Assembly Articulating Neuroendoscopic Forceps

STEIJN J. VAN SCHOOR
Delft University of Technology
November 26, 2021

Abstract

Minimally invasive surgery has some major benefits over traditional open surgery for the patient, but makes surgery more complex for the surgeon. Articulating instruments can regain some of the manoeuvrability that is lost by using a small incision. However, in endoscopic neurosurgery such articulating devices do currently not exist, due to scale dependent assembling and manufacturing challenges. We explored the use non-assembly additive manufacturing to circumvent the infeasible assembly and enable production of a 2 mm articulating forceps. Four different designs were made to explore different levels of articulation intricacy, with a distinction in planar or spatial, and concentrated or distributed bending. Eligible 3D printers capable of printing surgical instrument-sized parts including sub 2 mm mechanisms need relatively large clearances between moving parts. This poses a serious challenge that we solved by using compliant grasping and bending mechanisms. Three out of four designs were successfully 3D printed on a 5 mm and 2 mm scale, and their geometrical requirements were validated. The designs fitted through a 2.2 mm dummy trocar, reached bending angles up to 70°, and an forceps opening angle of 40°. The distributed planar and distributed spatial bending design were deemed infeasible due to their lack of bending stiffness upon external forces. The two remaining designs proof that 3D printed non-assembly forceps for neuroendoscopy are possible, with planar and spatial articulation. With these articulating devices, many more neurosurgeries could be executed in a minimally invasive manner. However, simulated surgical tasks should be performed to further test the designs, before they could be commercialised.

Keywords— Non-Assembly Mechanisms, Additive Manufacturing, 3D Printing, Minimally Invasive Surgery, Neurosurgery, Surgical Instrument

1 Introduction

1.1 Minimally invasive surgery

1.1.1 General procedure

Minimally invasive surgery (MIS), also known as keyhole surgery, is steadily gaining ground in the medical field [1]. An operation is minimally invasive when performed through one or several small incisions, or through the human body orifices. The surgeon no longer has a direct view on the surgical site. Instead, the surgeon uses an endoscope: an additional instrument with a camera to guide his or her actions. Surgical instruments usually enter the body through a trocar that is placed in the incision and serves as a pivot point. Major benefits of minimally invasive surgery include reduced patient pain, a shorter recovery time and reduction of scar tissue [2–5].

1.1.2 Endoscopic neurosurgery

New advancements in preoperative imaging techniques, endoscopic image quality, and better monitors enabled the use of minimally invasive approaches to neurosurgery [6, 7]. Neurosurgery

comprises all surgery on the nervous system, including the brain. Traditionally, a burr hole in the skull is cut or drilled, through which the surgeon has access to the brain tissue and ventricles. There is a direct view on the brain, which is sometimes enhanced with a microscope. By using an endoscope, the size of the burr hole can be significantly reduced, similar to other MIS applications. Furthermore, damage to the brain like brain retraction is reduced [8]. In infants below the age of one, the fontanelle can be used to enter the skull, and there is no need to damage the skull [9]. Endoscopic neurosurgery can be used for a variety of medical conditions, including the treatment of tumours, cysts, areas of increased pressure, and many other lesions [6, 7, 10–12]. The majority of these conditions take place in the brain’s ventricular system, a structure of inter-connected fluid-filled hollow cavities. A schematic drawing of the ventricular system is shown in Fig. 1. Endoscopic neurosurgery has proven to have superior recovery as opposed to conventional open brain surgery [7, 10].

Two general types of endoscopic neurosurgery exist: extra-axial, and coaxial [10]. In extra-axial procedures, the endoscope and instruments

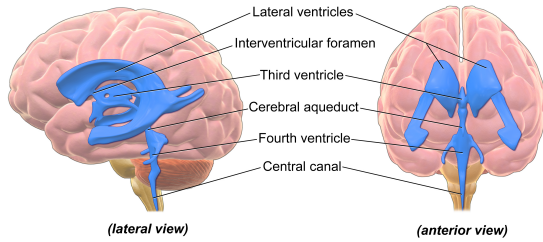


Figure 1: Schematic drawing of the brain’s ventricular system, including the separate ventricles and connecting ducts. Adopted from [13].

are separately inserted, and can be moved around individually. In coaxial procedures, like the one in Fig. 3, a special type of trocar is used that ensures all instruments are parallel. Unlike other trocars, it has a handle and holds different channels for all instrumentation, including the endoscope, and reaches all the way to the surgical site. On top of that, it can house channels for suction or irrigation, a channel to prevent overflow, and light fibres that illuminate the surgical site [7, 12]. The surgeon only needs to operate the trocar to move all instruments simultaneously. The trocar can also be fixed by a holding arm when the tip of the trocar has reached the surgical site; the trocar can no longer move, and only the instrument tips sticking out of the trocar can be controlled. Fixing the trocar does not only improve the surgeon’s ergonomics, but also frees one hand enabling the surgeon to use two surgical manipulators and operate ‘bi-manual’ [14]. The main reason not to use a holding arm is the ability to move the trocar, and thus endoscope and manipulators, which is called ‘freehand’ surgery.

1.1.3 Traditional manipulators for minimally invasive surgery

Traditional surgical instruments are not suitable for MIS; instruments used in MIS are usually long and slender (see Fig. 2a). A thinner instrument enables the use of a smaller trocar and thus a smaller incision. Manipulator instruments have an end effector that interacts with the surgical site, and a thin long shaft to connect the end effector to a handle. Common types of end effectors are needles, cutters, and forceps. The diameter of manipulators used in coaxial procedures is limited by the working channel diameter. Only the end effectors stick out of the trocar.

Angulated endoscopes exist to get a better view when an obstacle blocks the direct path of the endoscope. These endoscopes usually have a lens at the tip to change the direction of view

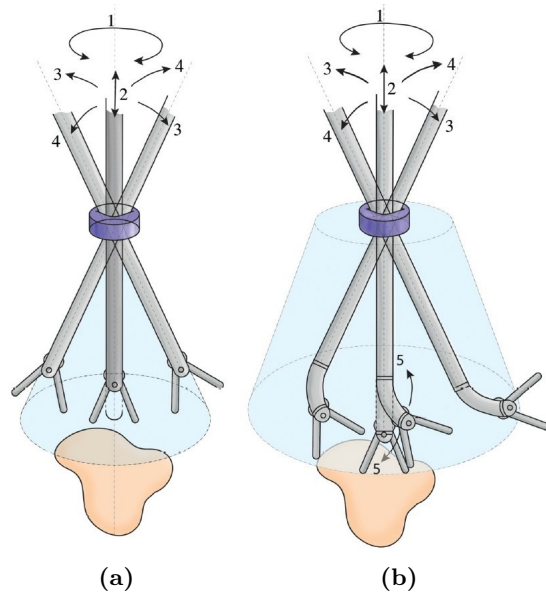


Figure 2: Workspace and DOF for general MIS manipulators. a) Traditional straight forceps. b) Articulating forceps. It can be seen that the articulating device has a larger workspace, and can approach the tissue from multiple angles due to the extra DOF (5). Adopted from [15].

from $0-70^\circ$ [8]. In open brain surgery also manipulating instruments with a pre-bent tip are used to work around obstacles, but these instruments do not fit through the straight trocar. With a rigid endoscope and straight instruments, sometimes multiple approaches are needed during the surgery [10]. Each new approach costs time and increases the risk of infection. The impossibility of using pre-bent instruments is one of the main reasons that in only a small portion of the potential cases a neuroendoscopic procedure is used [16, 17]. Sgouros [18] even goes as far as stating that “if an engineer was requested to design a new endoscope today from a ‘clean sheet’ ... it is unlikely that he would design such a difficult-to-manoeuvre ergonomically disadvantageous system”.

1.1.4 Articulating manipulators for minimally invasive surgery

Since the position of the trocar and thus pivot point is fixed, the surgeon cannot change the tissue approach angle after the incision is made. An incision may be optimally placed to reach one point in the body at one fixed angle, but sometimes that is not enough, which is where articulated instruments come into play. Articulation can regain one or more Degrees of Freedom (DOF) that are lost by using a small body entry point, as illustrated in Fig. 2. Instruments that have one or more extra joints in the tip can

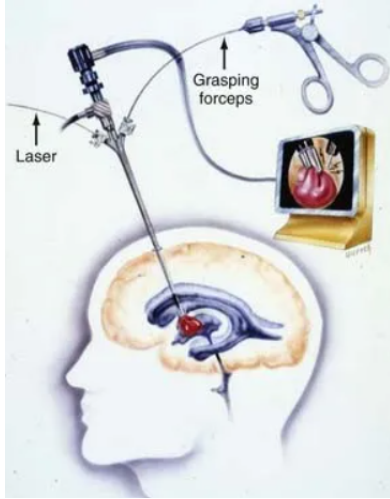


Figure 3: Schematic drawing of neuroendoscopic system, with all equipment running through a single trocar. This particular trocar holds a laser, forceps, light source, and endoscope. Adapted from [19].

steer the end effector in different positions and orientations, making them a versatile tool that depends less on obstacles and incision location [20]. Articulating instruments are no longer an exception in MIS, and research has shown that they add to the surgeon’s dexterity [21].

Many articulating instruments use cables or similar parts, like wires and tendons, to steer the end effector. Cables, wires and tendons are thin long features that are optimised for transfer of one-directional forces. Cables are a very efficient tool in surgical instruments, since they can transfer relatively large forces while taking up very little space. Furthermore, their flexibility in radial direction is low, which enables complex routing layouts.

Articulating instruments generally consist of many different parts to enable (multi-DOF) motion and motion actuation, on top of the existing instrument functions. Due to the instruments’ high complexity, in combination with the relatively low production quantities, assembling is often done manually [22].

1.2 Additive manufacturing

Additive manufacturing (AM), or 3D printing, is a fast-growing fabrication technology that enjoys popularity in the scientific, industrial, and the hobbyist community. In this technology, parts are built up layer by layer; each new layer is bonded to the previous to form one part. Due to its computer-controlled fabrication process, which is inherently different from all conventional production methods, 3D printing enables

production of parts that were previously very difficult to make.

As 3D printing technology advanced, so did its use in surgical instruments [23, 24]. The ease of printing a surgical instrument, as opposed to using conventional manufacturing, reduces the total production costs. When the production costs become lower than the sterilisation and reprocessing costs, it becomes economically beneficial to dispose the instrument after one-time use and reprocessing related design choices can be skipped. Furthermore, 3D printed instruments can be customised for each surgery, and instrumentation can be made accessible in remote or developing areas. Despite some of its substantial benefits over conventional manufacturing techniques, 3D printing of surgical instruments is not very common yet. Stainless steel is the golden standard for surgical equipment, but 3D printed metals suffer from porosity, residual stresses and rough surfaces. Other materials like polymers are currently best suited for 3D printing, but their material properties still lag behind on those of stainless steel.

One specifically interesting possibility is non-assembly AM: the fabrication of pre-assembled mechanisms—including moving parts—that are ready to use directly after they have been taken out of the 3D printer. With this promising new technique, mechanisms are fabricated in one step and assembly, traditionally one of the most costly and time-consuming production steps, can be completely avoided [25], reducing the production costs even further. Non-assembly AM could bring about a breakthrough in the development of instrumentation for MIS; where the functionality of micro-instruments is limited by the expensive and time-consuming fabrication and assembly process, non-assembly AM could provide a solution.

1.3 Problem statement

Neuroendoscopic approaches are rejected in the majority of potential cases, despite their superior patient recovery, due to the lack of pre-bent or steerable neuroendoscopic instruments; the complex shaped ventricular system with many different cavities and curvatures is difficult to navigate with straight instrumentation. Although steerable instruments for endoscopic neurosurgery could solve the rejection problem, they are difficult and expensive to make. Because of their small size—1-3 mm as opposed to 5-10 mm general MIS devices—both manufacturing and assembling is infeasible [26]. Additive manufacturing could provide a solution by circumventing the infeasible manufacturing and as-

sembling process. However, with additive manufacturing of surgical instruments a new challenge arises: many existing instruments are controlled with cables but using off-the-shelf steel cables in a 3D printed design still asks for manual assembling. On the other hand, 3D printing cables is infeasible; with current printing techniques the mechanical properties of cables—a low bending stiffness while also having a very high tensile stiffness—are still out of reach.

1.4 Project goal

The goal of this project is to explore the design of fully 3D printed non-assembly neuroendoscopic forceps, using planar and spatial articulation.

The above stated goal is built up from the following terms:

- *fully 3D printed:* Cables are allowed only if they can be printed with the rest of the device.
- *non-assembly:* The device must be printable in one step, i.e. using non-assembly AM.
- *neuroendoscopic:* The device must be suitable for use in an endoscope for neurosurgery. The device’s diameter is 2 mm.
- *forceps:* The device tip will have one degree of freedom for grasping.
- *articulation:* The device tip will have one or more degrees of freedom for bending, to achieve planar or spatial bending.

For simplicity, we choose to limit ourselves to a fully mechanical mechanism: no electric, hydraulic or magnetic components. Furthermore, the device will be disposable. Disposable devices are expensive since they need to be replaced after each intervention, but this is offset by the relatively low production costs of 3D printing.

1.5 Report outline

To solve the problem explained in Section 1.3 and fulfil the project goal, we start by summarising the state of the art in Section 2 and by thoroughly analysing the problem in Section 3. The design criteria, given in Section 4, follow from this problem analysis. Then, a general working principles design is constructed in Section 5, by looking at the device’s sub-functions. In Section 6, two planar bending concepts are deducted from the working principles design, with a different bending mechanism implementation. The designs are worked out in detail, and the

prototyping phase is described at the end of the section. In Section 7 we describe the experimental validation of the planar designs and discuss the test results. After that, we explore the design of two spatial bending devices in Section 8, along the same lines as the planar devices. Finally, we discuss our main findings and study limitations in Section 9 and conclude them in Section 10.

2 State of the art

2.1 Neuroendoscopic trocars

Unlike traditional trocars, neuroendoscopic trocars extend from the body opening, all the way to the surgical site, and have many additional integrated functionalities, as shown in Fig. 4. Due to these functionalities, such as irrigation and endoscopic vision, neuroendoscopic trocars are often referred to as neuroendoscopic systems. The main companies producing these neuroendoscopic systems are Storz [12], Aesculap [7], Wolf and Rudolf Medical [14]. Figure 4a shows the MINOP trocar by Aesculap, including two surgical manipulators. Currently, the endoscopic systems are not specialised for one type of surgery and are used in many different procedures. The working channels for manipulators range from 1.3 mm to 3.5 mm, and provide a rigid shaft for the instruments they hold [7, 12, 27]. Generally, the thinnest devices are used for paediatric surgery or certain very delicate procedures. To avoid instrument interference the main working channel follows a straight line through the entire trocar, while the endoscope, all tubes, and potential flexible instrument enter the trocar at an angle from the side (see Fig. 4a). The main working channel has a length of around 250-350 mm [7, 12].

2.2 Surgical articulation

The manipulator designed in this study is the forceps. Surgical forceps exist in many different types and forms, but they usually have two jaws that can be used to grasp, hold, or move tissue. In 1982 Chen reviewed the most used grasping mechanisms at that time [28]. Since then, another noteworthy type of grasper has been gaining ground: compliant forceps. For example, some grasping mechanisms have jaws that are mounted on flexible leaf springs, instead of using traditional joints [29–31]. More complex compliant solutions also exist, like the origami-inspired forceps by Edmonson et al. [32] shown in Fig. 5. To steer the grasper, an articulating mechanism is needed.

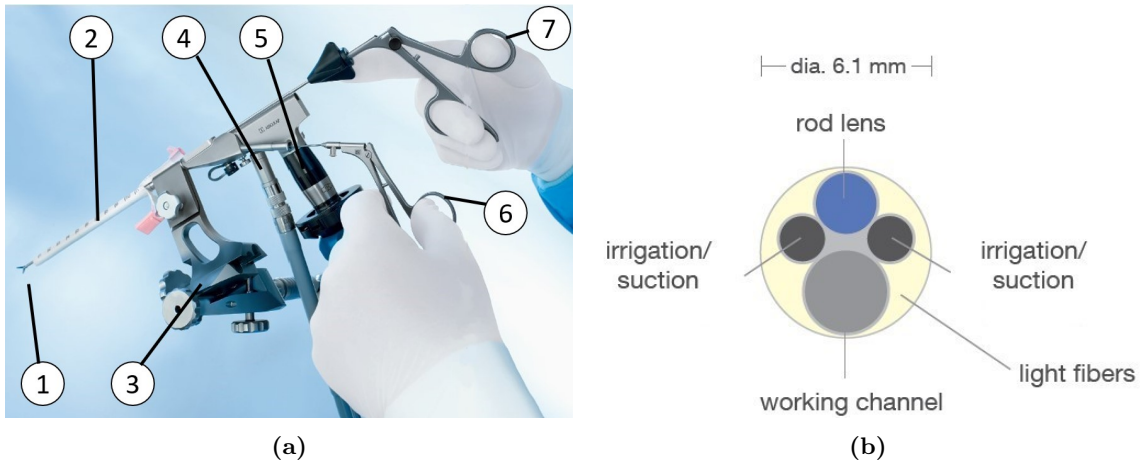


Figure 4: Neuroendoscopic system. a) system by Aesculap [7]. From left to right: 1, forceps; 2, trocar/endoscopic system; 3, holding arm; 4, irrigation supply; 5, endoscope; 6, instrument handle; 7, forceps handle. b) cross-section of endoscopic trocar. Adapted from [12].



Figure 5: 'Oriceps' surgical grasper by the Compliant Mechanisms Research Group from Brigham Young University [32].

Since articulating instruments are currently not used in neuroendoscopic surgery, it is helpful to look at how articulation is achieved in instruments from other MIS applications. Articulated instruments come in many forms. To analyse the different working principles, we divided the state-of-the-art solutions in planar and spatial bending mechanisms. Planar bending is fully 2D, i.e. within one bending plane, whereas spatial bending is 3D, i.e. in multiple bending planes. The solutions are then further divided in concentrated bending or distributed bending. Concentrated bending is achieved by at most one bending joint or mechanism per bending plane, and distributed bending is achieved by placing multiple joints in the same bending plane. The resulting categorisation consists of four categories and is visualised in Fig. 6: I) concentrated planar bending; II) distributed planar bending; III) concentrated spatial bending; IV) and distributed spatial bending.

More bending joints generally leads to higher

motion freedom and more dexterity for the surgeon, provided that the joints are correctly implemented. Some of the freedom that is lost by using a single body entry can be regained with extra articulation. Then why not aim for the largest possible number of degrees of freedom? Is a Category IV device not always better than one from Category I? With a higher manoeuvrability often comes higher complexity, and that has two main disadvantages: complex mechanisms require more space resulting in a larger diameter, and complex freedom of motion can be less intuitive to control. When a very thin device is required for a relatively simple surgical task, a Category I design could be used, but with a highly complex surgery where size is subordinated to manoeuvrability, Category IV is the way to go. Category II and III can be good middle ways when both size and articulation are key.

2.2.1 Concentrated planar bending (I)

The simplest adaptation from a rigid non-steerable instrument is the addition of a single, planar, bending joint. A large benefit of this category is the small size, which is crucial for neuroendoscopy. Zahraee et al. [34] described a prototype containing a single revolute joint to facilitate bending of the tip (see Fig. 7a). A driving shaft with two universal joints provides the transmission between the handle and the grasping mechanism. A different approach is used in the SATA mechanism by Tuijthof and Horeman [35] (see Fig. 7b). This mechanism consists of two concentric tubes that convert relative rotation into longitudinal translation through coupled inserts between the two tubes, which is then used to achieve a bending motion. The main advantage of this cableless mechanism is that

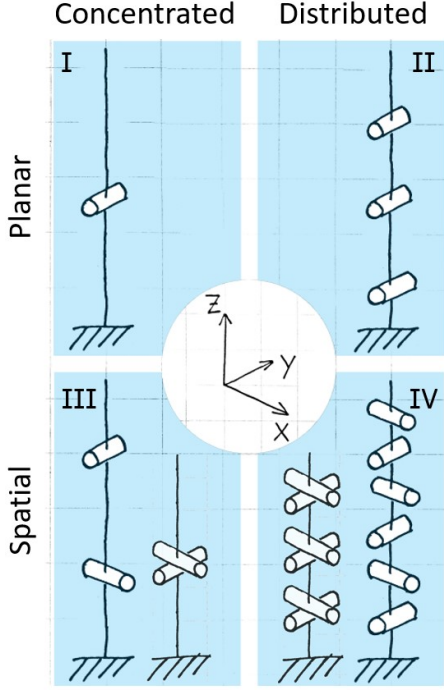


Figure 6: Schematic representation of four bending categories, using the Cans in series system by A. Schwab and J. Meijaard [33]. Each “can” represents one bending joint or mechanism. The two spatial bending categories can be accomplished by using 2DOF joints or by using complementary 1DOF joints. An example of both methods is shown.

the tubes are hollow, and endoscopic devices or driving cables for an end effector can be guided through the middle [36].

2.2.2 Distributed planar bending (II)

Some researchers designed devices that distribute the bending over multiple concatenated modules, resulting in a gradual bend and a larger bending radius compared to concentrated bending devices. A major advantage of distributed bending is the ability to reach around larger obstructions. In 1993, Müglitz et al. [37] published a MIS instrument using distributed bending (see Fig. 7c). This device consists of multiple concatenated four-bar mechanisms which are connected in such a way that they all move synchronous and the complete bending mechanism has one DOF. A cut-out is made along the neutral bending axis of the device, through which an endoscopic instrument can be guided. Another example of an instrument using planar distributed bending is the device by Minor and Mukherjee [38], which uses two layers of gear wheels on rigid links to couple the bending angle between each module (see Fig. 7d). Cables

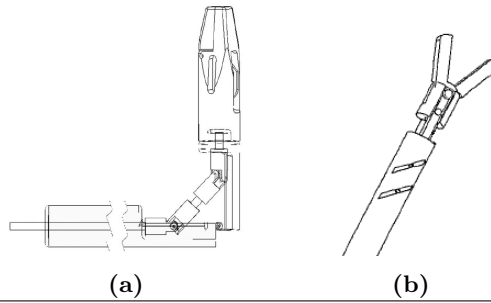
are used to actuate the end effector. On top of that, a third layer of gears driving a bevel gear serves as transmission for tip rotation around its own axis.

In the two articulated devices described above, the simultaneous bending of several concatenated mechanisms gradually changes the bending radius. A different approach is used by Zhang et al. [39] and Thompson et al. [40]: their instruments have a constant bending radius, but the length of the bending segment changes by actuating bending modules one by one (see Figs. 7e and 7f). The device by Zhang et al. has two modules. The most distal module moves first, until an end stop is reached and the second module starts moving. A constraint pin ensures the second module only starts rotating when the first module has reached its final rotation. The device by Thompson et al. consists of four modules. Each module has a driving link, whose joints are slightly misaligned from the joints between modules, thus restricting rotation. Only when the distally adjacent module has rotated, the joints align and the next module is free to rotate.

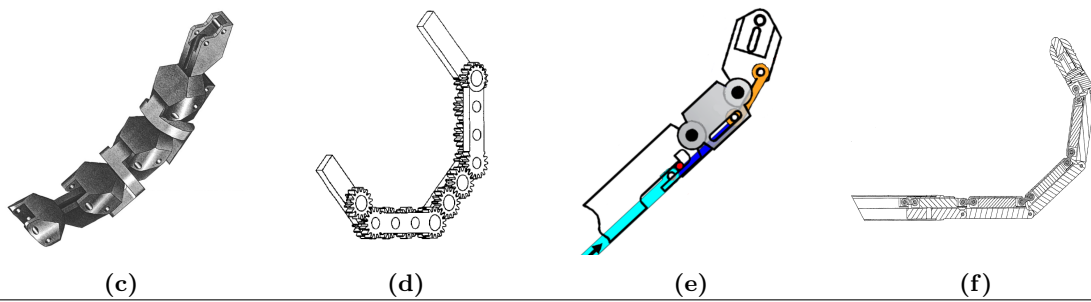
2.2.3 Concentrated spatial bending (III)

Spatial bending devices can move their end effector in any direction. This increases the possible angles of approach and could avoid interference with other instruments. Steege [41] patented a surgical tool with two bending joints that are placed in series with a 90° shift (see Fig. 7g). The bending is not distributed, since there is only one joint in each of the two bending planes. Both joints are ball-shaped and have slots to guide cables through that actuate the bending and gripping motion. The two jaws of the gripper share the same point of rotation, and are controlled by two skew sliding mechanisms. Another example is the DragonFlex by Jelínek et al. [42] that uses two bending joints in series (see Fig. 7h). Apart from actuation cables, the device is completely 3D printed. The designers opted for a novel rolling joint that minimises cable fatigue and play, a common problem in 3D printed mechanisms [46]. Sakes et al. [15] used independent control of grasper jaws to achieve bending, in combination with an extra bending joint for bending in the perpendicular direction (see Fig. 7i). Using the jaws for bending asks for large jaw rotations—for bending, both jaws need to rotate, after which there still needs to be room for opening—which they achieved by connecting pulleys to the jaws and cables to control them. Hardon et al. [43] describe a newer version of the SATA device with three concentric tubes, and an extra bending joint (see Fig. 7j). Cables

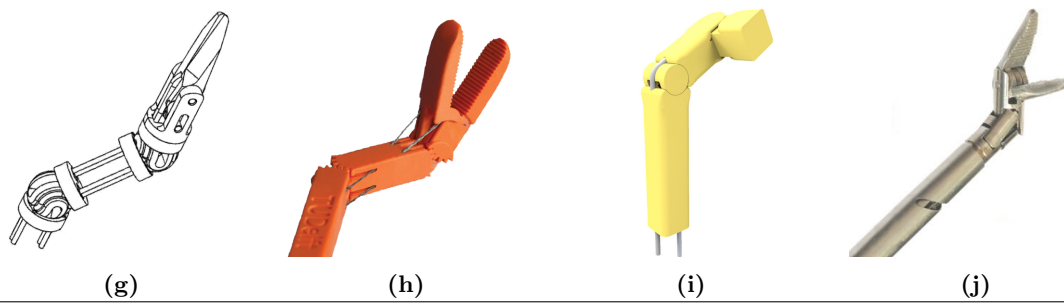
Concentrated planar bending (I)



Distributed planar bending (II)



Concentrated spatial bending (III)



Distributed spatial bending (IV)

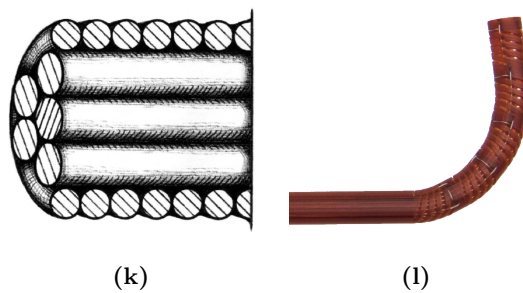


Figure 7: Overview of state-of-the-art articulating surgical devices. a-b) concentric planar bending, adapted from [34, 35], respectively. c-f) distributed planar bending, adapted from [37–40], respectively. g-j) concentrated spatial bending, adapted from [15, 41–43], respectively. k-l) distributed spatial bending, adapted from [44, 45], respectively.

guided through the proximal bending joint are used to transmit forces and motion to the more distal bending joint.

2.2.4 Distributed spatial bending (IV)

The most sophisticated devices combine distributed bending with a spatial range of motion. These devices can use complex paths to reach the surgical site and are highly adaptable. Breedveld et al. [44] designed an instrument that consists of three elements, from the inside outwards: a gripper driving cable, bending driving cables, and a spring holding the cables together (see Fig. 7k). A major advantage of this instrument is that it can be made from standard parts which reduces fabrication time and costs, benefiting mass production. Another device that can smoothly bend in 3D is the HelicoFlex by Culmone et al. [45] (see Fig. 7l). Apart from the driving cables, this instrument is completely 3D printed, with a total of only three parts. The bending part consists of a solid backbone, surrounded by flexible helicoids. The handle and device tip—similar in shape—are connected by 20 cables to couple their motion.

2.3 Non-assembly additive manufacturing

The solutions from Section 2.2 cannot directly be fed into a 3D printer with a small adjustment to make them suitable for neuroendoscopic trocars. Most mechanisms are not suitable for non-assembly AM without revising the design. The most notable differences between design for traditional and 3D printed mechanisms lie in the joints. Researchers have analysed different mechanisms and have tried to find optimal shapes and properties to 3D print certain joint types. Cuellar et al. [47] reviewed 3D printed non-assembly mechanisms and made a clear distinction between traditional rigid-body joints and compliant alternatives. Rigid-body joints can be printed by implementing a small clearance between the different joint parts, so they do not fuse together during printing. Compliant mechanisms can be printed when they are monolithic, i.e. the mechanism consists of one single-material part and flexible connections enable motion. With new multi-material 3D printing techniques it is possible to print the flexures with a different material than the stiff parts of the mechanism.

Prior to writing this report we performed a design review comparing design for non-assembly AM with design for conventional manufacturing [48]. The two design methods have more similarities than they have differences. Mechanism

functioning, for example, does not change when using non-assembly AM. In our report we focused on the differences. Interestingly, we found that sometimes seemingly opposing non-assembly AM design strategies can be used to achieve the same goal. At the base of this contradiction often was the trade-off between adding features and simplifying the mechanism. Both can be used to, for example, counteract excess play. We observed the same distinction that Cuellar et al. [47] made between rigid-body joints and compliant flexures; hybrids that used both in a single mechanism were scarce, whereas a combination between rigid and compliant joints—if material and printing properties allow—could be very useful.

One promising strategy we found is the stacking of (2.5D) compliant mechanisms to create a multi-layer mechanism and circumvent interference between flexures by placing them in different layers. 3D printing makes it easy to connect the layers locally, while keeping enough separation elsewhere. We found that many features and complex mechanisms can be made with non-assembly AM already, like one-way bearings, elaborate toy figures, nested helical gears and almost all existing compliant mechanisms. Unfortunately, printing cable-like structures is still a challenge and was mostly avoided. Other solutions to actuate a 3D printed instrument must be considered.

3 Problem analysis

3.1 Function analysis

The workings of the instrument can be split into four sub-functions, which all serve the goal of an articulated surgical forceps. Together they describe every action the instrument must be able to execute. The two main functional requirements are bending and (planar, 1 DOF) grasping (see Fig. 9). Both the grasping and bending can be further divided in two: a mechanism enabling just the bending or grasping motion, and a transmission mechanism to drive these motions. The bending requirement can be further refined for planar or spatial mechanisms, and for concentrated or distributed bending, since we will explore the design for all categories described in Section 2.2. The four functional requirements then become:

- **Bending:** Rotational motion(s) between shaft and grasper to manoeuvre tip behind obstacles, depending on category:

- I. Planar one DOF rotational motion

- II. Planar two (or more) DOF concatenated rotational motions
 - III. Spatial two DOF rotational motion
 - IV. Spatial four (or more) DOF concatenated rotational motions, in two (or more) bending planes
- **Bending transmission:** The bending motion must be actuated with a mechanism transmitting motion and forces.
 - **Grasping:** The tip must hold at least two jaws that can move towards each other (in the same plane), which means that at least one has to be able to rotate or translate.
 - **Grasping transmission:** The grasping motion must be actuated with a 1 DOF mechanism, transmitting motion and forces.

For simplicity, the designs will have the minimum amount (not more) of DOF as defined in the first functional requirement.

3.2 Small-scale challenges

With our 2 mm instrument, it is difficult to design and fabricate an articulation mechanism. Assembling becomes increasingly infeasible; parts can become so small that they are difficult to position correctly and without using too much force. We will use non-assembly AM for its advantages with fabricating very small assemblies. Reducing the size of existing designs by simply scaling them, however, is often not sufficient. Since length, area, and volume scale differently, properties depending on these measures will also scale differently. Furthermore, new scaling issues, such as low accuracy, strength, or isotropy, can arise when the minimum size limits of the 3D printer are approached. For example, simple features are better scalable than intricate features, and leaf flexures are preferred over notch flexures. At a small scale, it becomes increasingly important to make optimal use of the available space to maximise mechanical advantage and stiffness, which are often bottlenecks in small designs.

3.3 3D printer selection

Besides the micro-mechanisms in the 2 mm tip, our instrument needs a normal sized handle. We need a printer that has a high resolution to fabricate the small features in the 2 mm tip, but that must also fit a complete surgical instrument. Many printing techniques exist, but not many possess both features.

Han et al. [49] discussed six different 3D printing techniques and compared them: Fused Deposition Modelling (FDM), Stereolithography (SLA), Polyjet technology, Selective Laser Sintering (SLS), Binder Jetting (BJ) and Digital Light Processing (DLP). They summarised advantages and disadvantages of each technique and compared their specifications. Most printing techniques lack at least one property that we need. Fused Deposition Modelling (FDM) has a low printing resolution of 0.1 mm, which is too large for a 2 mm mechanism, especially when multiple layers are preferred [49]. Selective Laser Sintering (SLS) has a large layer height of 0.2 mm [49]. Both FDM and SLS have an accuracy of 0.3 mm or higher.

FDM, SLS, and Polyjet printers have advised minimum wall thicknesses of 0.6-1 mm [50–53], making a 2 mm mechanism infeasible. The minimum feature size for BJ is around 2 mm [54]. The remaining two processes are DLP and SLA. DLP and SLA have many similarities; both fall within the ISO/ASTM category [55] of Vat Photopolymerisation and use a light source to cure layers of liquid material. They have minimum feature sizes and wall thicknesses of around 0.2 mm [54], and can reach resolutions between 0.01-0.025 mm [49].

Despite the similar specifications, we prefer SLA for its ability of printing large volumes with high accuracy [43, 56]. With DLP a trade-off must be made between printing volume and resolution. We used Formlabs’ Form 3B printer for its 25 micron resolution, which is high enough to print the sub-millimetre features in the tip. To print, the build plate is lowered to the bottom of a tank filled with liquid photopolymer resin. A thin photopolymer layer between the build plate and the bottom of the tank is then cured using a laser beam. The build plate is raised one layer height, and a new layer between the previous layer and the bottom of the tank is cured. The Form 3B, originally developed for dental applications, can print multiple bio-compatible materials. The Form 3B has a resolution of 25 microns in x, y, and z direction, and layer fusion ensures an isotropic result.

We will print with the materials from the ‘Tough and Durable Resin Family’ [57]. This material group by Formlabs consists of three similar resins that are known for their good mechanical properties. The printed material will bend upon stresses, rather than fracture, which is critical for our purpose. The three materials have slightly different mechanical properties, with ‘Tough 2000’ being the stiffest, followed by ‘Tough 1500’ and ‘Durable’.

Ongoing advancements further exploit SLA’s

ability of printing multi-scale parts that are a combination of very precise sections and less critical large sections. Li et al. [58], for example, developed as SLA technique that is able of changing the laser spot size and the layer height to alter the print resolution and speed of different sections. SLA techniques are expected to develop higher printing speeds [59], larger build volumes [60], higher accuracy [61], and a wider material choice [62, 63].

3.4 Challenges and opportunities of AM

Using (non-assembly) AM enables us to design and fabricate a previously infeasible instrument, but it brings extra challenges and opportunities. They are summarised in Table 1. One of the main challenges with our chosen printing method is to achieve **tight clearances** between moving parts. Formlabs advises to use a minimum clearance of 0.3-0.5 mm [64] to avoid parts fusing together. On a 2 mm scale, this can cause excess play and it can limit part width. Minimum clearances can be decreased by using specific design techniques. Chen et al. [65] created design guidelines for minimising clearance in rigid body joints by using different shapes. Song and Chen [66] added markers and dents to locally minimise the clearance; since only a small area has a low clearance, the chance of parts fusing together is low, but it still results in lower play. A similar approach of locally minimising clearance was demonstrated by Wei et al. [67].

A weakness that many printing techniques have, is fabrication of **overhangs**. Overhangs describe every surface that is not directly supported by underlying material. SLA printers cannot print in mid-air, and the first layer in which an overhang occurs can collapse. The minimum surface angle that can still be printed with the Form 3B is 10°, almost horizontal [64]. Completely horizontal surfaces can only be printed when their length is less than 5 mm, or, when the surface is supported on both sides, less than 29 mm [64]. Due to the good overhang printing qualities of the Form 3B, overhangs are less relevant in the tip design. In the handle overhangs can introduce problems, but there is also more space to prevent it.

A challenge that is specific to Vat photopolymerisation processes is the presence of **peel forces**. Peel forces originate from a wiper that smooths out each new layer of liquid photopolymer. The wiper can cause strain in the previously printed layer, which can be minimised by minimising the flat surfaces in the horizontal plane printing plane. In practice, this means

Table 1: Challenges and opportunities of 3D printing.

Challenges	Opportunities
Tight clearances	Shape complexity
Overhangs	Design for stresses
Peel forces	Part consolidation
Post-processing	Intricate features
Mech. properties	Encapsulated structures

many parts on SLA machines are printed under an angle.

Ideally, the instrument is ready to use when taken out of the printer, but in reality it needs **post-processing**. When parts come out of the Form 3B printer, they first need to be washed in alcohol to remove residue liquid resin. Optionally, the printed part can be post-cured to enhance its mechanical properties. Finally, the support structures need to be removed. With intricate and delicate parts that need many supports, removal of supports can be time-consuming.

Lastly, the Form 3B has a limited range of materials. The **mechanical material properties** of these materials lack behind on those of surgical graded stainless steel. It will be a challenge to achieve a stiff enough mechanism for surgical use.

An important opportunity of AM is its ability of fabricating parts with high **shape complexity**. With conventional manufacturing techniques there is a strong relation between part complexity and manufacturing complexity, but with AM this relation is almost non-existent. 3D printers can print parts with many angles, curves and organic shapes. A part that will be 3D printed can be fully optimised for its functionality, without many of the limitations that conventional manufacturing imposes.

A result of the 'free' shape complexity is the ability to **design for stresses**. Parts can have a varying cross-section with just enough material in the right places to withstand the loads. Less material needs to be used, resulting in lower costs, lower fabrication times, and a lighter part with similar or improved strength.

Part consolidation is the combining of multiple parts into one, incorporating all functionalities. For example, many fasteners, washers, spacers and springs could be integrated in a single 3D printed part.

Although part consolidation can simplify a design and make it more efficient, AM is capable of printing many small and **intricate features** that take up the function of one larger feature. A bulky joint could be replaced by many small joints, distributing the forces, or multiple small

spacers could replace a single heavy one. In our tip design, splitting a single structure in multiple smaller ones has the risk of creating extra clearances, which should be avoided.

Lastly, it is possible to make **encapsulated structures**, that are hard to reach from the outside of the part. This is especially useful in small designs, or assemblies with many parts that obstruct the access to other parts.

3.5 Challenges and opportunities of compliant mechanisms

The combination of a 2 mm mechanism with multiple independent DOF and a minimum clearance of 0.3-0.5 mm poses a serious challenge. Fig. 8 visualises the influence of 0.3 mm clearance of a single rigid-body joint at a 2 mm scale. Even with a single joint the play takes up a significant portion of the device, and the joint pin and journal are thin (0.47 mm). Play can be reduced using special hinges, but the clearances will still severely limit the width of the structures. Compliant equivalents do not suffer from the large clearance since they have no play, and are suited for micro-scale and smaller [20].

Using rigid-body joints for our purpose is infeasible, but using compliance has some additional benefits. Compliant joints do not suffer from wear debris, need no lubrication and have no pinch points [20, 27, 68]. All three are highly unwanted in neurosurgery. Furthermore, compliant mechanisms are highly reliable and they simplify sterilisation [68]. Disadvantages of compliance include limited rotation, parasitic motion upon external forces, and reduced force feedback. Friction in traditional rigid-body joint instruments hampers haptic feedback, decreasing the surgeon’s instrument awareness. Even though compliant joints have no friction, they do require extra energy to deform, which also disturbs haptic feedback. This can be compensated for with static balancing [69].

A distinction can be made between lumped compliance and distributed compliance, based on the length of the compliant sections [70]. Notch joints are examples of lumped compliance; the deformation is concentrated in a short flexible section. Leaf flexures are examples of distributed compliance; the deformation and stresses are distributed over a longer length of material. Lumped compliant joints are compact, but have a very limited range of motion and are more prone to high stress concentrations and fatigue failure than distributed compliant joints [70, 71]. Cronin et al. [72] designed an endoscopic instrument for a 3.3 mm working channel and concluded that lumped, "hinge-like, com-

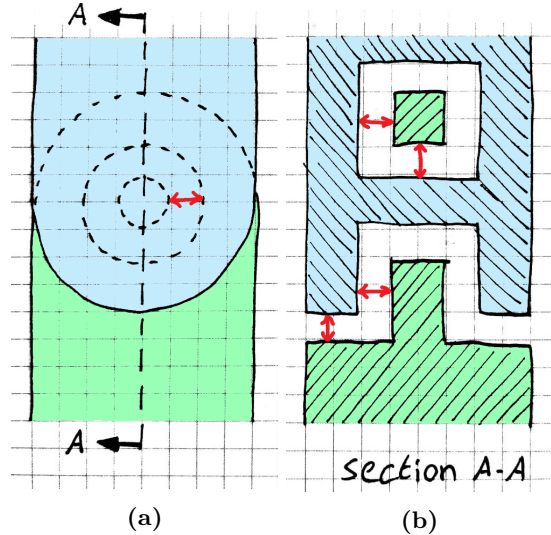


Figure 8: Visualisation of 0.3 mm clearance proportions in a 2 mm revolute joint. Note that this 2 mm square mechanism does not fit through a 2 mm round trocar. a) front view. b) side view cross-section.

pliant joints are also infeasible at this scale”. Since we need relatively large deformations for the bending and grasping, distributed compliance in the tip is preferred.

4 Design criteria

The criteria from Table 2 need to be taken into account during the design phase. The geometrical requirements ensure that the functional requirements from Section 3.1 are met and that the device can be used in an existing neuroendoscopic trocar. Figure 9 visualises the main geometrical requirements in a planar mechanism. The actuation requirements ensure that the surgeon is able to correctly operate the instrument. The printing limitations make sure the design can be printed with the Form 3B printer. The wishes are not critical, but ‘nice to have’. Criteria regarding sterilisation, re-usability, and aesthetics are not included, since we aim to design a disposable, single-use product.

The requirements for the different categories differ in one point: concentrated bending has a maximum bending radius of 6 mm, whereas distributed bending has a target bending radius of 12 mm. Most brain surgeries operate in and around the brain ventricles, which often have diameters of less than 10 mm. These surgeries benefit from devices with small bending radii. However, some operations require the instrument to navigate through the ventricles first, with curvatures around 12 mm [9, 73].

Table 2: Overview of design criteria**1 - Geometrical requirements**

Criterion	Target	Rationale
1.1 - Bending angle between shaft and tip	-60°–60°	60° is the standard bending angle in MIS instruments, in both directions.
1.2 - Bending radius	conc.: < 6 mm	Must be similar to that of existing pre-bent neurosurgical instruments. [74, 75]
	dist.: 12 mm	A larger bending radius can navigate through the ventricles' curves. [9, 73]
1.3 - Forceps opening angle	0°–40°	Must be similar to that of existing neuroendoscopic forceps. [7, 12, 75, 76]
1.4 - Maximum diameter	2 mm	The device must fit through a 2.2 mm working channel in a neurosurgical trocar.
1.5 - Shaft length	265 mm	The device must fit through a 250 mm working channel in a neurosurgical trocar.
1.6 - Maximum unwanted tip deflection	< 1 mm	The device must not significantly deform due to mean tissue forces of 0.68 N. [77]

2 - Actuation requirements

Criterion	Rationale
2.1 - Single hand control	Enables surgeons to operate the device with one hand.
2.2 - Adjustment of forceps opening angle	Enables surgeons to close the forceps and grasp different sizes of tissue.
2.3 - Precise adjustment of bending angle	Enables surgeons to adapt the direction of the forceps to reach behind obstacles.

3 - Form 3B printing limitations

Criterion	Target	Rationale
3.1 - Minimum clearance	0.3–0.5 mm	Minimum distance between moving surfaces. [64]
3.2 - Minimum wall thickness	0.2 mm	Minimum supported or unsupported wall thickness. [64]
3.3 - Minimum unsupported overhang angle	10°	The Form 3B printing is capable of printing very low overhang angles. [64]
3.4 - Materials	Form 3B materials	We are limited by the available materials by Formlabs. [64]
3.5 - Maximum printing volume	145 x 145 x 185 mm	The complete device must fit within the Form 3B printer. [64]

4 - Wishes

Criterion	Rationale
4.1 - Locking mechanism for bending	Enables surgeons to (mechanically) lock the forceps direction for improved ergonomics and precision.
4.2 - Shaft rotation	With shaft rotation the surgeon can maintain the same comfortable arm position whilst rotating the tip around its own axis.
4.3 - Tactile feedback of trocar emerging	The devices by Aesculap [7] have a sensible increase in friction when the tip exits the trocar to help the surgeon.
4.4 - Suitable for miniaturisation	Instruments for 1.3 mm trocars make the surgery even less invasive. [12]

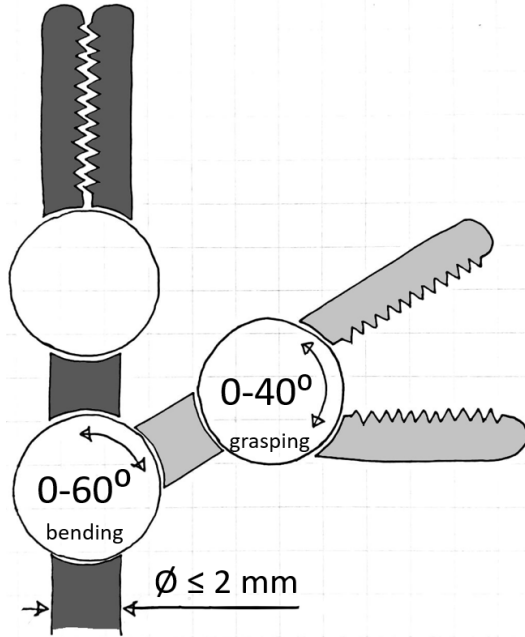


Figure 9: Schematic representation of functional requirements. On top of that, the maximum diameter criterion is indicated. The motions are planar.

The requirements from Table 2 also hold for the exploration of spatial bending designs. Since the Category III and IV designs can consist of multiple bending mechanisms, criterion 1.1 must be met for each separate mechanism. The distributed target radius of 12 mm can be achieved by the sum of multiple bending mechanisms.

5 Working principles concept

5.1 Concept generation

5.1.1 Methodology

The general solution functions as a minimum working example. The design must include all working principles but not yet their exact implementation. It should provide a framework from which a suitable design for each category can be derived, without the need for new design solutions. The differences between the derived designs can be kept small, because the reasoning behind choosing the underlying principles is universal to all categories.

To generate a suitable general solution to our problem definition that meets all design criteria, we made morphological overviews for each sub-function. The solutions to the different functional requirements in the morphological overviews can be combined to form many differ-

ent concepts. We considered two general rules that increase the chance of meeting the design criteria to generate our concepts:

1. Stick with compliance

Compliance will be used for its ease of printing and its suitability for joints in the millimetre range. At this scale, 3D printed rigid-body joints become fragile and clearances, which are fixed by the printing method, become relatively large, as explained in Section 3.5. Distributed compliance is preferred over lumped compliance for joints that need a significant range of motion.

2. Aim for mechanical simplicity

The diameter of the designs will largely be defined by the number of parallel parts and their complexity. Furthermore, a mechanically simple design with few joints and moving parts will be easiest to print. Note that we are not talking about geometrical complexity, like the number of different shapes, planes or edges, which is in fact a strength of 3D printing. Choosing less features saves space that can be used to increase part stiffness where needed.

These strict rules are necessary due to the complexity of designing a multiple DOF non-assembly mechanism smaller than 2 mm and with 0.3-0.5 mm clearances. A versatile design is preferred over a very specific solution that only works well for one of the Categories. Furthermore, mechanisms will be judged on properties such as diameter and stiffness. If, after applying these rules, more than one possible concept is generated, a detailed comparison will be made.

5.1.2 Morphological overviews

Fig. 10 shows a morphological overview of bending mechanisms, sorted by their number of joints. The rigid-body joints in the mechanisms could also be replaced by compliant notch joints to create (lumped) compliant equivalents. When multiple copies of one bending mechanism are concatenated, a gradual bend over a longer distance can be achieved, similar to the distributed mechanisms from Fig. 7. Figure 11 shows a morphological overview of grasping mechanisms. Opening and closing of the grasper can be achieved by moving or rotating the jaws towards and away from each other. To actuate either the bending or grasping, a mechanical transmission is needed between the handle and the tip. Potential transmission mechanisms are given in Fig. 12.

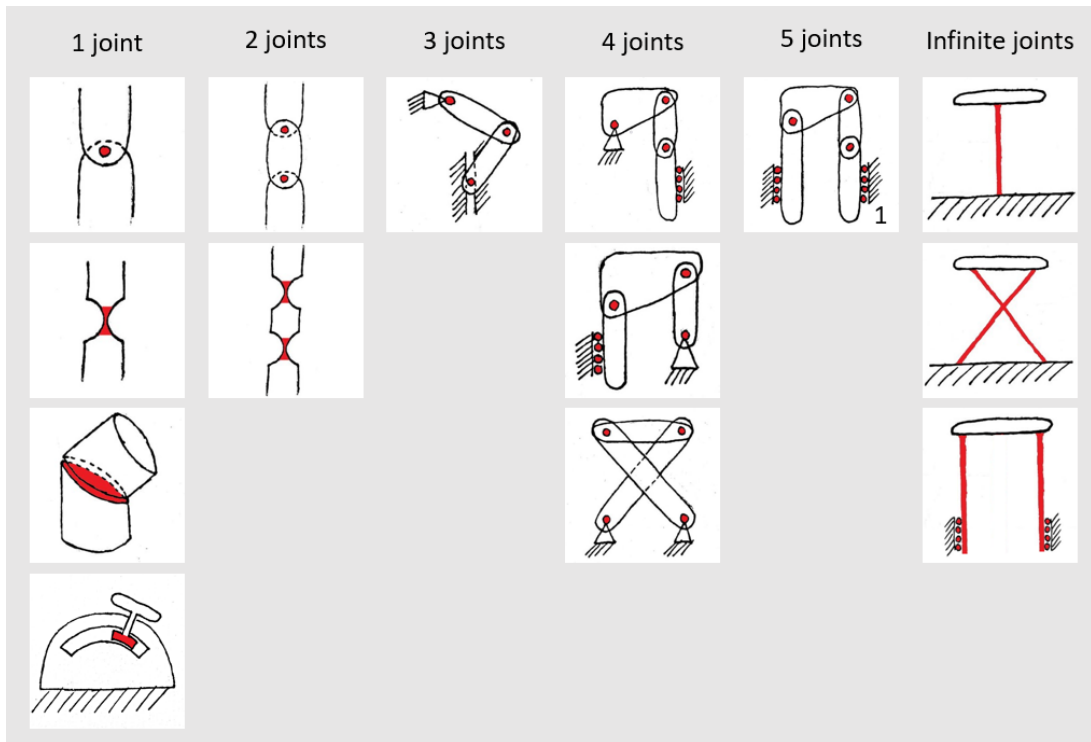


Figure 10: Morphological bending scheme. Different solutions to achieve planar bending are sorted by their number of joints (depicted in red). Notch joints are counted as single joints, and leaf flexures as an infinite series of infinitesimally small rigid links and joints. For a more detailed overview of single bending joints, see [78]. ¹Tuijthof and Horeman [35]

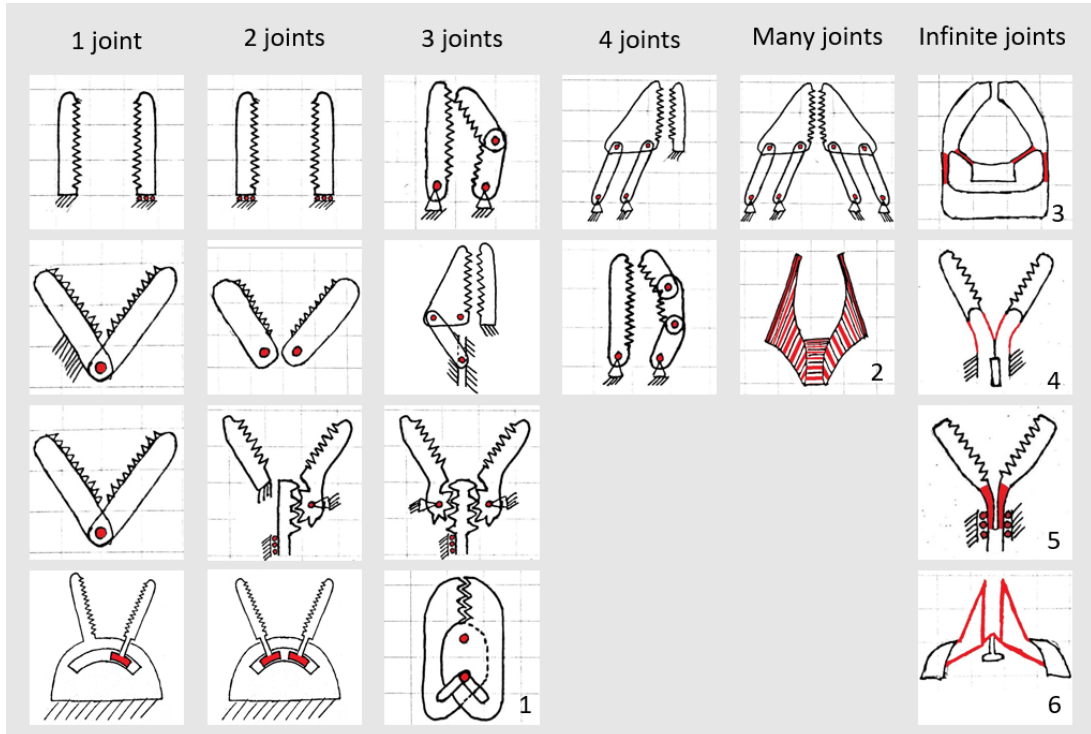


Figure 11: Morphological grasping scheme. Different solutions to achieve planar grasping are sorted by their number of joints (depicted in red). Notch joints are counted as single joints, and leaf flexures as an infinite series of infinitesimally small rigid links and joints. For an overview of traditional robotic grippers, see [28]. ¹Steeger [41]; ²Edmondson et al. [79, 80]; ³Berndsen [81]; ⁴Herder and Van den Berg [30]; ⁵D.O.R.C. [29] and Alcon [82]; ⁶Kota et al. [83]

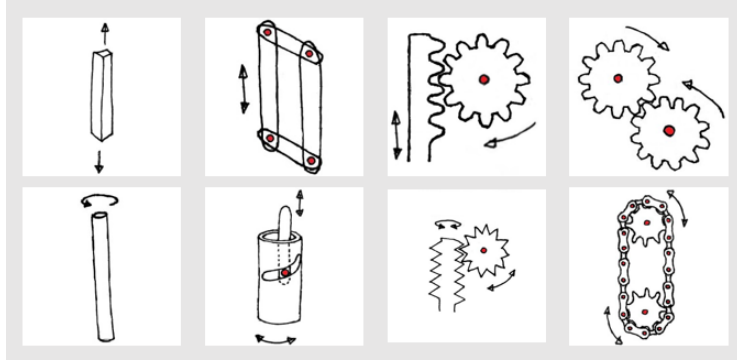


Figure 12: Morphological transmission scheme, including push-pull rod, rotating axle (possibly with universal joint), four-bar mechanism, cam mechanism, rack and pinion, worm wheel, gears, and chain. Note that the scheme applies to both transmission of bending and transmission of grasping forces or motions.

5.2 Sub-solutions

5.2.1 Bending mechanism

A 60° bending angle must be achieved. Applying rule 1 to Fig. 10, only the compliant solutions in the 'infinite joints'-column remain; all other solutions use rigid-body joints or lumped compliance. The remaining solutions are: a *single leaf flexure*, a *cross-flexure*, and *two parallel (sliding) leaf flexures*. All three solutions connect the tip with the base of the device with ordinary leaf flexures. Only the arrangement of the flexures differs, which makes it easy to compare them. The *single leaf flexure* scores highest on rule 2: mechanical simplicity. The *single leaf flexure* consists of only flexure, making it the simplest solution with the lowest part count. On top of that, the *single leaf flexure* is the thinnest mechanism of the three, and will not be a limiting factor for the diameter of the entire device.

This may seem like an easy choice, but there is a catch: the *single leaf flexure* and the *cross-flexure* need a transmission mechanism to actuate the distal part of the tip, and the *parallel leaf flexure* concept does not, since it is actuated by pushing/pulling the proximal side of the flexures themselves. The two sliding joints at the proximal side of the *parallel leaf flexures* enable the actuation of the flexures, and the actuation mechanisms of the other two solutions could have similar joints. If we take into account that the *single leaf flexure* and the *cross-flexure* need at least one, but preferably two, extra parts, the *parallel leaf flexure* solution has the fewest parts. This makes the *parallel leaf flexures* the simplest mechanism.

Since all three mechanisms consist of relatively long leaf flexures, a bending angle of 60° should be possible.

Note that the *single leaf flexure* solution with

an extra flexure used to actuate the tip is similar to the *parallel leaf flexures*. Despite being more complex, we will not rule out the *cross-flexure* mechanism yet. A comparison between concepts with *parallel leaf flexure* bending and *cross-flexure* bending will be made.

5.2.2 Grasping mechanism

Similarly, after applying rule 1 to Fig. 11, only the compliant solutions in the 'infinite joints'-column remain: Berndsen's *U-shape* design [81], Herder and Van den Berg's *V-shape* design [30], the design used in existing devices such as the *two-flexure* ones by D.O.R.C. [29] and Alcon [82], and the *triangular* design by Kota et al. [83]. The *U-shape* and *V-shape* designs are quite similar: they both have four flexures and three rigid parts, connected in the same arrangement. The only differences are the angle of the central flexures, and the relative sizes of the parts. Since the flexure orientation in the *U-shape* design limits their length, compliance will be lumped in a 2 mm instrument while a relatively large rotation is needed, and the *V-shape* design is preferred. The same reasons can be used to discard the *triangular* design; it has flexures that are oblique to the device's longitudinal axis, limiting their length and resulting in lumped compliance.

In terms of mechanical simplicity, the *two-flexure* design is better than the *V-shape* design: both have at most four parallel structures in a single cross-section, but the *two-flexure* design has half the number of flexures.

Both mechanisms should be able to achieve 40° opening angles. They can use similar jaws, that need to be closed during insertion in the endoscope.

The combined four flexures from the *V-shape* grasper can be made stiffer than the flexures of the *two-flexure* grasper, due to their wider base.

However, the flexures of the *two-flexure* grasper can be kept very short with only a small section sticking out of the tip. This is an advantage compared to the (outer) *V-shape* flexures which always extend a relatively large length from the tip. Furthermore, the shorter flexures keep the grasper jaws closer to the bending mechanism, which benefits actuation intuitiveness and minimises moment arms.

Its short flexures, together with its high simplicity—the grasper only needs two flexures—led us to opt for the *two-flexure* solution.

5.2.3 Transmission mechanism

Only the *push-pull rod* and the *axle* from Fig. 12 adhere to rule 1, since the other solutions use rigid-body joints. It is, however, also important to look at the compatibility of transmission mechanisms with the grasping and bending mechanisms. Following rule 2, we searched for the mechanism with the least parts and joints, whose output can be connected to the tip’s input in the easiest way. For both the *parallel leaf flexure* mechanism and the *cross-flexure* mechanism, the transmission output must be a push-or pull motion. The *push-pull rod* is the simplest way to achieve this motion.

Both bending mechanisms need two *push-pull rods*. The rigid push-pull rods can directly transition into the *parallel leaf flexures* without the need for a connecting joint, or they can be attached to the distal part of the *cross-flexure*. Choosing these solutions and attachments results in the simplest, thinnest mechanisms with a minimal number of joints and parallel parts, both in- and outside the shaft.

Also from a small-scale perspective *push-pull rods* outperform *axles*. For a solid cylinder, rotational stiffness scales with the radius to the power 4 ($k_{rot} = G \cdot \frac{\pi r^4}{L}$), and axial stiffness to the power 2 ($k_{ax} = E \cdot \frac{\pi r^2}{L}$). Since G and E are constant material properties, and given that the cylinders are properly constrained to prevent buckling, rotational stiffness will decrease quicker than axial stiffness during miniaturisation.

The grasper also needs a push-pull input. Here, the same line of reasoning applies. However, the grasper’s transmission mechanism needs to account for tip rotation. In other words, the output angle of the grasper’s transmission mechanism changes when the tip bends. We will solve this by using a *push-pull rod* with a decreased bending stiffness in the bending part. In this way, the grasping rod will bend with the bending flexures. Below the tip, the grasping

rod can have a higher bending stiffness because that part of the rod always remains straight.

5.3 Combination of sub-solutions

Appendix A provides an overview of the morphological schemes with the chosen bending mechanisms, grasping mechanism, and transmission mechanisms that lead to the two concepts. Figure 13 shows a sketch of the concepts, which are a combination of the sub-solutions. Only the bending mechanism and the shaft differ between concepts.

5.3.1 Parallel flexure concept

In total, this concept consists of three long flexures, of which two are for bending and one is part of the compliant grasping rod that follows the bending shape. Each of the three flexures springs from a rigid push-pull rod that runs from the handle. Moving the two bending push-pull rods in equal and opposite direction, i.e. sliding them along each other, will bend the tip. Pulling the grasper push-pull rod will pull the tapered grasper jaws through a rigid ring, closing the grasper. The trocar’s working channel keeps the push-pull rods together and serves as a sliding bearing.

The parallel flexure bending mechanism has many similarities with a grasper mechanism by Herder et al. [30]. A comparison of the two mechanisms is made in Appendix B.

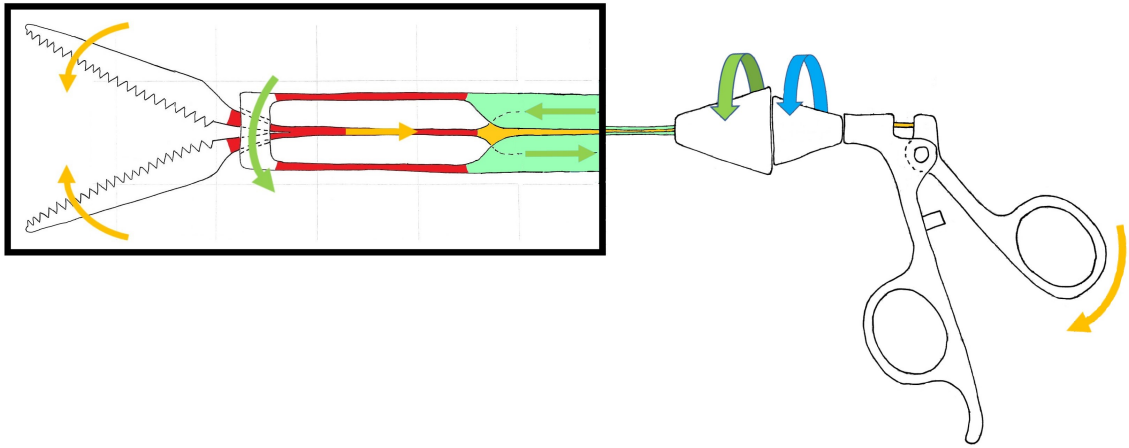
5.3.2 Cross-flexure concept

In total, this concept also consists of three long flexures, with the addition of two tendon-like structures to actuate the bending mechanism. The two bending flexures form a cross-flexure, which starts on a rigid base. A rigid rod connects the cross-flexure base with the handle, which is shown in pink in Fig. 13b. The tendons can be thinner than the flexures and are only used in tension. Pulling a pull rod that is connected to a tendon will bend the tip. Pulling the grasper push-pull rod will pull the tapered grasper jaws through a rigid ring, closing the grasper. The trocar’s working channel keeps the push-pull rods together and serves as a sliding bearing.

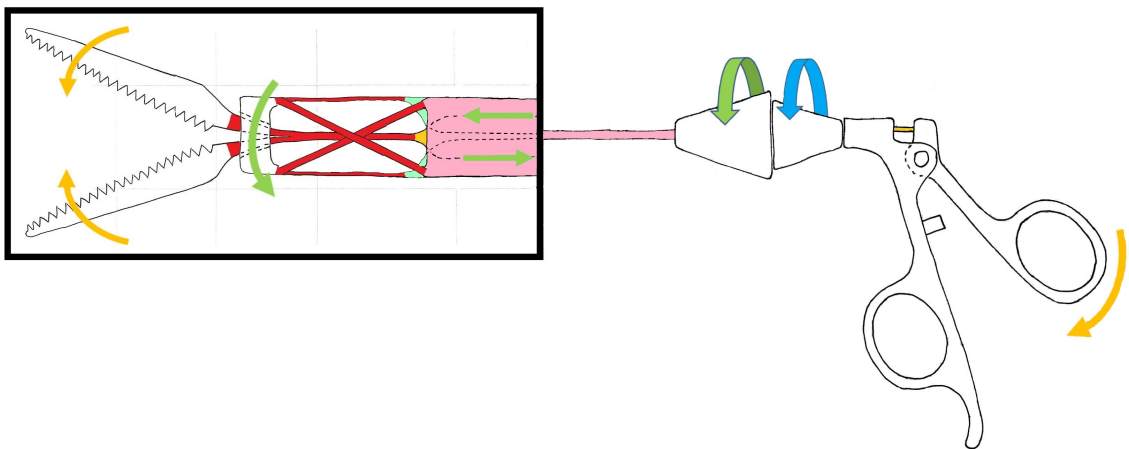
5.4 Concept selection

5.4.1 Concept comparison

In the comparison between the two concepts, we started with the simplest possible versions, shown on the top in Fig. 14. For the parallel flexure concept this means the bending flexures are



(a) Parallel flexure concept



(b) Cross-flexure concept

Figure 13: Close-up of concepts, indicated by the black frames. Compliant parts are depicted in red, the bending push-pull rods in green, and the grasping rods in orange. The grasper can be closed by pulling the trigger, which creates tension in the grasping rod. Then handle contains a mechanism to create an opposite sliding motion, which in turn bends the tip.

arranged in a square, and the grasping rod runs through the centre of the device's cross-section. The simplest possible version of the cross-flexure concept has one flexure in the front, and one in the back. The grasping rod runs through the centre of the device's cross-section, between the two bending flexures. Two rods to actuate the cross-flexure are placed in the same xz -plane as the grasping rod, between the two cross-flexure flexures. In the figures in Fig. 14 the concepts have a maximum diameter of 2 mm, and all clearances—indicated in red—are 0.3 mm.

An advantage of the cross-flexure concept is its small bending radius, which approximates zero. The centre of rotation lies roughly at the intersection of the cross-flexures. With the small bending radius the mechanism can make sharp turns and operate in limited spaces. The parallel flexure concept has a larger bending radius,

which depends on the length of the bending flexures.

The main weakness of the cross-flexure concept as opposed to the parallel flexure concept can best be explained by comparing their cross-sections. In the parallel flexure concept, the two bending flexures and the grasping rod do not interfere with each other; they are each in a different yz -plane, with a distance between them at all times. The cross-section is constant along the entire bending part. Even during bending the gap is maintained because all flexures bend in the same direction. In the cross-flexure concept, the bending flexures and grasping rod 'cross' in the middle; the cross-section at this height shows that the bending flexures and grasping rod are all on the same line, which severely limits their width. On top of that, not even the full line can be used because there need to be clearances

between the flexures. As can be seen from the cross-sections in Fig. 14, the total bending flexure width of the parallel flexure concept is 2.8 mm, and the total bending flexure width of the cross-flexure concept 0.6 mm: almost 5 times as low. When the width of the grasping rod is increased, this factor becomes even higher because there is a trade-off between the grasping rod and flexure width in the cross-flexure concept.

Another disadvantage of the cross-flexure design is the need for an extra pull-rod in the shaft of the cross-flexure concept to achieve two-way bending. The parallel flexure concept is already able of two-way bending since it uses two push-pull rods, as opposed to pull-rods. Using an extra rod for two-way bending increases the complexity of the shaft in three ways: 1) there are more features; 2) there need to be more clearances at the expense of the effective cross-section area; 3) the combination of thinner rods and more clearances increases the change of buckling and jamming in the shaft.

5.4.2 Stiffness related risks

When we critically look at the simplest versions of the concepts, both contain a risk that can lead to parasitic motion during bending: the long bending flexures of the parallel flexure concept are prone to bulging in the xz-plane (see Fig. E.1a) due to one flexure being loaded under compression, and the asymmetric cross-flexure of the cross-flexure concept is prone to torsion around the z-axis due to the moment that is introduced by the gap between the bending flexures. These risks do not necessarily have to get problematic, but they must still be addressed in the concept selection, in case they turn out more severe than expected. In the worst case parasitic motions could lead to low stiffnesses and unexpected bending behaviour.

For both risks a simple potential solution exists. Bulging could be avoided by constraining the perpendicular distance between the parallel bending flexures. There are several methods to do this, each with their own pros and cons, but for the comparison we will use one generic solution that enables us to continue the comparison between the concepts. In Appendix E we further analyse the problem and create a better informed solution, in case bulging turns out to be problematic. The generic solution consists of a 'spacing flexure' connecting the bending flexures, that only marginally contributes to the bending stiffness, but is stiff enough to keep the bending flexures from bulging. Asymmetric torsion of the cross-flexure can be avoided by introducing symmetry; the cross-flexure can be replaced by two thinner, mirrored cross-flexures.

Again, we opted to keep the solutions as simple as possible to make a comparison between 'minimum working examples'.

5.4.3 Final concept choice

Judged on the simplest designs from Fig. 14, most disadvantages of the cross-flexure concept rise from the 2 mm scale. On a larger scale, e.g. 10 mm, the cross-flexure concept may have been a better choice, but for our purpose it is infeasible, which is why we favour the parallel flexure concept. The infeasibility of the cross-flexure concept highlights the importance of rule 2 in the concept generation. Lastly, the two-plane symmetry of the parallel flexure design provides multiple opportunities to enhance the design's degrees of freedom.

The adjusted designs from Fig. 14 only strengthen the choice for the parallel flexure concept. The spacing flexure could solve bulging problems while leaving the initial parallel flexure concept intact; it can be added to the existing flexures, without changing them. The only geometrical disadvantage of the spacing flexure is that it constricts the maximum width of the grasping rod. The design of the cross-flexure, however, needs to change significantly to become symmetric, and these changes would amplify the concept's weaknesses. The adjusted design has two more flexures in the same yz-plane as the other flexures; the simplest design needs two clearances, but the adjusted design needs four. With a thickness of 0.3 mm, as used in the figures in Fig. 14, the resulting flexures have become leaf flexures in the wrong direction, and their width fails the minimum wall thickness.

6 Planar bending designs

6.1 Conceptual designs

6.1.1 Concept I – Concentrated planar bending

The working principles concept is already very similar to Category I from Fig. 6; with relatively short bending flexures, the bending mechanism resembles a single joint, with a bending radius that is smaller than the device's diameter. A 3D hand sketch of the concept can be seen in Fig. 15a. The shaft of the Category I design needs only two bending push-pull rods.

Compared to existing neuroendoscopic devices, this design only adds a single DOF. However, the ability to bend the tip highly increases the device's functionality. The bending mechanism makes it possible to manipulate tissue that

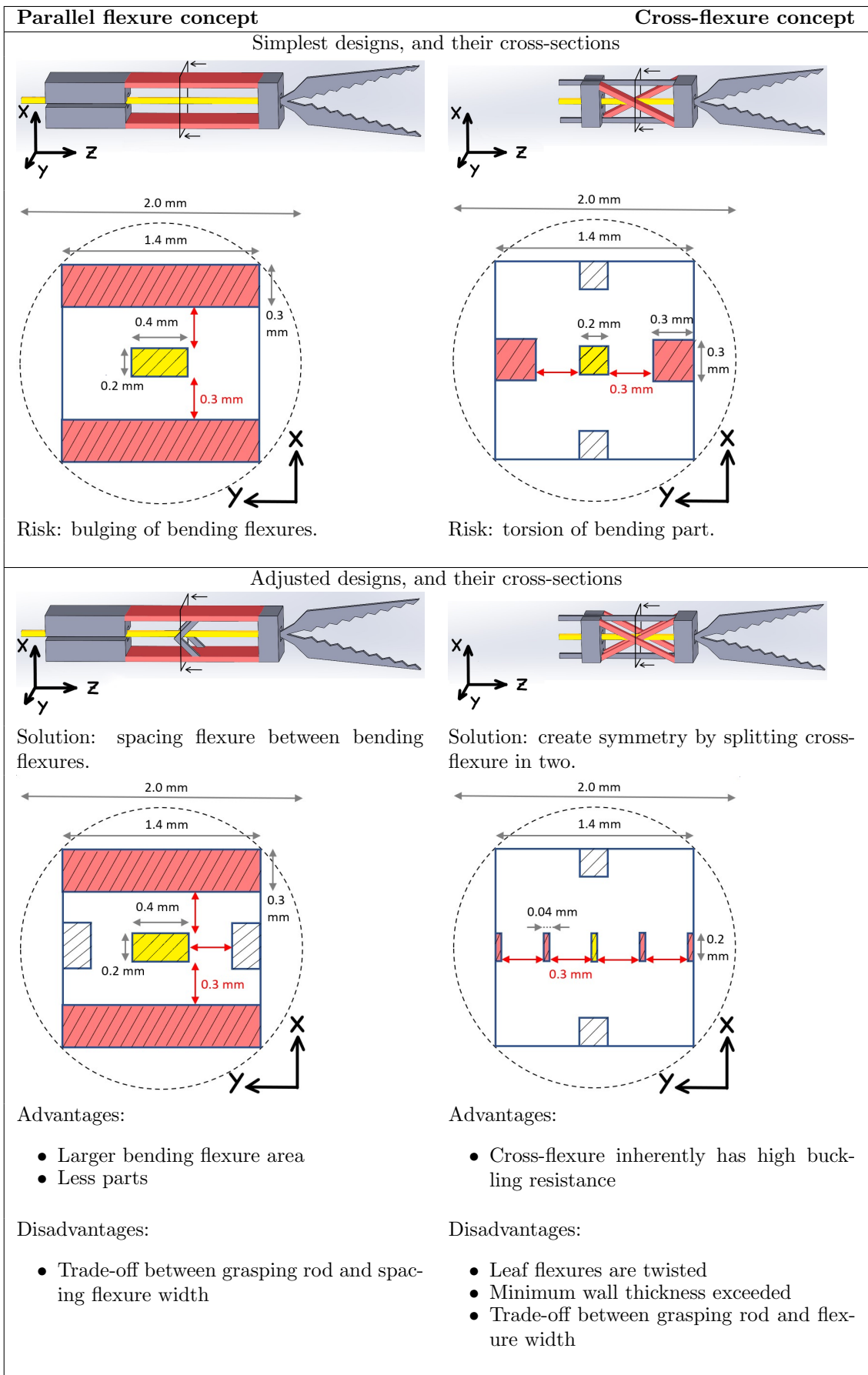


Figure 14: Concept comparison.

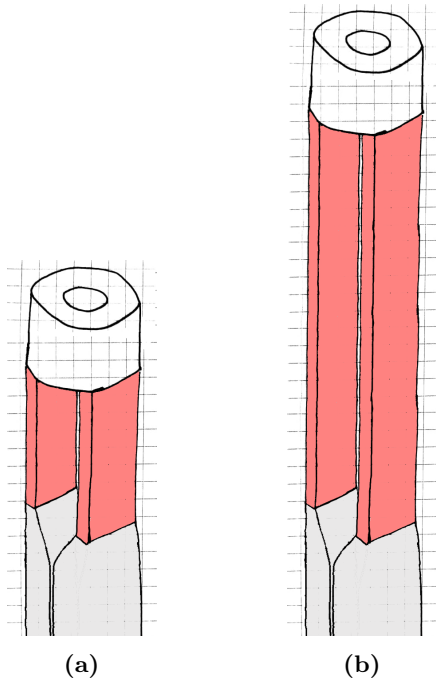


Figure 15: Conceptual planar bending designs. a) concentrated bending. b) distributed bending.

is not directly in line with the trocar. Furthermore, different approach angles can be used with the same instrument.

In theory, the concept can be adjusted to have a single fixed rotation axis and a bending radius of zero. It is a closer resemblance of the Cans in series model from Fig. 6, but the advantage of a slightly smaller bending radius does not outweigh the added complexity. An example of such design is included in Appendix D.

6.1.2 Concept II – Distributed planar bending

The simplest way to achieve distributed bending is to extend the bending flexures of the Category I design, as is shown in Fig. 15b. The bending mechanism works the same, but has a larger bending radius. The longer flexures come with a lower bending stiffness and the larger radius results in lower internal stresses. However, the device’s resistance to external forces will decrease. Theoretically, the bending radius and flexure length can be increased as long as the bending flexures maintain enough stiffness to support and move the tip. Instruments with different bending radii could be used to reach behind obstacles of different sizes, or move through different curves in the ventricular system.

The bending radius target for this category is 12 mm, i.e. six times the device’s diameter, to distribute the bending. Since the Category

II design is a longer version of the Category I design, the two share the same cross-sections. The shaft is exactly the same, and bending of the two concepts is actuated by moving the two bending rods in opposite directions.

Another concept could be made that more closely represents the Cans in series model from Fig. 6; distributed bending can be achieved by concatenating multiple copies of the parallel flexure bending mechanism, as is shown in Appendix D. Despite its higher level of bending control, we did not proceed with this design due to its higher complexity.

6.2 Bending flexure design

6.2.1 Cross-section geometry

The 2 mm tip diameter severely limits its stiffness and resistance to disturbances. High stiffness of the tip is therefore a priority in choosing the geometries in the tip mechanism. The stiffness is co-determined by the cross-sectional area of the bending flexures and their distance apart.

To determine the thickness of the bending flexures, we will start from the middle of the mechanism and work outwards. A minimum wall thickness of 0.2 mm will be used for the flexible grasping rod in the middle of the cross-section. Around the flexible grasping rod needs to be 0.3 mm of clearance on all sides (see Fig. 24a).

6.2.2 Bending flexure length: stiffness approach

To determine the bending flexure length and profile, and thus the stiffness of the bending mechanism, we need to have a thorough understanding of its workings. What makes the mechanism bend, and what forces are required to do so? Let us start with looking at the Free Body Diagram (FBD) of the general solution in Fig. 16a. The equal and opposite input forces are shown in green, the resultant lateral forces in yellow, and the resultant moments in purple. The system cannot be solved, since there are four equations ($\sum F_x = 0$, $\sum F_z = 0$, $\sum M_A = 0$, $\sum M_C = 0$), and six unknowns ($F_{A,x}$, $F_{C,x}$, $F_{A,z}$, $F_{C,z}$, M_A , M_C). The FBD’s in Fig. 16b and Fig. 16c could be solved, if we know the relation between the loads and the deformations.

Suppose we start from the bending mechanism’s neutral position: the bending flexures are straight and parallel, and there are no internal stresses. To start the bending, one flexure must be pulled downwards, and the other pushed upwards, while the bases of the flexures remain

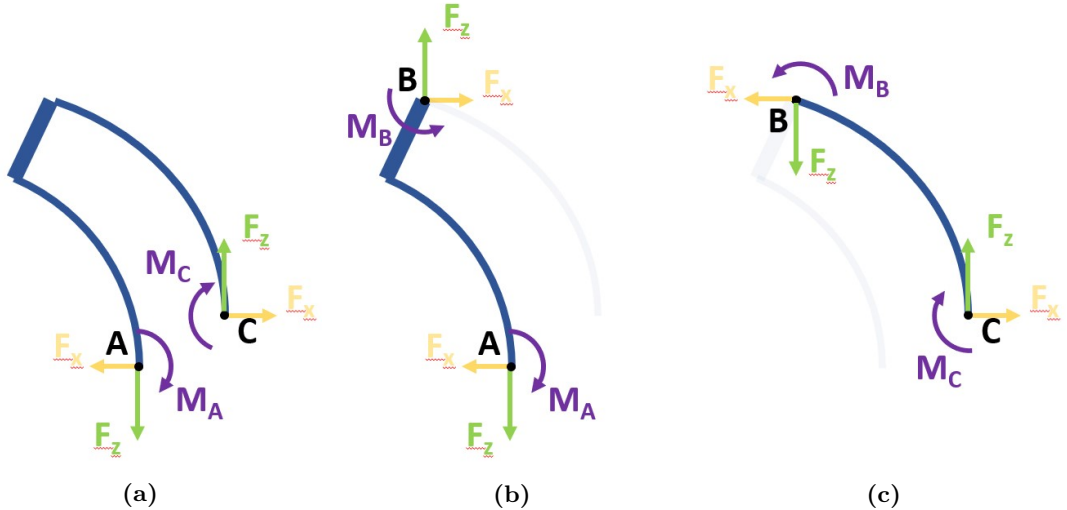


Figure 16: Free Body Diagrams of bending mechanism during bending. a) complete bending mechanism. b) left flexure and rigid grasper bearing. c) right flexure.

parallel. This will result in compression in one flexure, and tension in the other flexure. With the help of a small moment, due to the offset between the flexures, the compressed flexure will start to buckle. This type of buckling where the loads are not in line with the beams is called eccentric buckling [84]. Unlike classical buckling where the buckling happens instantaneously when the critical load is reached, eccentric buckling starts with any load. The eccentricity of the loads determines the bending direction, and when the load is increased, the buckling deformation increases. Both are crucial to control the bending mechanism.

Unfortunately, we cannot calculate the relation between force input and bending deformation. Buckling problems cannot be solved with classical beam theory, since it has a non-linear nature. Methods to solve the buckling differential equations exist, but we cannot use them for two reasons: first, the existing methods assume small deformations, whereas we need large deformations to achieve bending. Second, in our problem, the loads on the flexures change significantly during bending, and how they change depends on how the flexure buckles.

6.2.3 Bending flexure length: deformation approach

Since we cannot calculate the exact needed geometry of the bending flexures, we need to logically reason towards it. A trade-off can be made between a short bending mechanism with high flexure strains, and a longer bending mechanism which is less stiff. Our second approach to determine the flexure length, is to find the shortest possible length that does not break due to large

strains. A rough calculation can be made, using Eq. (1) to calculate arc lengths. In this calculation we assume perfect circular bending and the maximum strains on the surfaces of the inner bending flexure, which makes the shortest curve. θ is the bending angle, and r the bending radius at the neutral bending axis.

$$l = \frac{\theta\pi r}{180} \quad (1)$$

The maximum strain ϵ can be found by dividing the difference between the flexure surface arc length and initial length by the initial length. The initial length l_0 is equal to the neutral bending axis length during bending. Due to the flexure's symmetrical cross-section, the distance between the flexure's neutral bending axis and the maximum strain at the surface is half the flexure thickness, or $t/2$, leading to the arc length l_{max} in Eq. (2). Maximum strain ϵ is then given by Eq. (3).

$$l_{max} = \frac{\theta\pi(r+t/2)}{180} = l_0 + \frac{\theta\pi t/2}{180} \quad (2)$$

$$\epsilon = \frac{l_0 + \frac{\theta\pi t/2}{180} - l_0}{l_0} = \frac{\pi\theta t}{360l_0} \quad (3)$$

Formlabs Tough and Durable resins yield at a strain of 5% [57, 85]. When we set Eq. (3) equal to 5% and insert the right flexure thickness, the initial length l_0 can be calculated at which the flexure starts to yield when bent 60° . We apply a safety factor of 1.5 because the material data and calculation are rough.

6.2.4 Leaf flexure geometry

Using the method described above, we can finalise the geometry and dimensions of the Cat-

egory I and II designs. To maximise the cross-sectional area of the bending flexures, they will lie within a square, as can be seen in Fig. 18a. The largest square that fits within a 2 mm diameter circle has sides of $\sqrt{2} \approx 1.41$ mm. With a 0.2 mm flexible grasping rod, this leaves approximately 0.3 mm for each bending flexure. If the stiffness is still not sufficient, (part of) the grey areas in Fig. 18a could be added, at the cost of a non-rectangular leaf flexure. We have chosen to only include the grey parts on the sides of the flexures; adding these parts contributes to the stiffness while maintaining the leaf flexure shape with one preferred bending plane. The rounded edges make it easier to fit the tip through the round trocar.

Substituting flexure thickness $t = 0.3$ mm and bending angle $\theta = 60^\circ$ in Eq. (3), and solving for l_0 , results in a flexure length of roughly 4.5 mm, including the 1.5 safety factor. The bending radius can then be calculated with Eq. (1) and is 4.3 mm. This bending radius is below the 6 mm maximum bending radius from the design criteria. The bending radius of the Category II design can be freely chosen by altering the bending flexure length. With bending flexures of 11.25 mm, we opt for a bending radius of 10 mm.

6.3 Grasper design

6.3.1 Grasper principles

The grasper jaw surface will be copied from existing neurosurgical forceps and lies beyond the scope of this project. All categories have the same grasper. The jaws are shaped like half cones. When the grasper is closed, the widest parts of the two semicircular cross-sections form a circle that precisely fits through the endoscopic trocar and has a maximum cross-sectional area.

The closing mechanism will be adopted from existing grasper mechanisms used in other MIS disciplines like eye surgery. It consists of flexible jaw stems that are pulled through a rigid bearing. Figure 17 shows a cross-section of the grasper and its bearing. The shape of the grasper stems serves as a wedge that pushes against the bearing. The resulting wedge effect produces a force amplification; with a relatively low tension on the grasping rod a high grasping force can be achieved.

On the other hand, the wedge effect influences the required pulling motion; it ensures an inverse relation between grasping input displacement and closing force. If the required displacement is too large, the grasper tips retract and the complete device must be pushed forward to grasp something. The retraction effect is partly

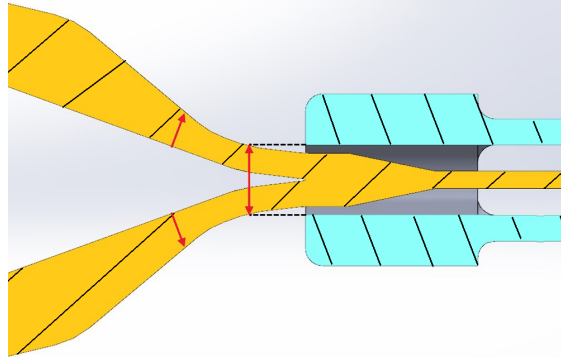


Figure 17: Close-up of grasper bearing, with the jaws in orange and the bearing in blue. When the long arrow reaches the bearing, closing of the grasper starts, and when the short arrows reach the bearing, the grasper is fully closed.

compensated for by the rotation of the jaw tips. To avoid it, the flexible jaw stems must be kept short, to minimise the retraction.

6.3.2 Grasping bearing

The grasping bearing is the stiff structure that makes sure the jaws close when pulled through it. To maximise the stiffness of the jaw stems, the inner bearing diameter will be as large as possible, i.e. spanning the full distance between the bending flexures. To maximise the stiffness of the bearing itself, it has the maximum outer diameter of 2 mm.

During printing, the grasper will be further extended from the grasping bearing, to meet the minimum clearance between the two. This means that the first bit of grasping trigger travel in the handle does not close the grasper yet.

6.3.3 Flexible grasping rod

The flexible part of the grasping rod runs along the central bending line of the bending mechanism, which means it will maintain a constant length during tip bending. To minimise the contribution to the bending stiffness, the flexible part will have the minimum wall thickness of 0.2 mm, as shown in Fig. 24a.

Since there is a clearance between the bending flexures and the flexible grasping rod, the grasping rod will tend to follow the shortest path during bending. This will be prevented by adding spacers to the bending flexures that push the grasping rod towards the central bending line. By keeping the spacers thin and narrow, they will minimally increase the bending stiffness, and chances of fusing together with the grasping rod are low, similar to the marks and

dents by Song and Chen [62]. Another method to make sure the end of the grasping rod is parallel to the tip, is to increase the length of the rigid bearing.

6.4 Shaft design

6.4.1 Shaft functions

The shaft consists of all structures between the handle and the tip of the device, i.e. two push-pull rods to actuate the bending of the tip, and one pull rod to close the grasper. During surgery the majority of the shaft is inside the endoscopic trocar, which provides a stiff shell. The parts that extend from the trocar on either side must be stiff enough on themselves. Similar to the tip, the shaft has a maximum diameter of 2 mm to fit through the 2.2 mm working channel. It must have a total length of 265 mm.

During pulling of the grasping pull-rod, the bending rods must stay in place. Vice versa, during motion of the bending push-pull rods, the grasper pull-rod must not be moved. The bending push-pull rods make an equal and opposite sliding motion. Buckling of rods in the shaft can lead to jamming, which must be prevented.

6.4.2 Shaft cross-section

The shaft will consist only of actuation rods. An extra shell to provide stiffness at the two shaft sections extending from the trocar has more disadvantage than advantages; it would take up space and it would need extra clearance between the shell and the rods, with a counteractive effect on the stiffness of the rods. Furthermore, it would complicate the printing process, for it takes away direct access to the rods and needs drainage holes. Since the grasping rod is only used in tension, it has no risk of buckling and can have a smaller cross-sectional area than the bending push-pull rods.

The simplest way to connect the rods to the bending mechanism is by placing the grasping rod in the middle, with bending rods equally spaced out around it. The diameter of the grasping rod will be 0.6 mm, which means it needs print supports roughly every 15 mm [64]. The bending push-pull rods surround the grasping rod as can be seen in Fig. 18b. With the minimum clearance of 0.3 mm, this configuration results in bending push-pull rods of 0.4 mm thick.

Due to the long rods in the shaft, there is a risk that the grasping rod gets jammed between the bending rods when one of the bending rods is pushed. The clearance between the grasping rod and the bending rods must be high enough so that the bending rods always collide with each

other first before jamming the grasping rod. In other words, when clamped together, there must still be enough clearance on the inside of the bending rods for the grasping rod to move.

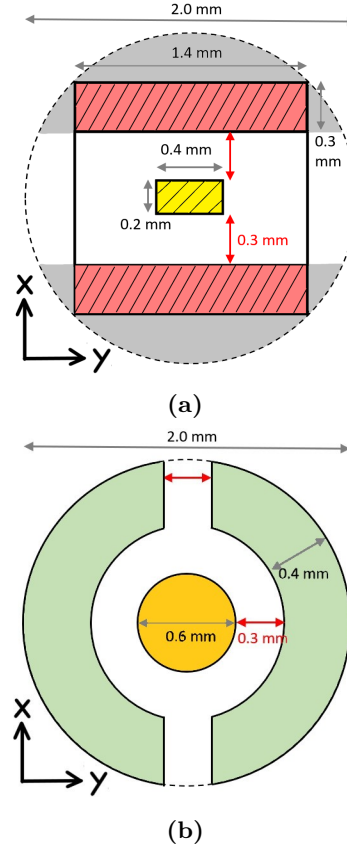


Figure 18: Initial planar bending design cross-sections. a) bending mechanism cross-section, with bending flexures in pink, grasping rod in yellow, potential expansion of bending flexures in grey, minimum clearance in red. b) shaft cross-section, with bending rods in green and grasping rod in orange.

6.4.3 Printing rods further apart

Despite only holding few parts, a significant portion of the shaft is lost to clearance between rods. To minimise the area loss, the rods can be designed with tight tolerances, but printed further apart. This is visualised in Fig. 19e. This printing configuration is possible if the bending flexures are slightly bend outwards at their very ends. An added benefit is that there is enough space for support structures. When the part is printed and support structures are removed, the rods are pushed together when inserted in a trocar to achieve a tight 0.1 mm clearance. The cross-sectional area of the bending rods has now increased more than 50%, and chances of jamming due to buckling are further reduced.

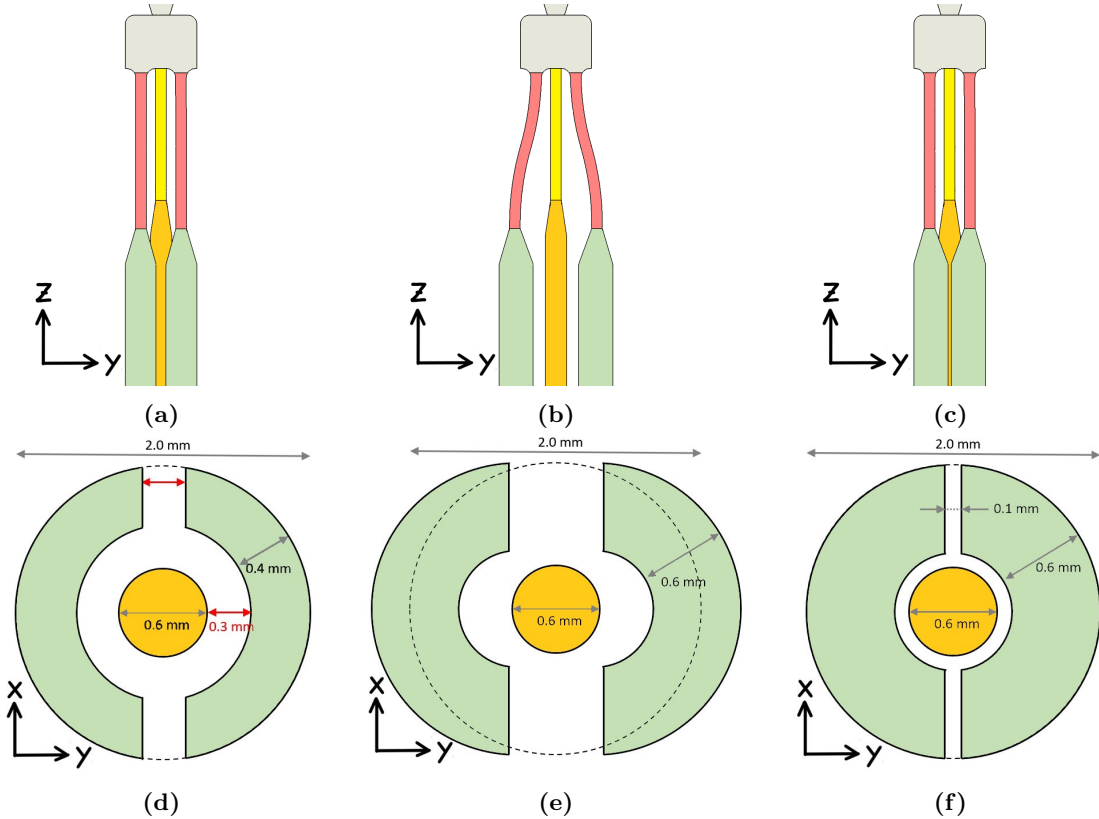


Figure 19: Three different designs to show how printing rods further apart can decrease clearances. Bending rods in green, grasping rod in orange, bending flexures in pink, and flexible grasping rod in yellow. a,d) design with minimum clearances of 0.3 mm. b,e) printing rods further apart. c,f) same design, after insertion in trocar, with clearances of 0.1 mm.

Detailed SolidWorks models of the tip designs are shown in Figs. 26a and 26b.

6.5 Prototyping

6.5.1 Prototype designs

Prototypes were made to validate that the designs also work in reality and to locate any existing design problems. We used a 1:2.5 scale for the prototypes to simplify fabrication and reduce measurement errors, resulting in 5 mm diameter devices. The prototypes were 3D printed on a Form 3B printer.

All dimensions in the tip are scaled by a factor 2.5, except the 0.3 mm clearances. Scaling all dimensions with the same factor results in a stiffer bending mechanism, but it gives the most insight in bending behaviour and plastic deformations. Scaling the bending flexures differently to maintain the bending stiffness would have an unknown effect on the bending characteristics, as explained in Section 6.2.2. The clearances were left unchanged because the ability to successfully print with 0.3 mm clearances is crucial for the 2 mm design to work.

Apart from the larger scale, the prototypes

differ from the real designs in two ways to be suitable for testing: the prototypes have no handle, and the shaft is only 50 mm long. Both differences make sure that the test results can be fully attributed to the device tip, without interference from the handle and long shaft. Instead of the handle, square blocks with holes were added at the end of the actuation rods. These blocks will be used to actuate the prototypes during testing.

6.5.2 Print orientation

Initially, the prototypes were printed upright, as can be seen in Fig. 20a. In this orientation overhangs are minimised and the prototypes almost completely support themselves. Only the grasper jaws and bottom of the prints have additional support structures. More importantly, there are no supports on surfaces that need to slide through the trocar or relative to each other. With this orientation the rods and flexures are built from many layers and printing could take up to 25 hours. Since the Form 3B prints with isotropic properties, this multi-layered orientation should not affect the prototypes' mechanical properties.

During fabrication the first the print results in the upright orientation were not satisfactory; the flexures came out irregular and warped, and the rods melted together. Despite adding extra supports and printing with different settings and materials, the problem persisted. Results were slightly better when the distance between the bending rods was increased, but still unacceptable. Eventually, printing the prototypes in a flat orientation solved our problem, at the cost of many supports. Printing with more supports increases the post-processing time, especially when the supports touch sliding surfaces, which was unavoidable.

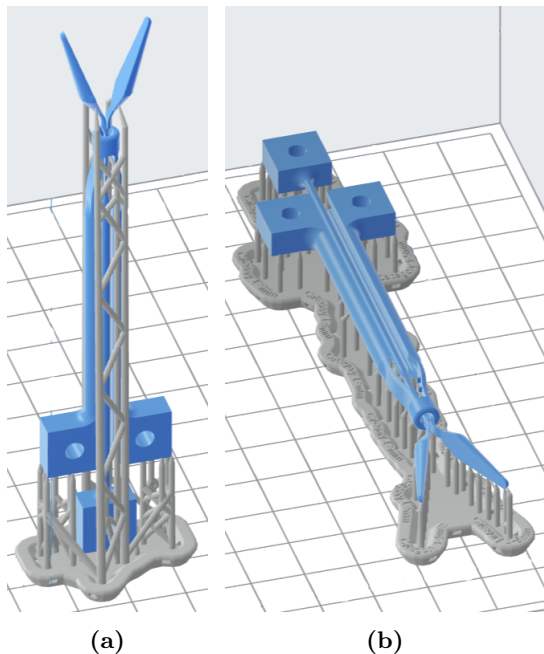


Figure 20: Sliced 5 mm Category I prototype in PreForm software, with support structures in grey. a) initial upright orientation. b) adjusted flat orientation.

6.5.3 Design iterations

During the prototyping phase we printed several iterations of the designs before getting satisfactory results. Apart from the changed print orientation, the following adjustments have been made to the prototypes:

- Increased width between rods to prevent melting together.
- A slightly elliptical grasper bearing to prevent jamming.
- Curved grasper stems.

The last two adjustments were necessary since the printed grasper successfully closed, but did

not automatically open again when the tension in the grasping rod was released; the grasper was jammed in the grasper bearing. With an elliptically—instead of perfectly round—grasper bearing, there is no more contact between the sides of the grasper and the grasper bearing during closing, reducing unnecessary friction. The curved grasper stems make sure that the force that the grasper bearing puts on the grasper stems during closing is in the same direction during the complete opening and closing motion. A similar curve in the grasper bearing opening makes sure the force always has a component that pushes the grasper out of the bearing, instead of just closing it.

6.5.4 Print settings

The final prototypes were printed using Tough 1500 resin and a 0.05 mm layer height. The default PreForm settings were used, except for the internal supports which were turned 'off'. To minimise the risk of rough sliding surfaces, all supports were manually placed and the touch-point size was lowered from 0.5 mm to 0.1–0.4 mm, depending on the support location. Printing both prototypes took less than 6 hours. Figure 21 shows a photo of the prototypes after printing.

After printing, the prototypes were cleaned in a Form Wash machine with isopropyl alcohol (IPA), and cured for 60 minutes at 70 °C in a Form Cure machine. The supports were manually removed using pliers and a hobby knife.

7 Experimental validation of planar bending designs

7.1 Experiments

7.1.1 Test setup

To validate whether the prototypes meet the set requirements, we conducted multiple experiments. The goals of these experiments, corresponding to the geometrical requirements, are to: 1) validate whether the prototypes can reach a 60° bending angle; 2) find the bending radii at 60° bending; 3) validate whether a 40° opening angle can be reached; 4) manually measure the diameters; 5) manually measure the shaft length; 6) evaluate the stiffness in different directions.

We designed and fabricated a test setup to adequately fixate the prototypes during the experiments, which can be seen in Fig. 22. The test setup consists of a fixture that can independently fixate the actuation rods of the pro-

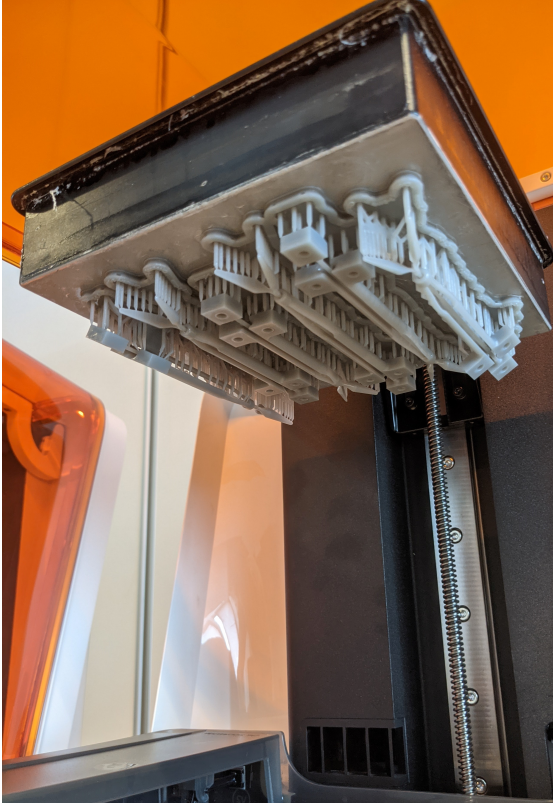


Figure 21: Six printed prototypes (two of each for Category I-III), still attached to the build plate.

prototypes, a 20 mm long dummy trocar, slots to operate the prototypes, and a phone holder to create a fixed point of view. A 5 mm black and white grid was placed directly below the prototypes to apply the correct scaling to the recordings. We applied small dots on all prototypes to precisely measure their deformations. The dots were tracked by manually clicking their position on individual video frames, with the help of the Matlab scripts in Appendix F and F. The results were then further processed and combined with the Matlab script in Appendix F.

Since the prototypes are 2.5 times larger than the detailed designs, some of the requirements must be scaled. Table 3 shows the original requirements as well as the scaled requirements. The bending angle, opening angle, and shaft length are unchanged. The maximum bending radius and diameter are scaled up by a factor of 2.5. The scaling of the maximum unwanted tip deflection can be found with Eq. (4), giving the deflection δ of a cantilever beam, where F is the force, E the Young's modulus and I the area moment of inertia [86].

$$\delta = \frac{Fl^3}{3EI}, \quad \text{with } I = \frac{1}{12}wd^3 - \frac{1}{12}w(d-2t)^3 \quad (4)$$

In our case, l is the length of the bending flexures, w and d the width and depth of the bending part, and t the flexure thickness. I is found by taking the area moment of inertia of the complete bending mechanism, minus that of the empty space between the bending flexures. Since l , w , d and t are all scaled with 2.5 and F and E remain the same, the deflection will be $1/2.5 = 0.4$ as high. That means that our maximum unwanted tip deflection of 1 mm in the embodiment designs corresponds to a deflection of 0.4 mm in the prototypes. In this calculation we assumed that the stiffness characteristics of the bending mechanism scale similarly in both straight and bent orientations, since we use the area moment of inertia of the straight mechanism.

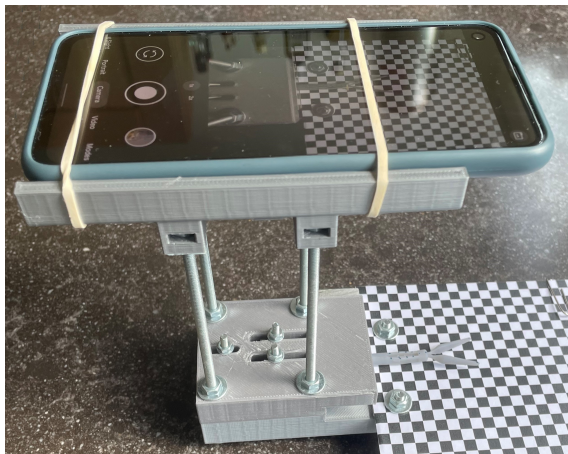
7.1.2 Bending test

The bending radius and angle can be found with the bending experiment. In this experiment the prototypes are filmed during a single bending cycle. During the experiment one bending rod is locked, with 10 mm sticking out of the trocar. The grasping rod is also locked. Then, the prototype is slowly bent to 60° , parallel to the black and white grid, and back. This cycle is repeated five more times, alternating between bending left and right. Figure 22c shows prototype I before and during bending, along with the applied forces (in orange), and the measured bending metrics; the bending angle is found by the blue line parallel to the grasping bearing. The bending radius is found by the red circle which is tangent to the blue line and the centre of the prototype where it starts to bend.

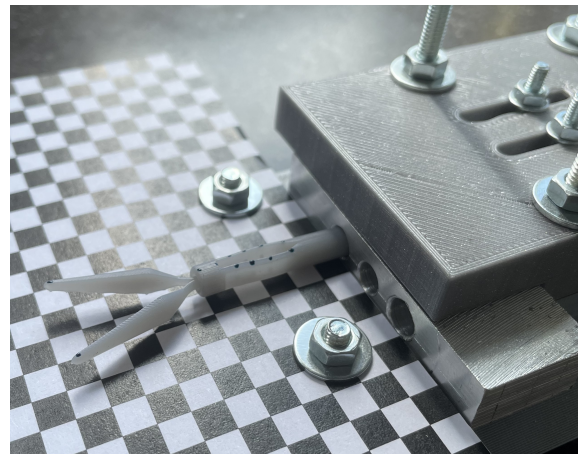
7.1.3 Stiffness test

According to criterion 1.6 from Table 3, the prototypes should have no unwanted tip deflections greater than 0.4 mm. Since the stiffness of the prototypes is different in different directions and orientations, this experiment is performed with three different prototype orientations: straight, bent, and with a closed grasper, as can be seen in Figs. 22d to 22f. In the first two orientations the force is applied at the grasper bearing, and in the last orientation the force is applied at the tip of the grasper, to simulate tissue grasping. In all three experiments we used small weights attached to a steel wire to put a 0.68 N force on the prototypes in their bending directions. The deflection, caused by the weights and measured at the force's point of application, was recorded by the phone's camera. As a final check, we also put the force perpendicular to the black and white grid. We expect the prototypes to be stiffer in

Test setup

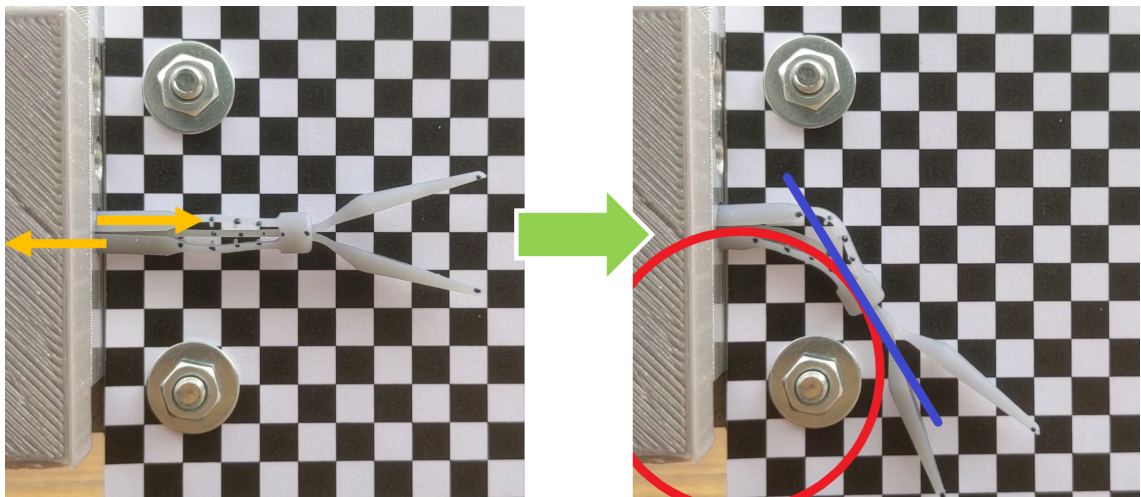


(a)



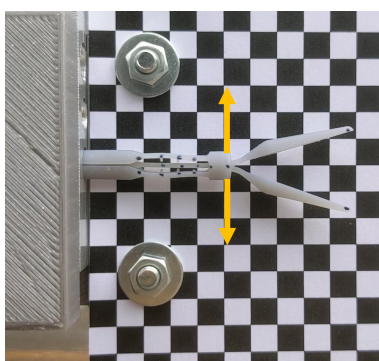
(b)

Bending experiment

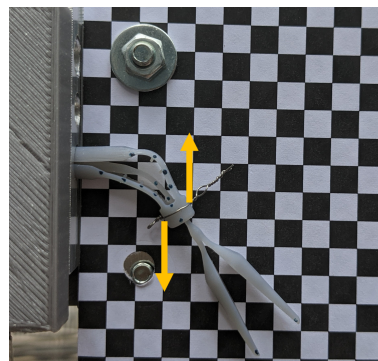


(c)

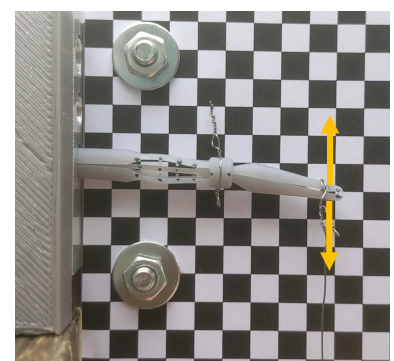
Stiffness experiments



(d)



(e)



(f)

Figure 22: a-b) photos of test setup, including prototype I. c) Bending experiment. The prototype on the left will bend like the prototype on the right due to the forces shown in orange. The blue line indicates the bending angle, and the red circle indicates the bending radius. d-f) Stiffness experiments. Straight, bent, and with a closed grasper, respectively. The orange arrows indicate where the 0.68 N force is applied (only one at a time).

Table 3: Overview of scaled design criteria for 5 mm prototypes**1 - Geometrical requirements**

Criterion		2 mm target	5 mm target
1.1 - Bending angle between shaft and tip		-60°-60°	-60°-60°
1.2 - Bending radius	conc.:	< 6 mm	< 15 mm
	dist.:	12 mm	30 mm
1.3 - Forceps opening angle		0°-40°	0°-40°
1.4 - Maximum diameter		2 mm	5 mm
1.5 - Shaft length		265 mm	265 mm
1.6 - Maximum unwanted tip deflection		< 1 mm	< 0.4 mm

this direction, so we took a single measurement for each prototype to verify whether the deflection in this direction is indeed lower.

7.2 Results and discussion**7.2.1 General measurements**

Criterion 1.4 is validated in two ways: first, the diameter of the prototypes is measured with a caliper, and second, the prototypes are pushed through a dummy trocar. Caliper measurements showed that the prototypes are indeed 5 mm in diameter. However, since the cross-section of the prototypes is not constant and sometimes consists of multiple parts with clearances, the second method is a better means to make sure the prototype will fit through a real trocar. Our dummy trocar has three holes of 5.2 mm, 5.4 mm, and 5.6 mm, respectively. Both prototypes fitted through the 5.2 mm hole, but only with the 5.4 mm hole they were free to move without significant friction. We expect that a real 5.2 mm trocar can be used with some lubricant, or with a slightly smaller prototype.

The 265 mm shaft length from **criterion 1.5** was abandoned in the prototype design due to the size limits of the 3D printer. We expect that if the prototypes work properly with a shorter shaft, they will also work with a 265 mm shaft.

The 0°-40° forceps opening angle from **criterion 1.3** was reached by both prototypes. We did notice that the maximum opening angle decreased to 30° after closing approximately three times. The elasticity in the device was no longer sufficient, and an extra force was needed to reach a 40° opening angle. This could be explained by hysteresis or plastic deformation in the grasper stem. Longer grasper stems could decrease the strains during closing and help to preserve elasticity.

7.2.2 Bending test results

The bending experiment showed that both prototypes easily meet **criterion 1.1**; bending angles up to 70° can be reached in both directions

Table 4: Bending radius at 60° bending – Planar bending

		Cat. I [mm]	Cat. II [mm]
Left		14.6	26.0
		14.6	27.1
		15.0	27.3
	SD	0.23	0.70
	Mean	14.77	26.76
Right		14.7	27.0
		15.3	28.3
		14.7	27.9
	SD	0.37	0.63
	Mean	14.90	27.74
	SD	0.28	0.80
	Mean	14.83	27.25

and the prototypes are still intact after running the experiments, without visual plastic deformations. This means that the bending radius measurements could be taken at the intended 60° bending angle. There were no notable differences between bending left and right, which was to be expected due to the prototypes' symmetry.

The resulting bending radii are given in Table 4, along with their mean value and standard deviation (SD). The first three values in each category correspond to bending to the left, and the second three values to the right. For Category I, the results show a mean bending radius at 60° bending of 14.83 mm, which is just below the 15 mm from **criterion 1.2**. For Category II, the 27.25 mm result is close to the aim of 30 mm.

Another interesting metric that can be extracted from the bending experiment is the input displacement needed to achieve a 60° bending angle, which is shown in Table 5. The input displacement is measured at the end of the actuated bending rod. This value is used to design the transmission ratio in the handle. A higher input/output displacement ratio can indicate more bulging, but improve precision. The mean input displacements of Category I and II,

Table 5: Input displacement at 60° bending – Planar bending

		Cat. I	Cat. II
		[mm]	[mm]
Left		5.6	5.3
		5.5	5.8
		6.0	5.7
	SD	0.27	0.26
	Mean	5.73	5.61
Right		5.1	5.2
		5.7	4.7
		5.5	4.8
	SD	0.32	0.23
	Mean	5.43	4.91
SD		0.31	0.44
Mean		5.58	5.26

5.58 mm and 5.26 mm respectively, are very similar. This similarity suggests that the bending motion of the parallel flexures is little dependent on the flexure length and is in line with Eq. (C.5), where the input displacement is also independent of flexure length.

7.2.3 Stiffness test results

The results from the stiffness experiments are shown in Table 6. Although there are large differences in deflections between the categories, the bent orientation has the lowest deflection within both categories, followed by the straight orientation. A possible explanation for this is that the bent prototypes are tensioned. The results show that the deflection in the bent direction (left) is lower than the deflection in the opposite direction, which also indicates that the tension in the prototype influences its stiffness. Ideally, all deflections would be below 0.4 mm, as defined in **criterion 1.6**, but only the results from the bent Category I prototype fulfil this.

Where the bent orientation seems stiffest, the measurements on the grasper indicate the least stiffness. This is partly expected since the grasper orientation is similar to the straight orientation, but with the applied force and measurement further away from the rigid trocar. However, the increase in deflections is so high that it cannot solely be explained by the measuring location. After examining the experiment photo’s, we concluded that the grasper can still move within the grasper bearing. In the experiment, the grasper was closed with metal wire, so the grasper stems were pushed together while there was no tension pulling the grasper into the bearing. More tension on the grasping rod, as with real grasping, could significantly improve the stiffness.

The single measurements of the upwards deflection are shown in the bottom row of Table 6. The upwards deflection is equal or lower than the mean sideways deflection for the straight and grasper orientations, as was expected. However, the upwards deflection exceeds the sideways deflection in the bent orientation. This means that in the bent orientation, the direction of minimal stiffness has changed. A possible cause is twisting of the bending flexures due to the introduced moment arm in bent orientations. Since the bent upwards deflections are still lower than the mean straight deflections, they are not critical.

7.3 Evaluation of experimental validation

The experiments gave useful results with which the designs were validated or can be improved. The prototype fixture made it possible to fixate and actuate the individual actuating rods of all prototypes and all experiments were successfully conducted. The markers on the prototype made it possible to track the prototype orientation, and the correct scaling factors could be found with the black and white grid. However, four improvements in the test setup and prototypes are possible to further increase result accuracy and consistency:

- **Add bending stop**

Since there was no precise method to know the bending angle during testing, we bent the prototypes a bit further to be sure a frame with 60° bending was captured. Extracting the bending angle from the videos, however, was error prone, so finding the right frame was difficult. A more consistent method would be to add a 60° physical bending stop to the test fixture.

- **Improve fixture tolerances**

During testing there was a bit of play when pulling the rods, caused by clearances between the prototypes and the fixture. Furthermore, the bending rods could separate slightly due to the 5.4 mm trocar, instead of 5.2 mm. Play can falsely decrease stiffness results, and introduce measurement errors. Reducing the clearances in the test setup could improve data accuracy.

- **Printed markers**

The markers on the prototypes that were used to extract the results can be improved. As of now, they were manually applied and manually clicked in Matlab. More precise results can be found by including the markers in the prototype CAD models as small dents or knobs. By printing the markers

Table 6: Deflection upon external 0.68 N force – Planar bending

		Cat. I			Cat. II		
		Straight [mm]	Bent [mm]	Grasper [mm]	Straight [mm]	Bent [mm]	Grasper [mm]
Left		1.4	0.3	5.5	9.5	2.7	20.5
		1.0	0.2	4.9	9.5	2.5	19.2
		1.1	0.2	4.9	9.1	2.4	19.1
	SD	0.20	0.06	0.38	0.25	0.18	0.78
	Mean	1.12	0.26	5.08	9.39	2.54	19.57
Right		1.5	0.4	7.0	7.9	5.6	19.0
		1.4	0.3	6.8	9.3	4.8	19.6
		1.4	0.2	7.2	8.9	5.0	19.4
	SD	0.05	0.08	0.2	0.71	0.41	0.32
	Mean	1.47	0.31	6.98	8.70	5.16	19.33
SD		0.23	0.07	1.08	0.62	1.46	0.55
Mean		1.29	0.28	6.03	9.02	3.85	19.45
Up*		1.3	0.4	5.0	2.5	6.9	9.5

they are exactly in the right place and constant between prototypes.

- **Printed attachment points**

Similar to the printed markers, the attachment points for the weights can be improved by adding small grooves to the grasper bearing and grasper tips. With these grooves the metal wire will better stay in place and the forces are always applied at the same point.

For further testing we advise to take more deformation measurements in the upwards direction. We expected this direction to be significantly stiffer than the other directions and tried to verify this with a single measurement. Since our hypothesis turned out false for the bent orientations, a minimal of three measurements could confirm the results with more certainty. Furthermore, the stiffness tests where the force was applied on the grasper could be repeated while pulling on the grasping rod, instead of closing the grasper with metal wire.

8 Spatial bending design exploration

8.1 Conceptual designs

8.1.1 Concept III – Concentrated spatial bending

Before discussing the planar designs in depth, we will explore their spatial equivalents. Even though the planar designs are not flawless yet, they showed that a non-assembly articulating neuroendoscopic forceps is realistic, affirming

that the exploration of spatial bending mechanisms is worthwhile. A hand sketch of the spatial bending designs is shown alongside the planar bending designs in Fig. 23.

The Category III design uses three parallel flexures, instead of two. The addition of a bending flexure creates a fully 3D bending mechanism; by pulling and pushing the three bending flexures different amounts, the tip can bend in all directions.

The three flexure concept could also work with four or more equally spaced flexures. Increasing the number of bending flexures mitigates the tendency towards some fixed bending axes. In theory, the number of parallel flexures can be increased infinitely, resulting in perfect homogeneous bending in all directions. We limited ourselves to using three bending flexures for two reasons. First, three is the minimal number of flexures to achieve spatial bending, making the mechanism exactly constrained; adding more flexures results in a statically indeterminate mechanism and introduces internal stresses. Second, with only three flexures, the number of rods and clearances is minimised for the degrees of freedom. Increasing the number of flexures would make the use of space less efficient; it is impossible to add flexures without losing stiffness.

Concentrated spatial bending can be achieved another way: by combining two separate 1DOF bending mechanisms with a phase shift, as shown in Appendix D. The alternative design is more complex and twice as long, without any significant advantages. Furthermore, the chosen solution in category III has fixed, intersecting bending axes, making it more intuitive.

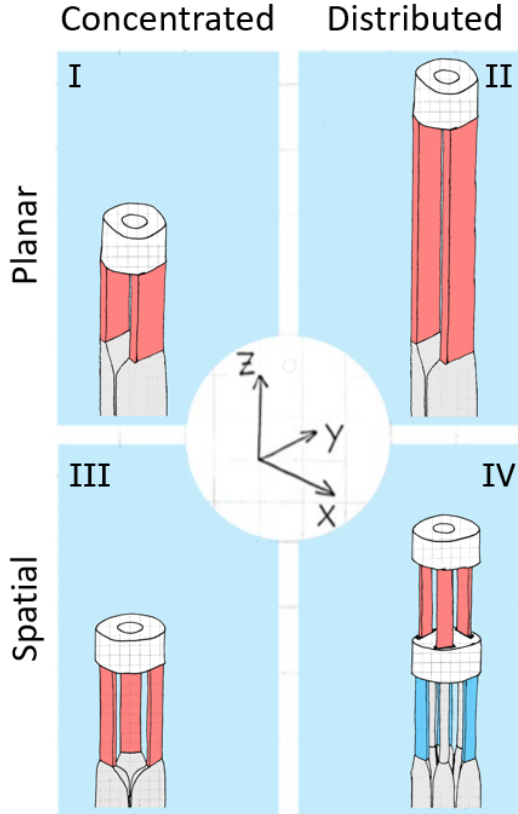


Figure 23: Overview with hand sketches of conceptual bending mechanism designs for each category, using parallel flexures.

8.1.2 Concept IV – Distributed spatial bending

The Category IV design consists of two concatenated Category III designs. The resultant mechanism can bend in 3D S-shapes, or multi-radius curves. In total, there are seven control rods in the shaft, three for each bending mechanism, and one for the grasper. The three flexible control rods of the upper (pink) mechanism run through the rigid part and along the blue flexures.

In theory, the distributed spatial bending design can be concatenated even further. Limiting factors are the material properties, since the stiffness decreases exponentially with thinner structures. Furthermore, the guiding of flexible control rods through the rigid parts can lead to high friction forces.

The cross-section of Category IV’s bending mechanism has two different versions: the top part is the same as Category III, but the bottom part is different. In the bottom part the bending flexures are shifted by 60° with respect to the top part, and there are three actuation rods in between.

The length of the bending flexures in both the top and bottom bending part is equal to that

of the Category III bending flexures. With the extra stiff part between the top and bottom, this results in a total bending part that is roughly twice the length of Category III’s bending part.

8.2 Final designs

8.2.1 Elliptical flexure dimensions

The extra flexure in Category III and IV enables bending in all directions, but to find the best flexure shape, a trade-off must be made. Flat and wide leaf flexures are less suitable for this design since they have a preferred bending direction and would need to twist during bending in other directions. Circular, or wire flexures can bend in each direction, but have a significantly smaller cross-section and thus lower stiffness. Instead, we used elliptical shapes as shown in Fig. 24b. Elliptically shaped flexures are stiffer than round flexures, but can still bend in different directions while twisting slightly.

The same methods from Section 6.2.1 and Section 6.2.3 can be applied to determine Category III and IV’s bending mechanism cross-sections. The cross-section of Category III, shown in Fig. 24b, is equal to the cross-section of the bottom part of Category IV. The top part of Category IV’s bending mechanism is shown in Fig. 24c. In these Categories a round flexible grasping rod is used to facilitate equal bending in each direction. The diameter of the flexible grasping rod is chosen equal to the thickness of the bending flexures. With the 0.3 mm clearance, that results in a thickness of 0.47 mm.

Since the flexible bending rods of Category IV (blue in Fig. 24c) would become too thin while maintaining a 0.3 mm clearance, the cross-section is shown with 0.2 mm clearances around the flexible rods. The decrease of the—already low—0.3 mm clearance will make the Category IV design infeasible with current printing techniques.

Despite the differently shaped flexures, flexure yielding will still occur at the flexure surface furthest away from the neutral bending axis, and Eq. (3) still applies. With the 1.5 safety factor, the shortest possible bending flexures for Category III and IV that do not yield are 7.3 mm long. This is longer than the flexures from Category I, due to the thicker flexures that will yield quicker.

8.2.2 Shaft design

The shaft cross-sections for the Category III and IV designs are shown in Figs. 25b and 25c, respectively. With two bending rods in the planar

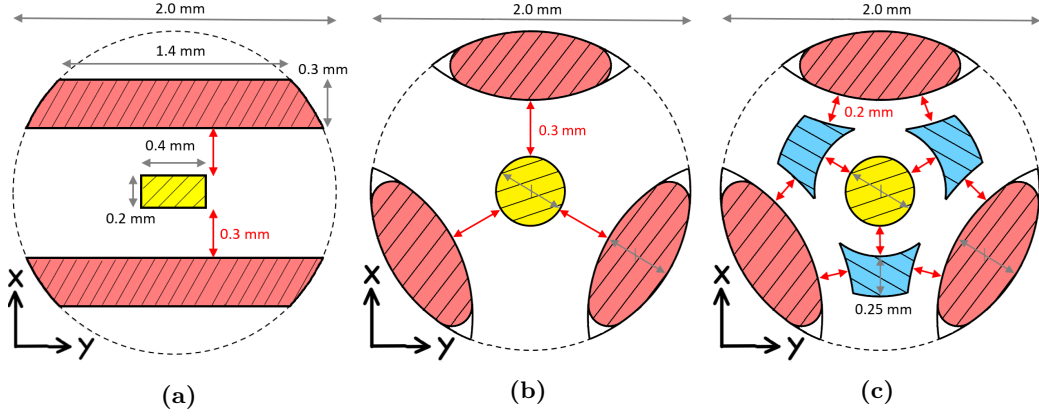


Figure 24: Cross-sections of bending mechanisms. Bending flexures in pink, (flexible part of) grasping rod in yellow, (flexible parts of) bending rods in blue, minimum clearance in red. a) Category I and II. b) Category III. c) Category IV.

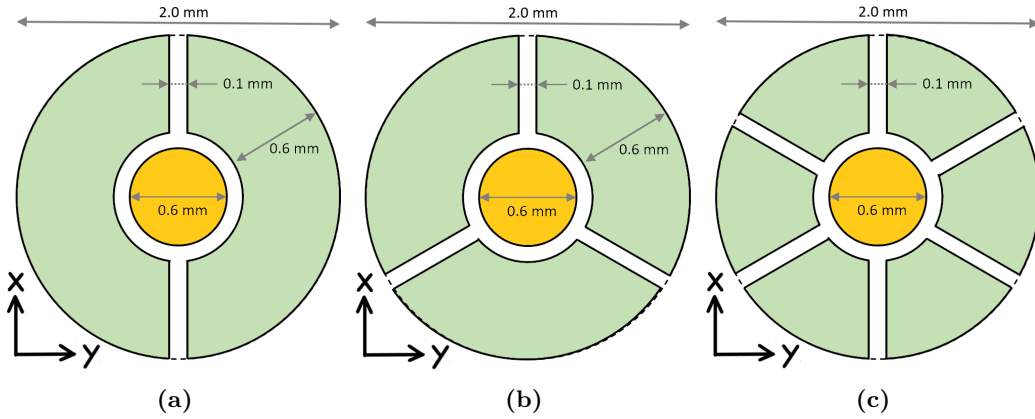


Figure 25: Shaft cross-sections. Bending rods in green and grasping rod in orange. a) Category I and II. b) Category III. c) Category IV.

designs, the grasping rod has a clearance on either side, and there is only one unit clearance between the bending rods, so the bending rods will never jam the grasping rod. With three bending rods, there is less, but still sufficient clearance for the grasping rod. With six bending rods or more, the clearance is no longer sufficient; the bending rods start to collide with the grasping rod when clamped together. This problem arises in the Category IV design, since it needs six bending push-pull rods, three for each bending mechanism layer. The risk of jamming could be reduced by increasing the clearance around the grasping rod while maintaining the clearance between the bending rods. The already thin bending rods of Category IV then need to become even thinner.

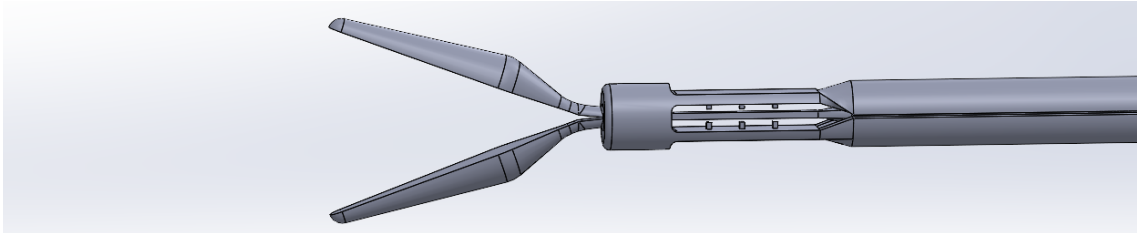
The three bending rods from Category III can be printed further apart like was done with the planar designs. The bending flexures can be printed in a S-shape, so the bending rods part with a 120° angle between. The same could be done for the six bending rods from Category IV.

However, printing the rods further apart only affects the parts below the distal bending mechanism, since the distal rods are held together by the stiff middle part. Since printability is limited by the lowest clearance and the clearances in the distal part are unchanged, printing the Category IV rods further apart is fruitless.

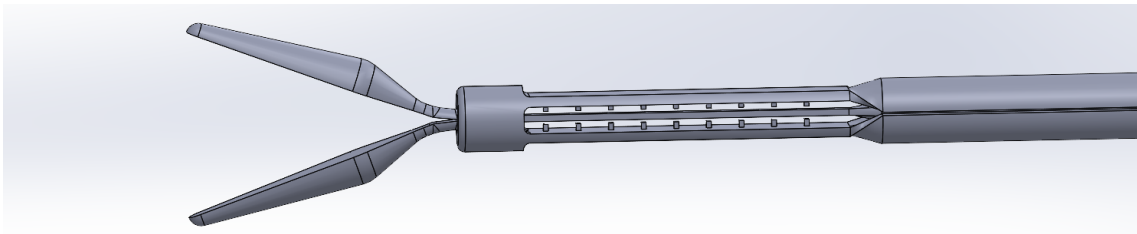
Detailed SolidWorks models of the tip designs are shown in Figs. 26c and 26d.

8.2.3 Prototyping

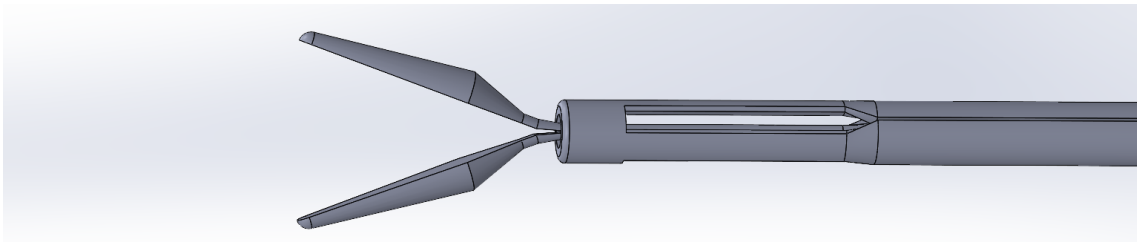
A Category III prototype was 3D printed using the same method as the Category I and II prototypes. Similar to the planar bending prototypes, 3D printing the spatial prototypes in an upright orientation was unsuccessful. A small chamfer was added to the upper located bending rod to prevent overhang in a location that cannot be reached by support structures in the flat printing orientation. No prototype was made for the Category IV design for it was deemed infeasible with current printing methods and materials, consid-



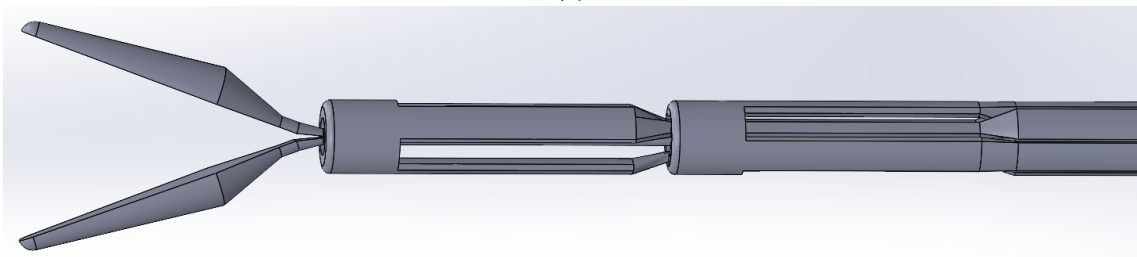
(a)



(b)



(c)



(d)

Figure 26: CAD model close-ups of the tip, made with SolidWorks. a-d) Category I, II, III and IV, respectively.

ering its 0.2 mm clearances and impossibility of printing the distal flexures further apart. Furthermore, printing the Category IV design flat would not be possible, because the many parallel rods and flexures prevent the accessibility of support structures in this orientation, as can be seen in Figs. 24c and 25c. The results from the other categories can still give insight in the potential workings of the Category IV design, as they share many of the same features.

8.3 Experimental validation of spatial bending designs

The general measurements on prototype III correspond with those on the other two prototypes; the prototype fitted through the 5.2 mm hole, but the 5.4 mm hole was used during testing. No notable differences in grasping behaviour were observed in the Category III prototype.

Bending radius and input displacement results are given in Tables 7 and 8, respectively. In these tables the previous results are repeated in a lighter colour. For Category II a larger bending radius was intended, but for Category III the flexures were elongated to prevent flexure failing, resulting in a mean radius of 25.65. The larger bending radius will make it harder to navigate through some of the small ventricles. If necessary, a 15 mm bending radius may still be reached with shorter and thinner flexures, at the cost of a lower stiffness.

The mean input displacement of 3.14 mm is significantly lower than for the planar designs. This could be explained by the smaller distance between the bending flexures—they are thicker and oriented in a triangle—and the difference in bending behaviour between the rectangular and elliptical flexures. The twisting that takes place in the elliptical flexures may help to avert bulging.

Stiffness results are given in Table 9. The measured deflections exceed the 0.4 mm requirement in all three directions. Again, the bent orientation has the lowest deflection within the category, followed by the straight orientation. The upwards deflection check of 1.0 mm is almost equal to the 0.95 mm bent orientation deflection, and thus not in the critical stiffness direction.

Mean stiffness values for each orientation in each Category are summarised in the bar graph in Fig. 27. It can be seen that the Category I design is stiffest overall, followed by the Category III design. This order corresponds with the length of each design’s bending flexures.

Table 7: Bending radius at 60° bending – Spatial bending

		Cat. I [mm]	Cat. II [mm]	Cat. III [mm]
Left		14.6	26.0	27.8
		14.6	27.1	26.2
		15.0	27.3	25.9
	SD	0.23	0.70	0.98
	Mean	14.77	26.76	26.63
Right		14.7	27.0	24.9
		15.3	28.3	23.0
		14.7	27.9	26.1
	SD	0.37	0.63	1.54
	Mean	14.90	27.74	24.66
	SD	0.28	0.80	1.58
	Mean	14.83	27.25	25.65

Table 8: Input displacement at 60° bending – Spatial bending

		Cat. I [mm]	Cat. II [mm]	Cat. III [mm]
Left		5.6	5.3	3.1
		5.5	5.8	3.0
		6.0	5.7	3.2
	SD	0.27	0.26	0.09
	Mean	5.73	5.61	3.08
Right		5.1	5.2	3.2
		5.7	4.7	3.3
		5.5	4.8	3.1
	SD	0.32	0.23	0.11
	Mean	5.43	4.91	3.20
	SD	0.31	0.44	0.11
	Mean	5.58	5.26	3.14

9 Discussion

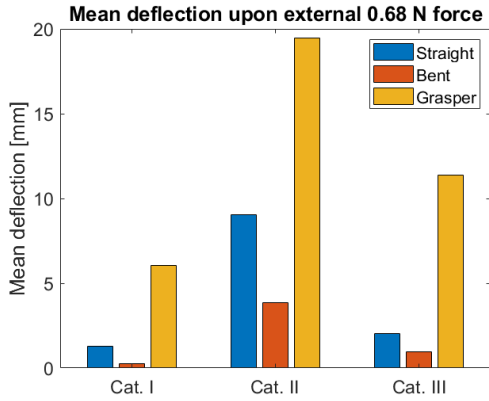
9.1 Handle design

An image of the handle can be seen in Fig. 28. Existing neuroendoscopic instruments use so-called ring handles [7, 12, 87, 88], with holes for a thumb and middle finger. Squeezing these fingers together will close the grasper. The ring for the middle finger is fixed to the shaft, and the rear ring for the thumb is attached to the shaft with a rotating link. A revolute joint near the shaft creates a lever that pulls on the grasping rod, running straight through the entire instrument. The lever must be designed in such a way that full closure of the handle corresponds to full closure of the grasper.

The grasper starts to close when the compliant jaw stems make contact with the grasping bearing, and it is fully closed when the tapered section of the jaw stems is reached. The input motion that must be generated in the handle is

Table 9: Deflection upon external 0.68 N force – Spatial bending

		Cat. I			Cat. II			Cat. III		
		Straight [mm]	Bent [mm]	Grasper [mm]	Straight [mm]	Bent [mm]	Grasper [mm]	Straight [mm]	Bent [mm]	Grasper [mm]
Left		1.4	0.3	5.5	9.5	2.7	20.5	2.4	0.9	12.1
		1.0	0.2	4.9	9.5	2.5	19.2	2.2	0.9	10.8
		1.1	0.2	4.9	9.1	2.4	19.1	2.4	0.7	11.7
	SD	0.20	0.06	0.38	0.25	0.18	0.78	0.13	0.13	0.66
	Mean	1.12	0.26	5.08	9.39	2.54	19.57	2.33	0.80	11.51
Right		1.5	0.4	7.0	7.9	5.6	19.0	2.3	1.5	10.9
		1.4	0.3	6.8	9.3	4.8	19.6	1.5	1.0	11.5
		1.4	0.2	7.2	8.9	5.0	19.4	1.4	0.8	11.3
	SD	0.05	0.08	0.2	0.71	0.41	0.32	0.47	0.39	0.33
	Mean	1.47	0.31	6.98	8.70	5.16	19.33	1.75	1.09	11.22
SD	0.23	0.07	1.08	0.62	1.46	0.55	0.44	0.31	0.49	
Mean	1.29	0.28	6.03	9.02	3.85	19.45	2.03	0.95	11.37	
Up*		1.3	0.4	5.0	2.5	6.9	9.5	1.8	1.0	10.1

**Figure 27:** Bar graph with mean deflection values from stiffness experiments. See Table 6 for full results.

0.4 mm. Since the grasper is printed further out from the grasping bearing, an extra 2.1 mm displacement of the grasping rod is needed before the grasper starts to close.

The input motion for the bending mechanism is an equal and opposite translation. The test results showed input displacements around 5.4 mm for the planar categories, and 3.1 mm for Category III, which would translate to 2.2 mm and 1.3 at true scale. To generate this motion, a mirrored version of the bending mechanism is placed in the handle, similar to the Dragon-Flex by Jelínek et al. [42]. This solution results in intuitive bending actuation without the need for rigid-body joints, which is simple to print. When the handle is rotated with respect to the shaft, the mirrored bending mechanism will move the bending rods in the shaft, and the tip will make an opposite motion. To ensure enough stiffness of the mirrored bending mech-

anism, it is 5 mm high, and 20 mm wide. Since the height is multiplied by 2.5 and the width does not influence the output displacement, the ratio between the handle angle and tip angle is 2.5:1. A similar handle can be used for spatial bending devices. By mirroring the spatial bending mechanism, the handle can also be moved spatially.

Since the needed input motions to bend the tip are so small, the motion must be amplified for accurate control. We choose to amplify the motion in the handle, since there is more space than in the tip or shaft. The part of the handle that is proximal to the mirrored bending mechanism serves as a lever arm; since bending is controlled by changing the angle in the handle, a longer proximal handle part increases control precision. With a 100 mm long handle, 60° tip bending corresponds to 24° handle bending and a 42 mm displacement of the surgeon’s hand.

Bending of the tip can be locked or unlocked on the side of the handle. As can be seen in Fig. 28, there are interlocking teeth on the touching surfaces of the bending rods. Two springs consisting of flexures, shown in grey, hold the bending rods together. The teeth make sure the bending angle is locked, unless the bending rods are pulled apart. To unlock the bending mechanism, the left and right end springs must be pushed together.

9.2 Main findings

9.2.1 Project goal

Now the designs are finished and validated, we can ask ourselves whether our solutions solve the problem described in Section 1.3. Can they contribute to the adoption of endoscopic ap-

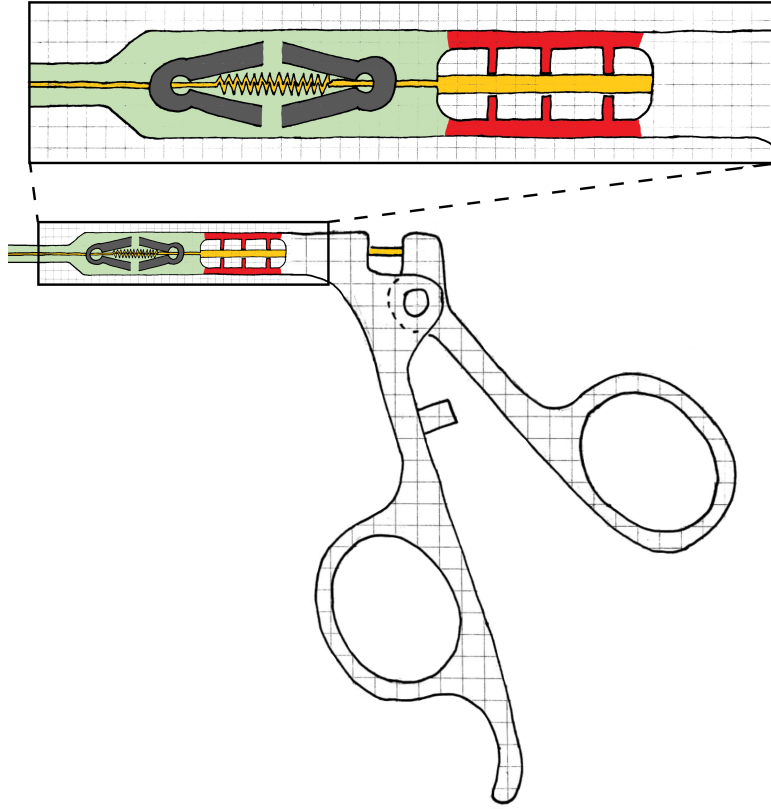


Figure 28: Schematic planar handle drawing, with the bending rods in green, the mirrored bending mechanism in red, the grasping rod in orange, and the bending lock in grey.

proaches in neurosurgery? All designs possess an increased manoeuvrability compared to traditional neuroendoscopic forceps, expanding the list of neurosurgical tasks that can be performed endoscopically. The fabrication of our designs is straightforward and relatively cheap; 3D printing omits the assembling step that made articulating 2 mm solutions infeasible with traditional manufacturing techniques. With these solutions, the step to choose for an endoscopic surgery is lowered.

The fulfilment of the design criteria is summarised in Table 10 using check-marks and cross-marks. Black marks indicate expected outcomes, and orange cross-marks indicate requirements that could be met with a relatively simple adjustment.

Reflecting on the (partly) failed geometrical requirements, the Category III design did not meet the bending radius requirement since we favoured a higher stiffness, as explained in Section 8.2.1. The maximum diameter can easily be achieved by using lubricant, or—if necessary—by slightly decreasing the width of the designs. The build plate of the Form 3B that was used to print the designs was too small for the 265 mm shaft requirement. However, a 3BL version with

identical print properties and a sufficiently large build volume is commercially available. The remaining requirement is the maximum unwanted tip deflection of less than 1 mm. The designs have much-needed articulations, but with their higher versatility comes lower stiffness, which is currently the largest downside compared to existing non-articulating instruments. The three tested prototypes failed this requirement. Results from the Category I and III designs are still in the same order as the benchmark value, but Category II showed deflections that were more than ten times too high, making the design infeasible.

The reason for the lower stiffness of the designs is twofold: the incorporation of bending mechanisms asks for more parallel parts and thus longitudinal splits, and the mechanical properties of the printed material are inferior to those of surgical stainless steel. Printing stiffer materials—even stainless steel—is possible, but accuracy and printability still lag behind [89]. It is worth noting that in brain surgery a low stiffness instrument does not always have to be a bad thing. Due to its vulnerability, brain tissue can easily be damaged by surgical instruments, and a slightly compliant device can help prevent

Table 10: Overview of design criteria fulfilment (expected outcomes in black)

	Cat. I	Cat. II	Cat. III	Cat. IV
1 - Geometrical requirements				
1.1 - Bending angle between shaft and tip	✓	✓	✓	✓
1.2 - Bending radius	✓	✓	✗	✗
1.3 - Forceps opening angle	✓	✓	✓	✓
1.4 - Maximum diameter	✗	✗	✗	✗
1.5 - Shaft length	✓	✓	✓	✓
1.6 - Maximum unwanted tip deflection	✗	✗	✗	✗
2 - Actuation requirements	designed for, but not validated			
3 - Form 3B printing limitations	complied			
4 - Wishes				
4.1 - Locking mechanism for bending	designed for, but not printed			
4.2 - Shaft rotation	unrealised			
4.3 - Tactile feedback of trocar emerging	designed for, but not printed			
4.4 - Suitable for miniaturisation	feasible			

this; most tasks require device-tissue interaction forces of less than 0.2 N [90, 91], and Payne et al. [92] even used a warning alert when the forces exceed 0.3 N.

The actuation requirements could not be validated with the performed experiments. However, they are accounted for throughout the design phase. The fabrication of our designs complied to all printing limitations imposed by the Form 3B printer. As for the wishes, the locking mechanism and tactile feedback are designed for in the handle and long shaft. Shaft rotation is not compatible with the mirrored bending mechanism in the handle, since it would take away the intuitive control. The designs have potential for miniaturisation, due to their lack of rigid body joints and low part count. Limiting factors are currently the need for 0.3 mm clearances and stiffness of printing materials, but both are expected to improve in the near future due to better printers and ongoing research of additive manufacturing.

Printing tight clearances without parts fusing together was the most challenging aspect in terms of prototype printability. To proof the designs can be manufactured with their intended dimensions, we successfully printed the prototypes again, but this time on true scale. The results can be seen in Fig. 29.

9.2.2 Expected functioning Category IV

Even though the Category IV design could not be printed and tested, the test results from the other categories can be extrapolated to gain insight in the design’s potential behaviour. First, the grasper is equal to that of the other designs. The flexible part of the grasping rod needs to make an extra bend, which can increase the friction when closing the grasper, but we expect no

new grasping problems. Furthermore, we expect similar bending radii to the Category III design, for it has the same bending flexures. The Category IV bending mechanism suffers from two impeding effects that are not present in the other designs. First, the workings of the proximal bending mechanism could be impeded by compression and tension forces that come from distal mechanism actuation. Second, the distal bending mechanism may suffer from insufficient compression stiffness of the flexible bending push-pull rods that run through the proximal mechanism.

The tested designs had a bending angle margin of at least 10° above the required 60°, but it is uncertain whether the bending margin is high enough to maintain 60° bending with these impeding effects. In terms of stiffness, the Category IV design will have an unwanted tip deflection of roughly eight times the deflection of the Category III design, since the length in Eq. (4) scales with the third power.

9.2.3 Design improvements

Several design improvements can be deduced from the test results to improve the devices’ functioning. First of all, the base of the grasper, including bearing, can be improved. In the experiments, a lot of stiffness was lost in the grasper stems; the unwanted deflections due to forces on the grasper were up to 5.5 times higher than when the force was applied on the grasper bearing. Part of the problem could be solved by pulling the grasper until it makes contact with the grasper bearing, but an adjustment to the design can also contribute to the solution. Figure 30 shows a cross-section of the prototype alongside a cross-section of an improved design. In the improved design, the thickness of the

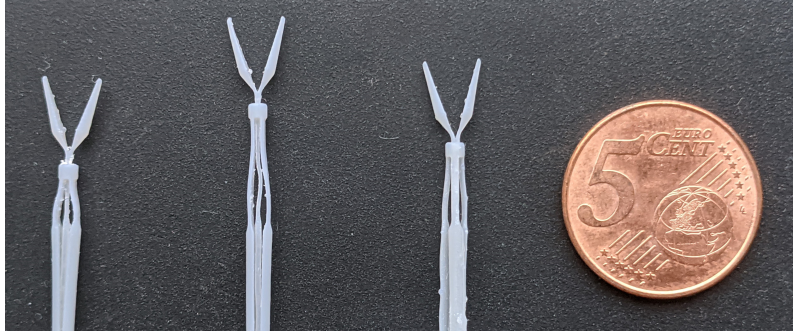


Figure 29: Photos of 2 mm 3D printed tips. From left to right: Category I, II and III.

grasper stems is doubled by increasing the diameter of the grasper bearing. To facilitate the larger diameter, the stiff bearing part was doubled in length. The radius of curvature of the grasper stems is increased by 250%, to account for the increase in thickness and the observed plastic deformation after closing three times.

From Eq. (3) and Eq. (4) follows that the bending radius of the Category III design could be reduced, while also increasing the stiffness of the straight mechanism, with thinner and shorter flexures. Doing so will also reduce the torsional stiffness of the skew flexures, and thus indirectly the bending stiffness of the bending mechanism, which mitigates the effect. To make sure the bending radius requirement is met, the new flexure length for Category III will be 4.5 mm, equal to that of Category I. Along with the 38% shortening from 7.3 mm to 4.5 mm comes a flexure thickness that is an equal factor thinner to prevent yielding, i.e. 0.29 mm. Caution is needed, however, since shorter flexures will weaken the assumptions that led to the equations. On top of that, the rotational and longitudinal stiffness will decrease with thinner flexures.

Another possible improvement in device stiffness could be achieved by using a different printing material. Tough 2000 resin, a stiffer version of the used Tough 1500, is known as a brittle material and was therefore previously dismissed. Brittle materials are not suitable for flexures, and can pose serious risks when failing inside the patient's body. However, according to the stress-strain curves from Formlabs [57], Tough 2000 has a similar yield strength to Tough 1500. Considering the observed bending margin above 60° without plastic deformations, printing with the stiffer Tough 2000 is worth trying. With a flexural modulus of 1.9 GPa, a potential 36% increase in stiffness could be achieved [85, 93].

Adding a spacing flexure to the design, as was proposed in Section 5.4.2, will be discarded. A spacing flexure primarily adds stiffness to

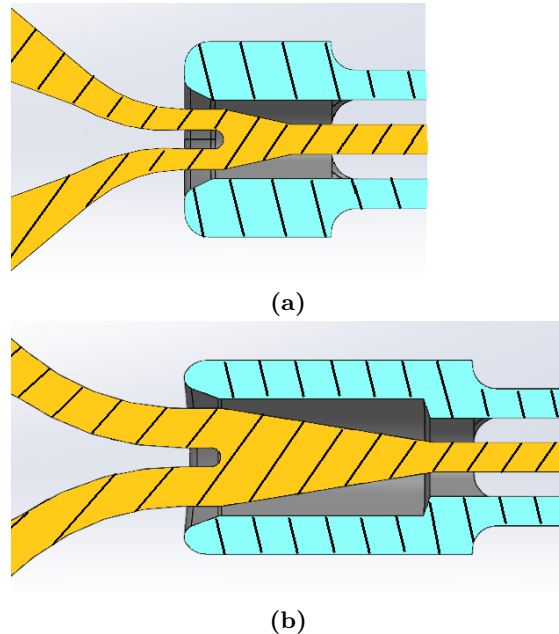


Figure 30: Grasper cross-sections, with the grasper stem in orange, and the grasper bearing in blue. a) Detailed design. b) Improved design.

the bent orientations by preventing excessive bulging, whereas the test results showed that the stiffness of the straight orientation is more critical. Furthermore, the prototypes bulged less than anticipated, and bulging did not increase significantly during stiffness testing.

9.2.4 3D printing opportunities used

In the goal of this study 3D printing is specified as a means to simplify the manufacturing of complex instruments. Since 3D printing is so different from traditional manufacturing techniques, it holds opportunities for fabricating design features that were previously infeasible. However, we did not explicitly favour 3D printing specific design features over general design features in our concept generation. In-

stead, the most promising design solutions were chosen, whether or not they could also be made with traditional manufacturing methods. This raises the question how many opportunities of 3D printing were actually used. Or, in other words, did we maximally exploit the strengths of additive manufacturing?

Even though the principle workings concept could be made with different manufacturing techniques, the implementation of the four concepts and the fine detailing are customised for 3D printing. Apart from the ability to create encapsulated structures, all opportunities from Table 1 were used. Since the devices have a maximum diameter of 2 mm, they consist of intricate features by definition. Furthermore, all parts are consolidated together with gradual transitions to prevent stress concentrations and maximise part strength. There is no need for space consuming and relatively weak joints or connections between parts. 3D printing’s ability to print complex shapes is used to improve the cross-sectional shape of the bending flexures and bending rods. The same holds for the grasper stems, which have a double curvature. Lastly, 3D printing enabled us to print the actuation rods further apart, as discussed in Section 6.4.3, despite the resulting complexly shaped bent rods.

After exploiting all these opportunities, the designs consist of only two parts—excluding the handle—that are printed in a single step. There is no need for assembling, but cleaning, curing, and support removal is required. Although cleaning and curing require very little manual labour, support removal takes approximately 20 minutes of full focus. All combined, the use of non-assembly AM led to a significantly less labour-intensive manufacturing process than would be possible with traditional manufacturing techniques.

9.3 Study limitations

9.3.1 Categorisation

The categorisation in planar or spatial and concentrated or distributed bending helped to structure the concept generation. It was not used to find optimal solutions, but to explore whether non-assembly planar and spatial instruments are possible. Four different designs were generated that each have their own bending behaviour. By exploring whether all the designs from different categories were feasible, we have been able to conclude that the Category I and III designs are feasible. However, even though our Category II and IV designs were deemed infeasible, we may not conclude that all possible designs in these

categories would be infeasible; other designs or AM techniques that do work may exist.

The four final designs arguably deviate from the four categories as specified in Section 2.2. As described before, the Category I and III designs do have a small bending radius, instead of a pure rotation joint. With the minimum flexure length of 4.5 mm to prevent yielding, the bending radius exceeded the device diameter, despite meeting the 6 mm requirement. The designs are kept as short as possible, but can no longer be called purely ‘concentrated’. The Category II design is ‘distributed’, because its bending part is elongated more than strictly necessary for it to function. The Category IV design is ‘distributed’ since the bending is split over two mechanisms in series.

In theory, Category II and IV could be further divided into ‘coupled’ and ‘decoupled’ bending motion. Our Category II design has coupled motion, just like the four existing distributed planar bending devices in Fig. 7; a single rod is used to actuate a single degree of freedom bending mechanism. Our Category IV design, however, has two decoupled bending motions; the two bending mechanisms can be independently controlled, which adds to possibility of bending in (3D) S-shapes.

Lastly, our distributed designs have a limited number of concatenated bending mechanisms, and thus degrees of freedom. In other words, distribution of bending is possible up to a certain extent. The Category IV design, which already proved infeasible as it is, has two bending layers and six degrees of freedom. To navigate through even more complex paths, extra degrees of freedom are necessary. As a comparison, the HelicoFlex by Culmone et al. [45] has ten.

9.3.2 Experimental validation

To keep the bending behaviour of the prototypes as representative as possible, all dimensions were scaled with the same factor. Scaling with a single factor ensured that the potential occurrence of plastic deformation remained unchanged. Furthermore, the prototypes visually look the same as the 2 mm designs, both in a straight orientation and during bending. Scaling up the device had an inversely proportional effect on the bending stiffness, which was accounted for in the new stiffness requirement. However, the torsion stiffness—which plays a part in the spatial bending mechanisms—scales with the inverse power of three. This means that the scaled up elliptical flexures twist less than in the original 2 mm design. Since the elliptical flexures are close to circular and twisting is not necessary to bend the mechanism, the effect will

be small.

Even when a design meets all set requirements, that does not mean it will turn into a useful surgical instrument. Our experiments did not test the dexterity and usability of the prototypes, so impeding effects may be overlooked. Three examples of potential risks are:

- **Grasper retraction**

The retraction of the grasper during closing, as discussed in Section 6.3, may complicate grasping control. There is a trade-off between retraction and closing force, induced by the wedge effect in the grasper bearing. A workable balance must be found. In instruments for posterior eye surgery, where similar graspers are used, the problem is avoided by pushing the bearing forward instead of retracting the grasper. Our bending mechanism prevents us from using this solution.

- **Bending interference**

Opening and closing the grasper could potentially interfere with the bending mechanism by tensioning it in two ways. First, when in a straight orientation, pulling the grasping rod puts a compression load on the bending flexures, which could result in a jerky bending start. With the force amplification in the grasper bearing the required pulling force is lowered, and bending mechanism tensioning is largely prevented. In addition, the bending flexures are made as stiff as possible. Second, in a bent orientation, opening or closing the grasper could change the bending angle. Again, this effect is mitigated by the relatively stiff bending flexures and the amplification of the pulling force, but it could not have been properly examined with our experiments.

- **Grasping interference**

On the other hand, bending the tip could also impede the grasping function. Since there still is a small bulging effect during bending, the inner bending flexure makes a shorter turn than the outer one. When tensioned, the flexible grasping rod will follow this short turn, which means that the tension on the grasping rod changes during bending. In the worst case, a grasped object could be released, or tissue is grasped with too much force. A potential solution to this problem could be a spring in the handle that always maintains tension on the grasping rod during grasping.

To validate whether these concerns are grounded, experiments using simulated surgical

tasks could be used. A widely used example of such a task is the transfer of rings between pegs [94]. Only when the instrument is pleasant and intuitive to use, surgeons will add it to their arsenal.

9.4 Future recommendations

Apart from the additional experiments mentioned above, we can make many recommendations to further develop the designs, ranging from small adjustments to major design reconsiderations:

- Further work out handle
The handle must be worked out in more detail.
- Multi-material printing
Aguirre and Frecker [95] 3D printed a hybrid grasper, using different materials. By optimising mechanical properties of each part, overall stiffness can be increased.
- Multi-scale printing
Li et al. [58] developed an SLA printer that can print with different accuracy within a single print. Printing time could be drastically decreased, since a large part of our device needs no high printing resolution.
- Non-linear Finite Elements Modelling
With non-linear solvers the bending behaviour can be modelled for better flexure design.
- Grasper/flexure topology optimisation
With topology optimisation, the stiffness can be optimised with minimal material.
- Force-feedback
Force feedback by static balancing like researched by Stapel and Herder [96] could benefit the surgeon's instrument awareness.
- Repeat in five years
With the rate at which new research on minimally invasive surgery and non-assembly AM is generated, it would be interesting to repeat this study in a few years' time.

10 Conclusion

The goal of exploring the design of 3D printed non-assembly articulating neuroendoscopic forceps was achieved; designs were made for four different bending categories, either planar or spatial, and concentrated or distributed. Each design has its own bending behaviour, along

with its own strengths and weaknesses. We aimed to evaluate which designs are possible with non-assembly AM, and which are not. Two of the designs were deemed feasible with the help of 5 mm prototypes. Non-assembly additive manufacturing enables the creation of these articulating instruments that were previously infeasible to produce and assemble, by using flexures instead of rigid links and cables.

The two feasible designs—both possessing concentrated bending—were successfully 3D printed on a 2 mm scale; one can bend in a plane with a single DOF, and the other can bend spatially with two DOF. Their stiffness could be increased by widening the grasper stems, adjusting the flexure geometry, and changing the printing material. Simulated surgical tasks must be performed to further assess and improve usability, but the devices prove that non-assembly additive manufacturing of 2 mm surgical manipulators, planar and spatial, is feasible.

When neurosurgeons have access to articulating instruments that fit through an endoscope, the scope of treatments that can be performed endoscopically is greatly enlarged, and many more patients could profit from the benefits of minimally invasive surgery. The ongoing advancements in both minimally invasive surgery and additive manufacturing will only increase the potential of non-assembly 3D printed surgical devices, and could change healthcare forever.

References

- [1] IMARC Group. *Minimally Invasive Surgery Market: Global Industry Trends, Share, Size, Growth, Opportunity and Forecast 2020-2025*. Tech. rep. 2020.
- [2] Jim C. Hu. “Comparative Effectiveness of Minimally Invasive vs Open Radical Prostatectomy”. In: *JAMA* 302.14 (Oct. 2009), p. 1557. DOI: 10.1001/jama.2009.1451.
- [3] V. Velanovich. “Laparoscopic vs open surgery”. In: *Surgical Endoscopy* 14.1 (Jan. 2000), pp. 16–21. DOI: 10.1007/s004649900003.
- [4] Paul Breedveld et al. “Manipulation in Laparoscopic Surgery: Overview of Impeding Effects and Supporting Aids”. In: *Journal of Laparoendoscopic & Advanced Surgical Techniques* 9.6 (Dec. 1999), pp. 469–480. DOI: 10.1089/lap.1999.9.469. URL: <https://doi.org/10.1089/lap.1999.9.469>.
- [5] Marco Braga et al. “Laparoscopic versus open colorectal surgery - A randomized trial on short-term outcome”. In: *Annals of surgery* 236 (Jan. 2003), 759–66, discussion 767. DOI: 10.1097/01.SLA.0000036269.60340.AE.
- [6] Roberto Dezena. *Endoscopic third ventriculostomy : classic concepts and a state-of-the-art guide*. Cham: Springer, 2020. ISBN: 978-3-030-28657-6.
- [7] The Aesculap Advisory Board for “Minimally Invasive Neurosurgery and Neuroendoscopy”. *Neuroendoscopy – Offering more for patients through less invasive techniques*. Brochure Aesculap, Inc. 2019. URL: <https://www.aesculapusa.com/en/healthcare-professionals/or-solutions/or-solutions-neuroendoscopy/endoscope-assisted.html>.
- [8] Henry W. S. Schroeder. “Current Status and Future Developments of Neuroendoscopically Assisted Neurosurgery”. In: *Neuroendoscopy*. Springer Berlin Heidelberg, Aug. 2014, pp. 65–80. DOI: 10.1007/978-3-642-39085-2_6.
- [9] Roberto Alexandre Dezena. *Atlas of Endoscopic Neurosurgery of the Third Ventricle*. Springer International Publishing, 2017. DOI: 10.1007/978-3-319-50068-3.
- [10] Nancy McLaughlin et al. “Endoscopic Approaches to Skull Base Lesions, Ventricular Tumors, and Cysts”. In: *Principles of Neurological Surgery*. Elsevier, 2012, pp. 681–694. DOI: 10.1016/b978-1-4377-0701-4.00044-0.
- [11] Kyu Won Shim et al. “Neuroendoscopy : Current and Future Perspectives”. In: *Journal of Korean Neurosurgical Society* 60.3 (May 2017), pp. 322–326. DOI: 10.3340/jkns.2017.0202.006.
- [12] Henry W. S. Schroeder. *The LOTTA System for Intracranial Neuroendoscopy*. Brochure KARL STORZ - Endoskope. 2017. URL: <https://stopler.nl/uploads/media/5bdc4ac0dfb26/http-www-stoplerftp-comwebsitebrochureswww-0048-brochure1-endoworld-the-lotta-system.pdf>.
- [13] BruceBlasus. *Ventricles of the Brain*. 2013. URL: https://commons.wikimedia.org/wiki/File:Blausen_0896_Ventricles_Brain.png (visited on 10/12/2021).
- [14] André Grotenhuis. “Neuroendoscopic Instruments and Surgical Technique”. In: *Neuroendoscopy*. Springer Berlin Heidelberg, Aug. 2014, pp. 81–91. DOI: 10.1007/978-3-642-39085-2_7.
- [15] Aimée Sakes et al. “Design of a Novel Three-Dimensional-Printed Two Degrees-of-Freedom Steerable Electrosurgical Grasper for Minimally Invasive Surgery”. In: *Journal of Medical Devices* 12.1 (Jan. 2018). DOI: 10.1115/1.4038561.
- [16] Paolo Cappabianca et al. “Application of neuroendoscopy to intraventricular lesions”. In: *Neurosurgery* 62.suppl.2 (Feb. 2008), SHC575–SHC598. DOI: 10.1227/01.neu.0000316262.74843.dd.
- [17] Khan W. Li et al. “Neuroendoscopy: past, present, and future”. In: *Neurosurgical Focus* 19.6 (Dec. 2005), pp. 1–5. DOI: 10.3171/foc.2005.19.6.2.
- [18] Spyros Sgouros. “Man-to-Machine Interface in Neuroendoscopy: The Importance of Human Interface in the Development of Neuroendoscopy”. In: *Neuroendoscopy*. Springer Berlin Heidelberg, Aug. 2014, pp. 213–224. DOI: 10.1007/978-3-642-39085-2_19.
- [19] Kim Eagle and Alan R. Cohen. “Endoscopic Laser Third Ventriculostomy”. In: *New England Journal of Medicine* 328.8 (Feb. 1993), pp. 552–552. DOI: 10.1056/nejm199302253280806.

- [20] S. Kota et al. “Design and Application of Compliant Mechanisms for Surgical Tools”. In: *Journal of Biomechanical Engineering* 127.6 (July 2005), pp. 981–989. DOI: 10.1115/1.2056561.
- [21] Geoffrey Chow et al. “Rigid vs articulating instrumentation for task completion in single-port surgery”. In: *The American Journal of Surgery* 211.5 (May 2016), pp. 903–907. DOI: 10.1016/j.amjsurg.2016.01.017.
- [22] Med-Tech Inovation. *The tools that go into manufacturing small surgical instruments at a high volume*. 2019. URL: <https://www.med-technews.com/news/how-to-manufacture-small-surgical-instruments-at-a-high-volu/> (visited on 06/03/2021).
- [23] unknown. *2020 Additive Manufacturing Market Outlook and Summary of Opportunities*. Tech. rep. SmarTech Markets Publishing LLC, Dec. 2019.
- [24] Costanza Culmone, Gerwin Smit, and Paul Breedveld. “Additive manufacturing of medical instruments: A state-of-the-art review”. In: *Additive Manufacturing* 27 (May 2019), pp. 461–473. DOI: 10.1016/j.addma.2019.03.015.
- [25] Geoffrey Boothroyd. “Product design for manufacture and assembly”. In: *Computer-Aided Design* 26.7 (July 1994), pp. 505–520. DOI: 10.1016/0010-4485(94)90082-5.
- [26] Julien Catherine, Christine Rotinat-Libersa, and Alain Micaelli. “Comparative review of endoscopic devices articulations technologies developed for minimally invasive medical procedures”. In: *Applied Bionics and Biomechanics* 8.2 (2011), pp. 151–171. ISSN: 1176-2322. DOI: 10.3233/ABB-2011-0018.
- [27] Andrew Lim et al. “Design and Comparison of Magnetically-Actuated Dexterous Forceps Instruments for Neuroendoscopy”. In: *IEEE Transactions on Biomedical Engineering* 68.3 (Mar. 2021), pp. 846–856. DOI: 10.1109/tbme.2020.3007581.
- [28] Fan Yu Chen. “Gripping mechanisms for industrial robots”. In: *Mechanism and Machine Theory* 17.5 (Jan. 1982), pp. 299–311. DOI: 10.1016/0094-114x(82)90011-8.
- [29] D.O.R.C. Dutch Ophthalmic Research Center. *Disposable Microforceps Ultra peel 27 gauge / 0.4mm*. <https://dorcglobal.com/product/disposable-microforceps-ultra-peel-27-gauge-04mm>. Online; accessed 25 September 2020.
- [30] J.L. Herder and F.P.A. van den Berg. “Statically balanced compliant mechanisms (SBCM’s), and example and prospects”. In: *ASME DETC 26th Biennial, Mechanisms and Robotics Conference* (Baltimore, Sept. 10–13, 2000). ASME, 2000.
- [31] Man Bok Hong and Yung-Ho Jo. “Design and Evaluation of 2-DOF Compliant Forceps With Force-Sensing Capability for Minimally Invasive Robot Surgery”. In: *IEEE Transactions on Robotics* 28.4 (Aug. 2012), pp. 932–941. DOI: 10.1109/tro.2012.2194889.
- [32] Bryce J. Edmondson et al. “Oriceps: Origami-Inspired Forceps”. In: *Volume 1: Development and Characterization of Multifunctional Materials; Modeling, Simulation and Control of Adaptive Systems; Integrated System Design and Implementation*. American Society of Mechanical Engineers, Sept. 2013. DOI: 10.1115/smasis2013-3299.
- [33] A. L. Schwab and J. P. Meijaard. “How to Draw Euler Angles and Utilize Euler Parameters”. In: *Volume 2: 30th Annual Mechanisms and Robotics Conference, Parts A and B*. ASMEDC, Jan. 2006. DOI: 10.1115/detc2006-99307.
- [34] Ali Hassan Zahraee et al. “Toward the Development of a Hand-Held Surgical Robot for Laparoscopy”. In: *IEEE/ASME Transactions on Mechatronics* (Dec. 2010). DOI: 10.1109/tmech.2010.2055577.
- [35] Garbielle J. M. Tuijthof and Tim Horeman. “Surgical device, in particular for minimally invasive surgery”. 2014. URL: <https://research.tudelft.nl/en/publications/surgical-device-in-particular-for-minimally-invasive-surgery-2>.
- [36] T. Horeman et al. “Design and Preliminary Evaluation of a Stiff Steerable Cutter for Arthroscopic Procedures”. In: *Journal of Medical Devices* 9.4 (Aug. 2015). DOI: 10.1115/1.4030506.
- [37] J. Mueglitz et al. “Kinematic problems of manipulators for minimal invasive surgery”. In: *Endosc Surg Allied Technol* (June 1993).

- [38] M. Minor and R. Mukherjee. “A dexterous manipulator for minimally invasive surgery”. In: *Proceedings 1999 IEEE International Conference on Robotics and Automation (Cat. No.99CH36288C)*. IEEE, 1999. DOI: 10.1109/robot.1999.770410.
- [39] Boyu Zhang et al. “Robotic Visible Force Manipulator With a Novel Linkage Bending Mechanism”. In: *Journal of Mechanisms and Robotics* 11.1 (Dec. 2018). DOI: 10.1115/1.4041941.
- [40] Mark Thompson et al. “Device and system for surgical dissection and or guidance of other medical devices into body”. 2007. URL: <http://v3.espacenet.com/textdoc?DB=EPODOC&IDX=EP1983904>.
- [41] Adam T. C. Steege. “Surgical tool”. 2013. URL: <https://patentscope.wipo.int/search/en/detail.jsf?docId=W02013166409>.
- [42] Filip Jelínek, Rob Pessers, and Paul Breedveld. “DragonFlex Smart Steerable Laparoscopic Instrument”. In: *Journal of Medical Devices* 8.1 (Jan. 2014). DOI: 10.1115/1.4026153.
- [43] Sem F. Hardon et al. “A new modular mechanism that allows full detachability and cleaning of steerable laparoscopic instruments”. In: *Surgical Endoscopy* 33.10 (May 2019), pp. 3484–3493. DOI: 10.1007/s00464-019-06849-0.
- [44] P. Breedveld et al. “A new, easily miniaturized steerable endoscope”. In: *IEEE Engineering in Medicine and Biology Magazine* 24.6 (Nov. 2005), pp. 40–47. DOI: 10.1109/memb.2005.1549729.
- [45] Costanza Culmone et al. “Exploring non-assembly 3D printing for novel compliant surgical devices”. In: *PLOS ONE* 15.5 (May 2020). Ed. by Tommaso Ranzani, e0232952. DOI: 10.1371/journal.pone.0232952.
- [46] Filip Jelínek et al. “Method for minimising rolling joint play in the steerable laparoscopic instrument prototype DragonFlex”. In: *Minimally Invasive Therapy & Allied Technologies* 24.3 (Nov. 2014), pp. 181–188. DOI: 10.3109/13645706.2014.968170.
- [47] Juan Sebastian Cuellar et al. “Additive manufacturing of non-assembly mechanisms”. In: *Additive Manufacturing* 21 (May 2018), pp. 150–158. DOI: 10.1016/j.addma.2018.02.004.
- [48] Steijn van Schoor, Costanza Culmone, and Kirsten Lussenburg. “Design of non-assembly mechanisms for desktop 3D printers – A design review (unpublished)”. In: (Aug. 2020).
- [49] Tao Han et al. “3D Printed Sensors for Biomedical Applications: A Review”. In: *Sensors* 19.7 (Apr. 2019), p. 1706. DOI: 10.3390/s19071706.
- [50] Materialise. *Design Guidelines - PolyJet Materials*. URL: <https://www.materialise.com/en/manufacturing/materials/composite-materials/design-guidelines> (visited on 03/29/2021).
- [51] Proto3000. *PolyJet 3D Printing Technology*. 2021. URL: <https://proto3000.com/service/3d-printing-services/technologies/polyjet/> (visited on 03/29/2021).
- [52] Protolabs. *Design Guidelines: PolyJet*. URL: <https://www.protolabs.com/services/3d-printing/polyjet/design-guidelines/> (visited on 03/29/2021).
- [53] formlabs. *Minimum Wall Thickness for 3D Printing*. URL: <https://formlabs.com/eu/blog/minimum-wall-thickness-3d-printing/> (visited on 03/29/2021).
- [54] Sourabh Manoj Saptarshi and Dr. Chi Zhou. “Basics of 3D Printing”. In: *3D Printing in Orthopaedic Surgery*. Elsevier, 2019, pp. 17–30. DOI: 10.1016/b978-0-323-58118-9.00002-6.
- [55] *Guidelines for design for additive manufacturing*. Standard. International Organization for Standardization, American Society for Testing and Materials, Jan. 2017.
- [56] Ian Gibson, David Rosen, and Brent Stucker. *Additive Manufacturing Technologies*. Springer New York, 2015. DOI: 10.1007/978-1-4939-2113-3.
- [57] formlabs. *Resin family - tough and durable*. URL: <https://formlabs.com/eu/materials/tough-durable/> (visited on 03/30/2021).
- [58] Yuanrui Li et al. “Bioinspired Functional Surfaces Enabled by Multiscale Stereolithography”. In: *Advanced Materials Technologies* 4.5 (Feb. 2019), p. 1800638. DOI: 10.1002/admt.201800638.

- [59] Xiangfan Chen et al. “High-Speed 3D Printing of Millimeter-Size Customized Aspheric Imaging Lenses with Sub 7 nm Surface Roughness”. In: *Advanced Materials* 30.18 (Mar. 2018), p. 1705683. DOI: 10.1002/adma.201705683.
- [60] Eric Barnett and Clément Gosselin. “Large-scale 3D printing with a cable-suspended robot”. In: *Additive Manufacturing* 7 (July 2015), pp. 27–44. DOI: 10.1016/j.addma.2015.05.001.
- [61] Ran He et al. “Fabrication of circular microfluidic channels through grayscale dual-projection lithography”. In: *Microfluidics and Nanofluidics* 21.1 (Jan. 2017). DOI: 10.1007/s10404-017-1851-5.
- [62] Xuan Song et al. “Ceramic fabrication using Mask-Image-Projection-based Stereolithography integrated with tape-casting”. In: *Journal of Manufacturing Processes* 20 (Oct. 2015), pp. 456–464. DOI: 10.1016/j.jmapro.2015.06.022.
- [63] Ran He et al. “Three-dimensional printing of large objects with high resolution by scanning lithography”. In: *The International Journal of Advanced Manufacturing Technology* 105.10 (June 2019), pp. 4147–4157. DOI: 10.1007/s00170-019-03862-4.
- [64] formlabs. *Design specifications for 3D models (Form 3/Form 3B)*. 2020. URL: https://support.formlabs.com/s/article/Design-specifications-for-3D-models-form-3?language=en_US (visited on 03/29/2021).
- [65] Yonghua Chen and Jianan Lu. “Minimise joint clearance in rapid fabrication of non-assembly mechanisms”. In: *International Journal of Computer Integrated Manufacturing* 24.8 (Aug. 2011), pp. 726–734. DOI: 10.1080/0951192x.2011.592995.
- [66] Xuan Song and Yong Chen. “Joint Design for 3-D Printing Non-Assembly Mechanisms”. In: *Volume 5: 6th International Conference on Micro- and Nanosystems; 17th Design for Manufacturing and the Life Cycle Conference*. American Society of Mechanical Engineers, Aug. 2012. DOI: 10.1115/detc2012-71528.
- [67] Xiangzhi Wei, Yaobin Tian, and Ajay Joneja. “A study on revolute joints in 3D-printed non-assembly mechanisms”. In: *Rapid Prototyping Journal* 22.6 (Oct. 2016), pp. 901–933. DOI: 10.1108/rpj-10-2014-0146.
- [68] Larry L. Howell. “Compliant Mechanisms”. In: *21st Century Kinematics*. Springer London, 2013, pp. 189–216. DOI: 10.1007/978-1-4471-4510-3_7.
- [69] J. Lassooij et al. “A statically balanced and bi-stable compliant end effector combined with a laparoscopic 2DoF robotic arm”. In: *Mechanical Sciences* 3.2 (Dec. 2012), pp. 85–93. DOI: 10.5194/ms-3-85-2012.
- [70] Luzhong Yin and G. K. Ananthasuresh. “Design of Distributed Compliant Mechanisms”. In: *Mechanics Based Design of Structures and Machines* 31.2 (Jan. 2003), pp. 151–179. DOI: 10.1081/sme-120020289.
- [71] D. Farhadi Machekposhti, N. Tolou, and J. L. Herder. “A Review on Compliant Joints and Rigid-Body Constant Velocity Universal Joints Toward the Design of Compliant Homokinetic Couplings”. In: *Journal of Mechanical Design* 137.3 (Mar. 2015). DOI: 10.1115/1.4029318.
- [72] James A. Cronin, Mary I. Frecker, and Abraham Mathew. “Design of a Compliant Endoscopic Suturing Instrument”. In: *Journal of Medical Devices* 2.2 (May 2008). DOI: 10.1115/1.2931551.
- [73] Elaine Nicpon Marieb and Katja Hoehn. *Human anatomy & physiology*. Pearson education, 2007.
- [74] Aesculap. *SENSATION Micro Instruments*. Brochure Aesculap. 2017. URL: <https://www.aesculapusa.com/en/healthcare-professionals/or-solutions/or-solutions-neurosurgical-instruments/micro-instruments.html>.
- [75] Surgical Holdings. *Neuro/Spinal Surgery*. Brochure Surgical Holdings. URL: <https://www.surgicalholdings.co.uk/media/files/new%5C%20catalogue/SH%5C%20Catalogue%5C%20-%5C%20Neuro%5C%20%5C%26%5C%20Spinal.pdf>.
- [76] Symmetry Surgical. *Neuro Portfolio*. Brochure Symmetry Surgical. URL: <https://www.symmetrysurgical.com/en/Image/GetDocument/48>.
- [77] Aida Kafai Golahmadi et al. “Tool-tissue forces in surgery: A systematic review”. In: *Annals of Medicine and Surgery* 65 (May 2021), p. 102268. DOI: 10.1016/j.amsu.2021.102268.

- [78] Filip Jelínek et al. “Classification of Joints Used in Steerable Instruments for Minimally Invasive Surgery—A Review of the State of the Art”. In: *Journal of Medical Devices* 9.1 (Mar. 2015). DOI: 10.1115/1.4028649.
- [79] Bryce Edmondson et al. “Surgical forceps”. 2014. URL: <https://patents.google.com/patent/US20150057702A1/en>.
- [80] BYU-CMR. *Oriceps: Origami Inspired Forceps*. THING id: 2988740. 2018. URL: <https://www.thingiverse.com/thing:2988740>.
- [81] Berndts23; Bernd Berndsen. *Compliant Pliers / Gripper*. THING id: 4177201. 2020. URL: <https://www.thingiverse.com/thing:4177201>.
- [82] Alcon Vision, LLC. *SURGICAL RETINA PRODUCT CATALOG*. Borchure Alcon. 2019. URL: <https://alcon.widen.net/s/zrlg779yi0>.
- [83] Sridhar Kota et al. “Mission adaptive compliant wing — design, fabrication and flight test”. In: *RTO Applied Vehicle Technology Panel (AVT) Symposium*. American Institute of Aeronautics and Astronautics, 2009. DOI: 10.2514/6.2009-2126.
- [84] Bob McGinty. *Buckling of Eccentrically Loaded Columns*. 2014. URL: <https://www.continuummechanics.org/eccentriccolumnbuckling.html> (visited on 03/29/2021).
- [85] formlabs. *Tough 1500 Technical Data Sheet*. 2018. URL: https://formlabs-media.formlabs.com/datasheets/Tough_1500_TDS_EN.pdf (visited on 03/30/2021).
- [86] S. P. Timoshenko J. M. Gere. *Mechanics of materials - Fourth SI edition*. Cheltenham: Stanley Thornes, 1999. ISBN: 074873998X.
- [87] U. Matern and P. Waller. “Instruments for minimally invasive surgery”. In: *Surgical Endoscopy* 13.2 (Feb. 1999), pp. 174–182. DOI: 10.1007/s004649900934.
- [88] U. Matern et al. “MIS instruments”. In: *Surgical Endoscopy* 13.8 (Aug. 1999), pp. 756–762. DOI: 10.1007/s004649901093.
- [89] Filip Jelínek and Paul Breedveld. “Design for Additive Manufacture of Fine Medical Instrumentation—DragonFlex Case Study”. In: *Journal of Mechanical Design* 137.11 (Oct. 2015). DOI: 10.1115/1.4030997.
- [90] Marco Aggravi et al. “Hand–tool–tissue interaction forces in neurosurgery for haptic rendering”. In: *Medical & Biological Engineering & Computing* 54.8 (Dec. 2015), pp. 1229–1241. DOI: 10.1007/s11517-015-1439-8.
- [91] Gmaan AlZhrani et al. “Proficiency Performance Benchmarks for Removal of Simulated Brain Tumors Using a Virtual Reality Simulator NeuroTouch”. In: *Journal of Surgical Education* 72.4 (July 2015), pp. 685–696. DOI: 10.1016/j.jsurg.2014.12.014.
- [92] Christopher J. Payne, Hani J. Marcus, and Guang-Zhong Yang. “A Smart Haptic Hand-Held Device for Neurosurgical Microdissection”. In: *Annals of Biomedical Engineering* 43.9 (Jan. 2015), pp. 2185–2195. DOI: 10.1007/s10439-015-1258-y.
- [93] formlabs. *Tough 2000 Technical Data Sheet*. 2018. URL: <https://formlabs-media.formlabs.com/datasheets/2001340-TDS-ENUS-OP.pdf> (visited on 03/30/2021).
- [94] Venkata S. Arikatla et al. “Face and construct validation of a virtual peg transfer simulator”. In: *Surgical Endoscopy* 27.5 (Dec. 2012), pp. 1721–1729. DOI: 10.1007/s00464-012-2664-y.
- [95] Milton E. Aguirre and Mary Frecker. “Design and Optimization of Hybrid Compliant Narrow-Gauge Surgical Forceps”. In: *ASME 2010 Conference on Smart Materials, Adaptive Structures and Intelligent Systems, Volume 1*. ASMEDC, Jan. 2010. DOI: 10.1115/smasis2010-3732.
- [96] Aaron Stapel and Just L. Herder. “Feasibility Study of a Fully Compliant Statically Balanced Laparoscopic Grasper”. In: *Volume 2: 28th Biennial Mechanisms and Robotics Conference, Parts A and B*. ASMEDC, Jan. 2004. DOI: 10.1115/detc2004-57242.

Appendix A Morphological schemes

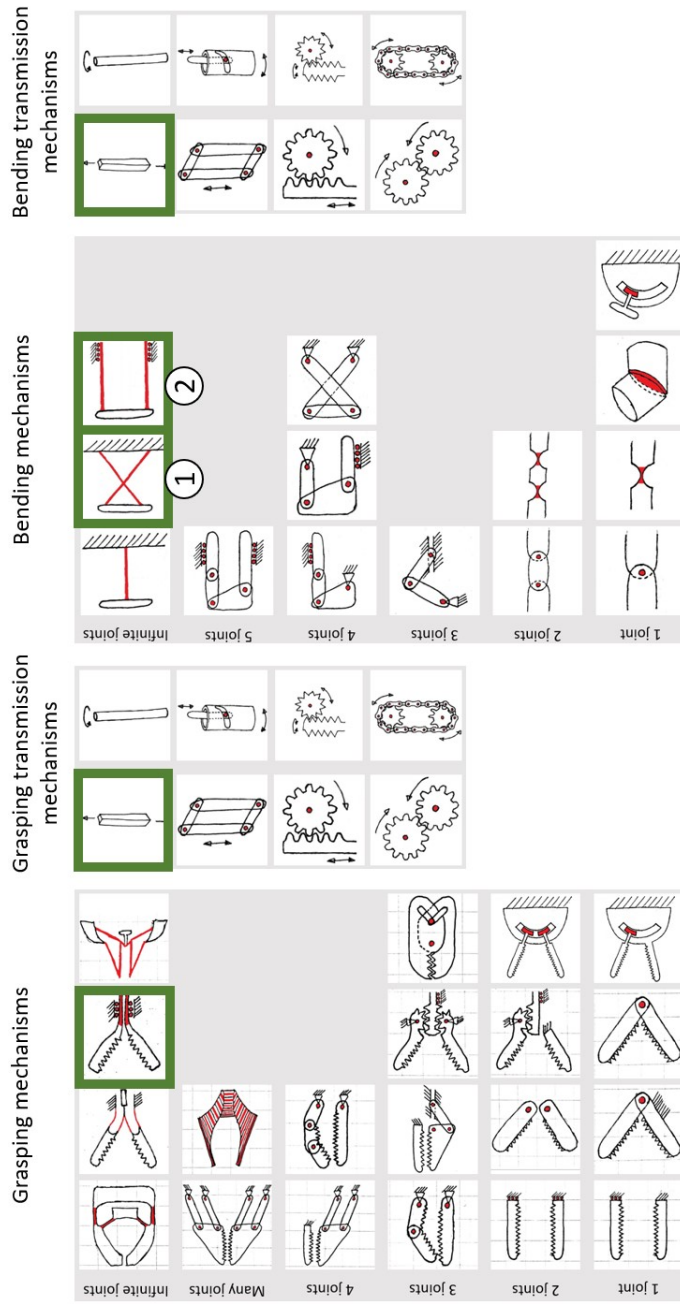
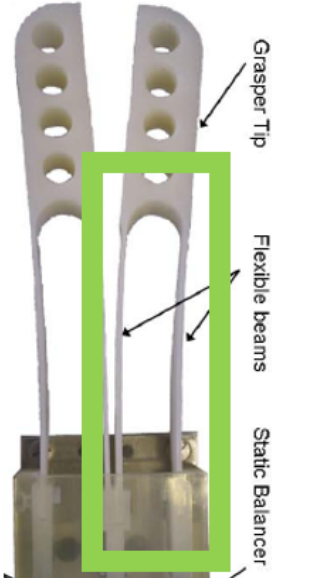
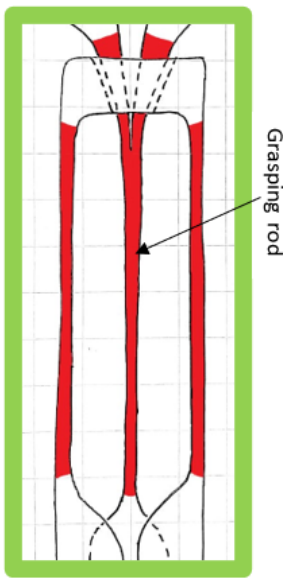


Figure A.1: Schematic overview that shows the combination of solutions that leads to the two concepts in Section 5. The concepts use the same grasping and transmission mechanisms, but have a different bending solution.

Appendix B Comparison with compliant grasper

Table B.1: Comparison between our bending mechanism and the mechanism in the compliant grasper by Herder and Van den Berg [30]. The relevant part in both figures is indicated by the green frame.

Grasper by Herder et al.	Our bending concept	Remarks
		
Similarities		
<p>Two leaf flexures Equal length Actuated by push/pull motion Symmetric mechanism (one flexure slightly longer in Herder <i>et al.</i>) Bending motion (rotation of top part) Bottom parts of flexures remain parallel</p>		
Differences		
<p>Used for grasping Push/pull one flexure Displacement of one flexure is constraint (by collision with second mechanism) Half the width of device (since there are two mechanisms besides each other) High forces in one direction (grasping) Neutral position is bend</p>	<p>Used for bending Push/pull both flexures No constraints on flexure displacement Full width of device Forces in both directions Neutral position is straight</p>	<p>Same FBD due to reaction forces Looking at our prototypes, buckling does not exceed midline</p>
<p>No extra bending stiffness Metal</p>	<p>Grasping rod adds stiffness Only printable materials possible</p>	<p>Full width is an advantage We need twice the range of motion, unless designing for one-side bending Ideally, $k_{grasping} \ll k_{bending}$</p>

Appendix C Bending calculations

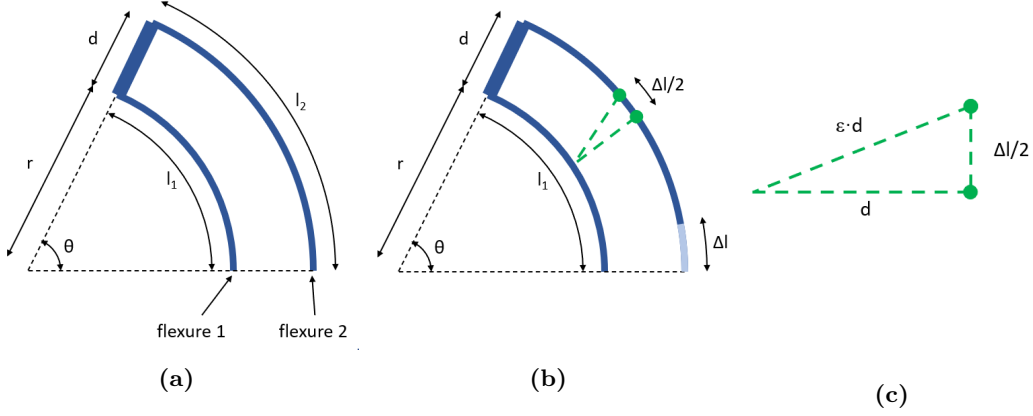


Figure C.1: Schematic representation of flexures during bending.

The following geometric calculation can be used to describe the flexure behaviour during bending. The (sub-)results of the calculation can be used to support design choices and finalise design dimensions. In this calculations the following assumptions are made:

1. The flexures bend in a perfect circular shape, i.e. they take the shape of a circle arc.
2. The bending flexures maintain a constant (perpendicular) distance during bending.
3. The bending flexures are parallel at the base.

The length of flexure 1 (see Fig. C.1) is given by:

$$l_1 = \frac{\theta}{360} 2\pi r, \quad (\text{C.1})$$

where θ denotes the bending angle and r the bending radius of flexure 1. The length of flexure 2 can be calculated in the same way, by replacing r with $r + d$, where d is the distance between flexures 1 and 2:

$$l_2 = \frac{\theta}{360} 2\pi(r + d) \quad (\text{C.2})$$

If we rewrite Eq. (C.2) as a function of r and substitute in Eq. (C.1), we get:

$$\begin{aligned} l_1 &= \frac{\theta}{360} 2\pi \left(\frac{360}{\theta} \frac{1}{2\pi} l_2 - d \right) \\ &= l_2 - \frac{2\pi\theta}{360} d \end{aligned} \quad (\text{C.3})$$

The difference between l_1 and l_2 , Δl , is:

$$\Delta l = l_2 - l_1 = \frac{2\pi\theta}{360} d \quad (\text{C.4})$$

Δl denotes the maximum shear between the two bending flexures, or maximum input displacement, which takes place at the base. Note that Δl is independent from the bending radius r and flexures lengths. For the maximum bending angle $\theta = 60^\circ$:

$$\Delta l = 1.0472d \quad (\text{C.5})$$

Halfway the bending flexures, where a potential spacing flexures could connect them, the shear is halved. With Fig. C.1c we can calculate the required elongation ϵ of a spacing flexure with Pythagoras theorem:

$$\epsilon = \sqrt{1 + \frac{1.0472^2}{4}} = 1.13, \quad (\text{C.6})$$

meaning a required elongation of approximately 13%.

Appendix D Alternative bending concepts

Direct Cans in series equivalents

Figure D.1 shows the original Cans in series representation of the four categories and their corresponding parallel flexure designs side by side. The designs in the figure are the most equivalent counterparts of the Cans in series drawings. Since the Cans in series models are merely a tool to structure the design configuration, their direct equivalents are not necessarily the best solutions for our purpose. The five designs from Fig. D.1b that were discontinued are further explained in the next sections.

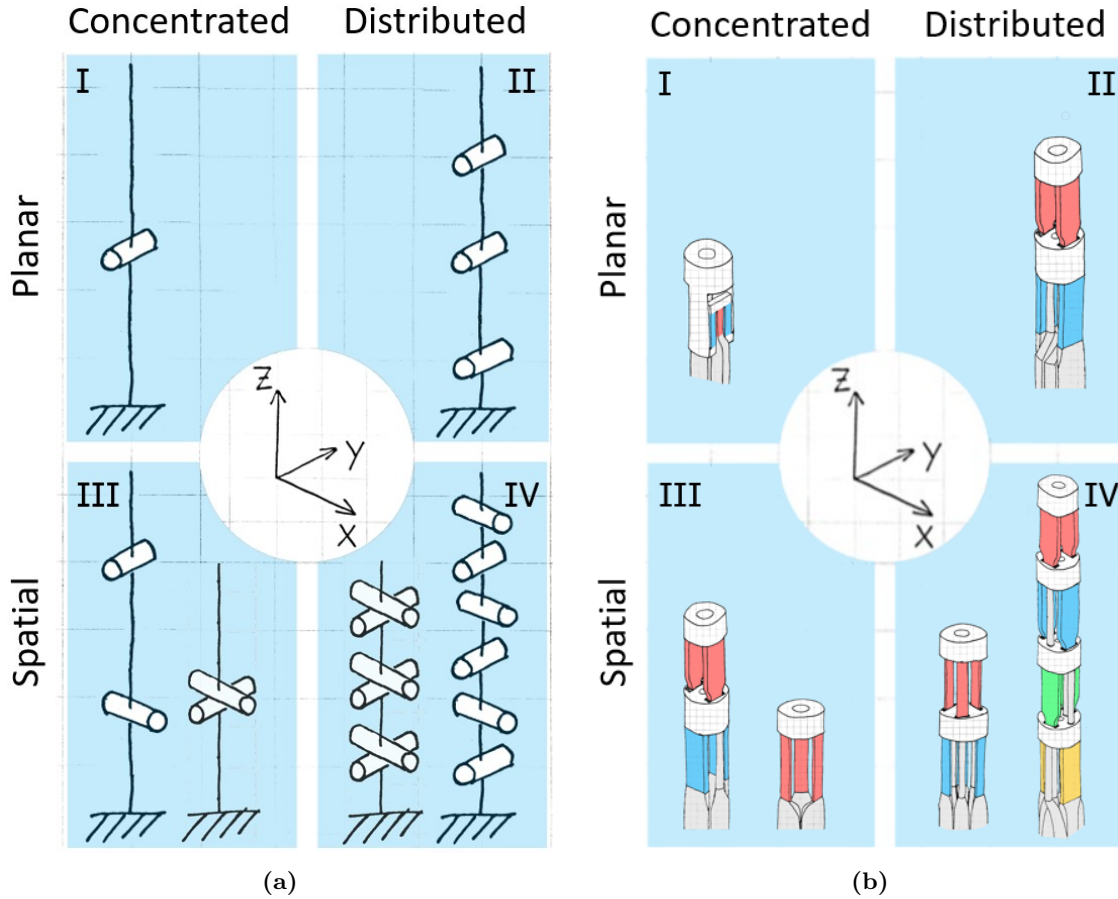


Figure D.1: Four bending categories. a) schematic representation using the Cans in series system by A. Schwab and J. Meijaard [33], a duplicate of Fig. 6. b) concept hand sketches for each category, using parallel flexures.

Alternative concentrated planar bending concept

Fig. D.2 shows a concept that resembles concentrated planar bending, using leaf flexures. The concentrated bending is achieved by splitting the bending flexures from the parallel flexure concept (see Section 5) in two parts and reconnect the upper (blue) parts upside down, besides the lower (pink) parts. To create symmetry, the blue flexure is split in two. With this new flexure orientation, the concept still works the same, but the bending mechanism is shortened, and it cancels out all translations during bending. What remains is a purely rotational bending motion around a single fixed axis.

Even though this concept fits better with category I from Fig. 6 than the parallel flexure concept, it has no clear advantages, whilst having increased complexity and many parallel parts. Another drawback to this concept is that the bending mechanism sticks out in the opposite direction during bending, as can be seen in Fig. D.2b.

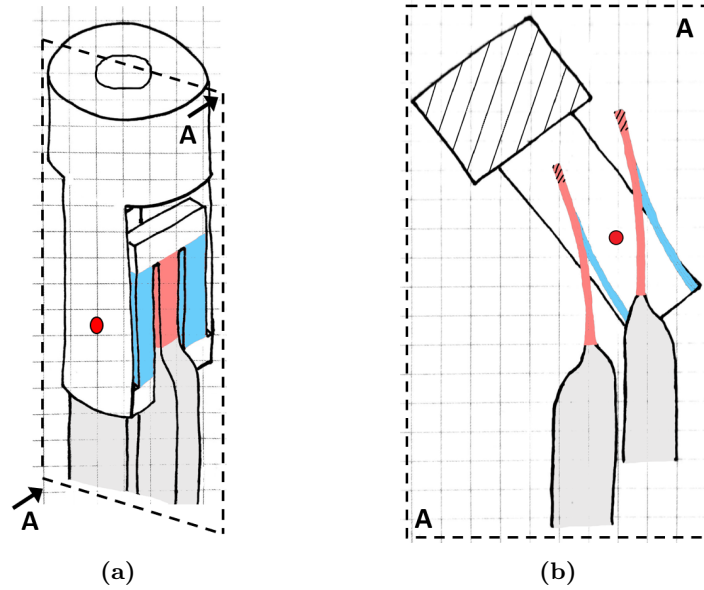


Figure D.2: Hand sketches of zero-radius bending concept, with the single axis of rotation indicated by the red dot. a) 3D sketch. b) cross-section during bending.

Alternative distributed planar bending concept

Fig. D.3b shows a concept that resembles distributed planar bending, using leaf flexures. The distributed bending is achieved by a concatenation of — in this case two — bending mechanisms. Each mechanism can be individually controlled, but all motions remain in the same plane. This makes it possible to manoeuvre the device in complex shapes that would not be possible with the two flexure concept from Section 6.1.2

Each new concatenated mechanism needs two new rods to actuate it. To use the optimum configuration with all bending flexures from each layer oriented collinear, the rods need to be guided around the lower laying bending flexures. In the two-layer example from Fig. D.3b the extra rods are guided towards the centre of the device, to minimise their contribution to the bending stiffness. Adding a third layer would mean the new rods need to be guided around the bending flexures and the rods of the second layer. The two flexure concept can make the same large radii, without the added complexity that comes from the extra flexures and rods.

Alternative concentrated spatial bending concept

Two parallel flexure bending mechanisms with a 90° shift create one 2DOF system, as is shown in Fig. D.3a. Between the two bending mechanisms needs to be a rigid part that the bending flexures of the lower (blue) mechanism attach to. Flexible rods to control the upper (pink) mechanism need to run through the rigid part and along the blue flexures. The actuation of the two bending mechanisms is decoupled when the actuation rods of the red flexures remain in the xz -plane and are thin enough to bend along with the blue mechanism. This means that the two degrees of freedom can be actuated independently and simultaneously. The blue bending flexures must be actuated to bend the tip around the x -axis, and the pink bending flexures provide rotation around the y -axis. The distance between the bending axes, caused by the non-zero bending radii and the rigid part between the bending mechanisms, makes the control of the device less intuitive; the bending axis of the pink mechanism moves during bending of the blue mechanism.

Alternative distributed spatial bending concept

Figure D.3c shows a concept consisting of two concatenated versions of the alternative Category III concept, or four concatenated Category I concepts. This concept has nine control rods in the shaft, two for each bending mechanism, and one for the grasper. It becomes increasingly difficult to efficiently guide all control rods past the bending mechanisms, especially when they must stay in their xz - and yz -planes to keep a constant length during bending.

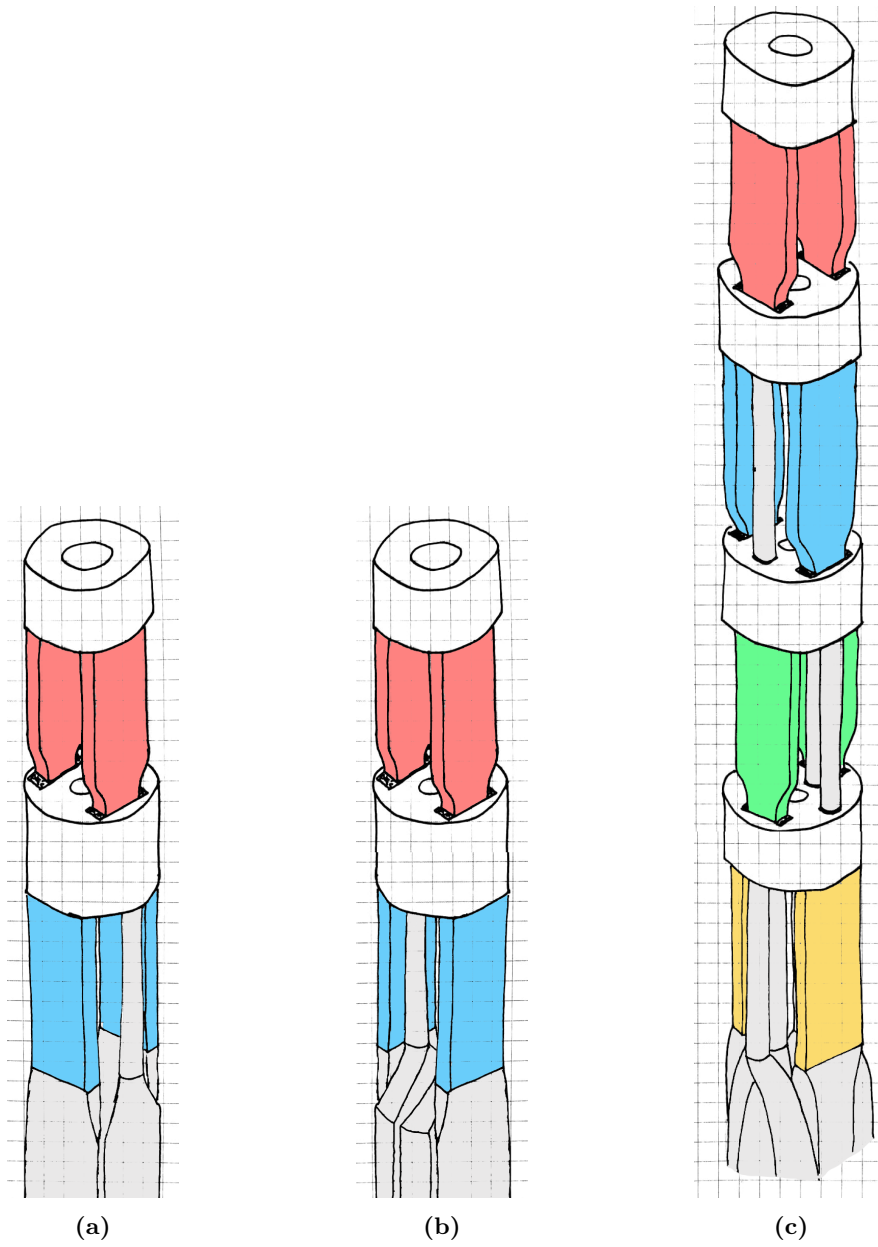


Figure D.3: Hand sketches of alternative concepts. a) distributed planar bending. b) concentrated spatial bending. c) distributed spatial bending.

Appendix E Design of a spacing flexure

Bulging of bending flexures: problem analysis

Both bending flexures bend due to reactant forces and moments, but since they are counter-loaded—one under tension and one under compression—they will bend differently. Figure E.1a shows the expected bending behaviour of both flexures. The tension in the flexure on the inside of the bend partially counteracts its bending: the flexure will be slightly straightened. Conversely, the compression in the outside flexure amplifies its bending and leads to a higher outward buckling deflection. The difference in bending leads to a local increase in device diameter and can reduce the device's stiffness, especially at larger bending angles. Furthermore, a larger input displacement is needed to achieve a certain tip rotation, and hysteresis can occur when moving back to the undeformed position. When the difference between the flexures is too large, the maximum bending angle of the tip may not be reached.

The local separation of bending flexures, henceforth called 'bulging', was present in a 10 mm proof of concept, as well as the printed prototypes used in the experiments. Figure E.1b shows the theoretical bulging besides a photo of the 10 mm proof of concept. Bulging of the bending flexures could decrease the stiffness of the device. A part or mechanism that prevents bulging could contribute to a high stiffness device, which is one of the major challenges in our true scale design.

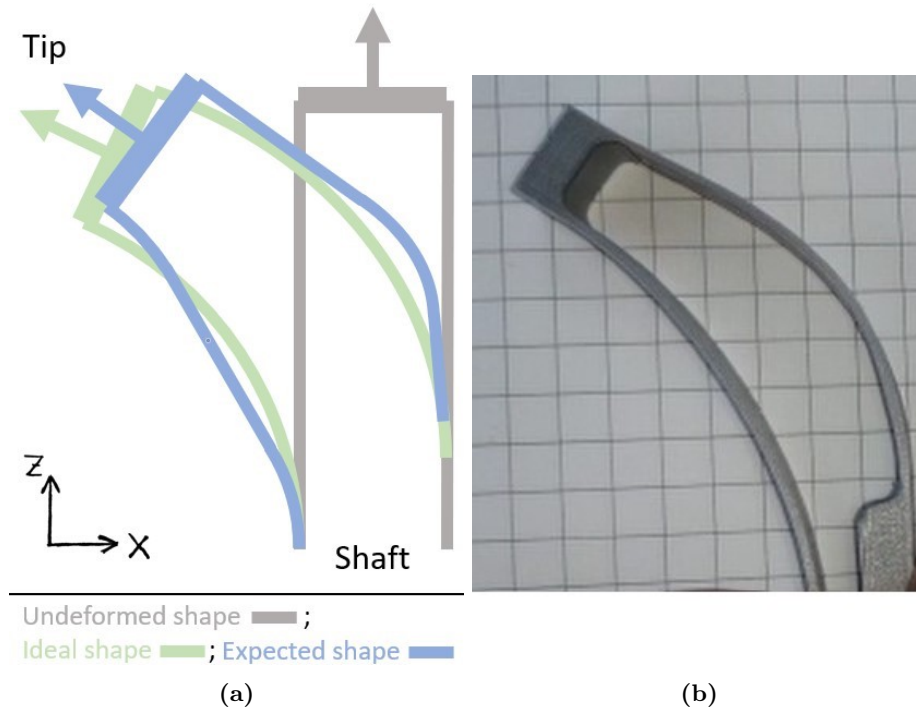


Figure E.1: Bending behaviour of the tip. a) theoretical undeformed position in grey, ideal bending shape in green, and exaggerated expected 'bulging' bending shape in blue. b) 10 mm proof of concept. The bending shape has a lower bending angle of the tip, despite having a larger input motion. Furthermore, it has a local increase in diameter.

Potential bulging solutions

Bulging can be avoided by constraining the distance between the flexures, while still allowing relative motion. This can be done in three ways: 1) by adding a flexible sliding mechanism between the bending flexures, 2) by constructing a cage around the bending flexures, which can also be seen as an external sliding mechanism, or 3) by adding a monolithic flexible connection—or spacing flexure—between the flexures. The first method will interfere with the bending of the flexures and with the grasping rod. Furthermore, the minimum clearance in the sliding mechanism will still allow for some bulging. Since the second method surrounds the bending flexure and grasper width. Furthermore, it will increase the bending

stiffness. The third solution is preferred since it can be used without changing the rest of the mechanism.

Performing a simple test with the 10 mm proof of concept from Fig. E.1b showed that a single spacing flexure halfway the bending flexures significantly reduces bulging. The spacing flexure must maintain a constant width between bending flexures that make a relative sliding motion. This means that the spacing flexure needs to elongate approximately 13%, as is calculated in Appendix C. When the spacing flexure is rigidly connected to the bending flexures its rotation at its two ends is limited, and the required elongation will be higher. The spacing flexure must be stiff enough to prevent bending flexure separation, but its contribution to the bending stiffness must be low. We used three approaches to find the best spacing flexures:

1. **Find the flexure equivalent of a cable**, see Table E.1

A cable connecting the bending flexures could constrict the maximum distance between them when fully bent. The first approach is to find a 3D printable cable equivalent. The first step in Table E.1 is a rigid link, which would need revolute joints. The next step is to replace the rigid link by a helical spring. A benefit of a spring is that the spacing stiffness increases with the bending, to keep up with the increasing tendency to bulge. Because a 2 mm helical spring is unfeasible, it can be replaced by a flexure alternative, as is shown in the bottom row. This structure can be printed, but is equally stiff in each direction.

2. **Geometrical reasoning starting from simple leaf flexure**, see Table E.2

The second approach is to start with a straight leaf flexure. Placing the leaf flexure at an angle would result in lower stress concentrations in one direction, but higher stress concentrations in the other direction. When a triangle is formed by using two shorter leaf flexures at an angle, stress concentrations in both directions are reduced. A final improvement can be made by making the triangle very narrow, as in the bottom row of Table E.2. The contribution to the bending stiffness and the spacing stiffness are now uncoupled; the horizontal flexures can be kept thin to minimise the bending stiffness, and the vertical flexures provide the spacing stiffness.

3. **Geometrical reasoning starting from compliant slider**, see Table E.3

The third approach starts with a compliant slider, consisting of a rigid beam and a back-and-forth flexure. The back-and-forth flexure provides a linear DOF, like a slider. Rotating the back-and-forth flexures by 90° will increase the spacing stiffness, since the bending direction of the leaf flexures is now perpendicular to the bulging direction. The configuration can be further improved by moving one leaf flexure to the other side, introducing symmetry, reducing the number of clearances, and leaving more space for the grasping rod in the middle.

The first approach succeeds in adding spacing stiffness, but fails at keeping the bending stiffness low. Theoretically, the third approach results in the solution that is most mechanically sound; the compliant leaf flexures marginally contribute to the bending stiffness, while being stiff in the bulging direction. However, this design adds clearances to the design which limit the size of the other mechanisms. The 'Spike' flexure from approach 2 makes a good trade-off between good stiffness control and simplicity.

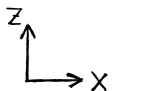
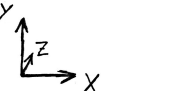
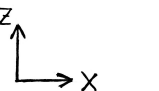
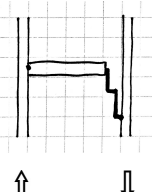

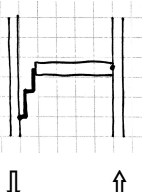
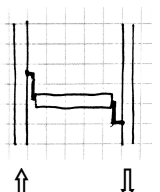
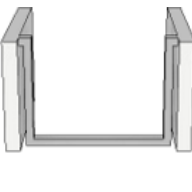
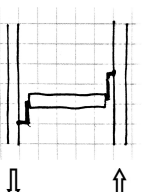
Table E.1: Spacing flexure design, approach 1: Flexure equivalent of a cable

Expected bending behaviour	Undeformed shape	Expected bending behaviour	
			<p>Cable</p> <ul style="list-style-type: none"> • Zero stiffness until fully bent • Cable cannot be printed
			<p>Rigid link with revolute joints</p> <ul style="list-style-type: none"> • Revolute joints not feasible • Bending flexures are pulled together
			<p>Helical spring</p> <ul style="list-style-type: none"> • Stiffness increases with bending • Printing helical spring not feasible
			<p>Flexure alternative of helical spring</p> <ul style="list-style-type: none"> • Stiffness increases with bending

Table E.2: Spacing flexure design, approach 2: Geometrical reasoning starting from a simple leaf flexure

Expected bending behaviour	Undeformed shape	Expected bending behaviour	
			<p>Straight leaf flexure</p> <ul style="list-style-type: none"> • Bending flexures are pulled together • Attachment points remain horizontal
			<p>Skew leaf flexure</p> <ul style="list-style-type: none"> • Left: bending flexures are slightly pulled together • Right: bending flexures are severely pulled together
			<p>Triangular flexure</p> <ul style="list-style-type: none"> • High bending stiffness compared to spacing stiffness
			<p>Spike flexure</p> <ul style="list-style-type: none"> • High spacing stiffness compared to bending stiffness

Table E.3: Spacing flexure design, approach 3: Geometrical reasoning starting from a compliant slider

Expected bending behaviour	Undeformed shape	Expected bending behaviour	
			<p>Sliding mechanism</p> <ul style="list-style-type: none"> • Difficult to print stacked flexures • Very low bending stiffness • Flexures take up relatively much space
			<p>Sliding mechanism</p> <ul style="list-style-type: none"> • Very low bending stiffness • Relatively high spacing stiffness
			<p>Sliding mechanism</p> <ul style="list-style-type: none"> • Symmetric • Very low bending stiffness • Relatively high spacing stiffness

Appendix F Matlab scripts

Processing experimental data

```
1 saveI = false;
2 saveII = false;
3 saveIII = false;
4
5 %% crop and scaling settings
6 % videoframes
7 crop1.window = [532, 0, 1110];
8 crop1.row = 1008; % start looking at row ..
9 crop1.col1 = 77; % start looking at column ..
10 crop1.col2 = 997; % start looking at column ..
11 crop1.squares = 12; % number of squares for scaling
12
13 % photos
14 crop2.window = [1180, 590, 2190, 1885];
15 crop2.row = 172; % start looking at row ..
16 crop2.col1 = 377; % start looking at column ..
17 crop2.col2 = 2019; % start looking at column ..
18 crop2.squares = 12; % number of squares for scaling
19
20 % photos small
21 crop3.window = [];
22 crop3.row = 92; % start looking at row ..
23 crop3.col1 = 1119; % start looking at column ..
24 crop3.col2 = 3843; % start looking at column ..
25 crop3.squares = 10; % number of squares for scaling
26
27 % photos
28 crop4.window = [1180, 590, 2190, 1885];
29 crop4.row = 95; % start looking at row ..
30 crop4.col1 = 341; % start looking at column ..
31 crop4.col2 = 1956; % start looking at column ..
32 crop4.squares = 12; % number of squares for scaling
33
34
35 %% Bending category I
36 expI1 = BendingMetrics('I Bending 1a.jpg', 'I Bending 1b.jpg');
37 expI2 = BendingMetrics('I Bending 2a.jpg', 'I Bending 2b.jpg');
38 expI3 = BendingMetrics('I Bending 3a.jpg', 'I Bending 3b.jpg');
39 expI4 = BendingMetrics('I Bending 4a.jpg', 'I Bending 4b.jpg');
40 expI5 = BendingMetrics('I Bending 5a.jpg', 'I Bending 5b.jpg');
41 expI6 = BendingMetrics('I Bending 6a.jpg', 'I Bending 6b.jpg');
42
43 if saveI
44     save('expI1.mat', 'expI1')
45     save('expI2.mat', 'expI2')
46     save('expI3.mat', 'expI3')
47     save('expI4.mat', 'expI4')
48     save('expI5.mat', 'expI5')
49     save('expI6.mat', 'expI6')
50 end
51
52 expI.alpha = [expI1.alpha expI2.alpha expI3.alpha expI4.alpha ...
53             expI5.alpha expI6.alpha];
54
55 expI.disp = [expI1.disp expI2.disp expI3.disp expI4.disp ...
56            expI5.disp expI6.disp];
57
58 expI.radius = [expI1.radius expI2.radius expI3.radius expI4.radius ...
59              expI5.radius expI6.radius];
60
61 %% Stiffness category I
62
63 % neutral
64 expI7 = StiffnessMetrics('I Stiffness neutral 1a.jpg', ...
65                          'I Stiffness neutral 1b.jpg', crop1);
66 expI8 = StiffnessMetrics('I Stiffness neutral 2a.jpg', ...
67                          'I Stiffness neutral 2b.jpg', crop1);
```

```

68 expI9 = StiffnessMetrics('I Stiffness neutral 3a.jpg', ...
69     'I Stiffness neutral 3b.jpg', crop1);
70 expI10 = StiffnessMetrics('I Stiffness neutral 4a.jpg', ...
71     'I Stiffness neutral 4b.jpg', crop1);
72 expI11 = StiffnessMetrics('I Stiffness neutral 5a.jpg', ...
73     'I Stiffness neutral 5b.jpg', crop1);
74 expI12 = StiffnessMetrics('I Stiffness neutral 6a.jpg', ...
75     'I Stiffness neutral 6b.jpg', crop1);
76
77 if saveI
78     save('expI7.mat', 'expI7')
79     save('expI8.mat', 'expI8')
80     save('expI9.mat', 'expI9')
81     save('expI10.mat', 'expI10')
82     save('expI11.mat', 'expI11')
83     save('expI12.mat', 'expI12')
84 end
85
86 expI.stiffness.neutral = [expI7.defl expI8.defl expI9.defl ...
87     expI10.defl expI11.defl expI12.defl];
88
89 % bent
90 expI13 = StiffnessMetrics('I Stiffness bent 1a.jpg', ...
91     'I Stiffness bent 1b.jpg', crop2);
92 expI14 = StiffnessMetrics('I Stiffness bent 2a.jpg', ...
93     'I Stiffness bent 2b.jpg', crop2);
94 expI15 = StiffnessMetrics('I Stiffness bent 3a.jpg', ...
95     'I Stiffness bent 3b.jpg', crop2);
96 expI16 = StiffnessMetrics('I Stiffness bent 4a.jpg', ...
97     'I Stiffness bent 4b.jpg', crop2);
98 expI17 = StiffnessMetrics('I Stiffness bent 5a.jpg', ...
99     'I Stiffness bent 5b.jpg', crop2);
100 expI18 = StiffnessMetrics('I Stiffness bent 6a.jpg', ...
101     'I Stiffness bent 6b.jpg', crop2);
102
103 if saveI
104     save('expI13.mat', 'expI13')
105     save('expI14.mat', 'expI14')
106     save('expI15.mat', 'expI15')
107     save('expI16.mat', 'expI16')
108     save('expI17.mat', 'expI17')
109     save('expI18.mat', 'expI18')
110 end
111
112 expI.stiffness.bent = [expI13.defl expI14.defl expI15.defl ...
113     expI16.defl expI17.defl expI18.defl];
114
115 % grasper
116 expI19 = StiffnessMetrics('I Stiffness grasper 1a.jpg', ...
117     'I Stiffness grasper 1b.jpg', crop1);
118 expI20 = StiffnessMetrics('I Stiffness grasper 2a.jpg', ...
119     'I Stiffness grasper 2b.jpg', crop1);
120 expI21 = StiffnessMetrics('I Stiffness grasper 3a.jpg', ...
121     'I Stiffness grasper 3b.jpg', crop1);
122 expI22 = StiffnessMetrics('I Stiffness grasper 4a.jpg', ...
123     'I Stiffness grasper 4b.jpg', crop1);
124 expI23 = StiffnessMetrics('I Stiffness grasper 5a.jpg', ...
125     'I Stiffness grasper 5b.jpg', crop1);
126 expI24 = StiffnessMetrics('I Stiffness grasper 6a.jpg', ...
127     'I Stiffness grasper 6b.jpg', crop1);
128
129 if saveI
130     save('expI19.mat', 'expI19')
131     save('expI20.mat', 'expI20')
132     save('expI21.mat', 'expI21')
133     save('expI22.mat', 'expI22')
134     save('expI23.mat', 'expI23')
135     save('expI24.mat', 'expI24')
136 end
137
138 expI.stiffness.grasper = [expI19.defl expI20.defl expI21.defl ...
139     expI22.defl expI23.defl expI24.defl];
140

```

```

141
142
143
144 %% Bending category II
145 expII1 = BendingMetrics('II Bending 1a.jpg', 'II Bending 1b.jpg');
146 expII2 = BendingMetrics('II Bending 2a.jpg', 'II Bending 2b.jpg');
147 expII3 = BendingMetrics('II Bending 3a.jpg', 'II Bending 3b.jpg');
148 expII4 = BendingMetrics('II Bending 4a.jpg', 'II Bending 4b.jpg');
149 expII5 = BendingMetrics('II Bending 5a.jpg', 'II Bending 5b.jpg');
150 expII6 = BendingMetrics('II Bending 6a.jpg', 'II Bending 6b.jpg');
151
152 if saveI
153     save('expII1.mat', 'expII1')
154     save('expII2.mat', 'expII2')
155     save('expII3.mat', 'expII3')
156     save('expII4.mat', 'expII4')
157     save('expII5.mat', 'expII5')
158     save('expII6.mat', 'expII6')
159 end
160
161 expII.alpha = [expII1.alpha expII2.alpha expII3.alpha ...
162               expII4.alpha expII5.alpha expII6.alpha];
163
164 expII.disp = [expII1.disp expII2.disp expII3.disp ...
165              expII4.disp expII5.disp expII6.disp];
166
167 expII.radius = [expII1.radius expII2.radius expII3.radius ...
168                expII4.radius expII5.radius expII6.radius];
169
170
171 %% Stiffness category II
172
173 % neutral
174 expII7 = StiffnessMetrics('II Stiffness neutral 1a.jpg', ...
175                            'II Stiffness neutral 1b.jpg', crop2);
176 expII8 = StiffnessMetrics('II Stiffness neutral 2a.jpg', ...
177                            'II Stiffness neutral 2b.jpg', crop2);
178 expII9 = StiffnessMetrics('II Stiffness neutral 3a.jpg', ...
179                            'II Stiffness neutral 3b.jpg', crop2);
180 expII10 = StiffnessMetrics('II Stiffness neutral 4a.jpg', ...
181                             'II Stiffness neutral 4b.jpg', crop2);
182 expII11 = StiffnessMetrics('II Stiffness neutral 5a.jpg', ...
183                             'II Stiffness neutral 5b.jpg', crop2);
184 expII12 = StiffnessMetrics('II Stiffness neutral 6a.jpg', ...
185                             'II Stiffness neutral 6b.jpg', crop2);
186
187 if saveII
188     save('expII7.mat', 'expII7')
189     save('expII8.mat', 'expII8')
190     save('expII9.mat', 'expII9')
191     save('expII10.mat', 'expII10')
192     save('expII11.mat', 'expII11')
193     save('expII12.mat', 'expII12')
194 end
195
196 expII.stiffness.neutral = [expII7.defl expII8.defl expII9.defl ...
197                            expII10.defl expII11.defl expII12.defl];
198
199 % bent
200 expII13 = StiffnessMetrics('II Stiffness bent 1a.jpg', ...
201                             'II Stiffness bent 1b.jpg', crop3);
202 expII14 = StiffnessMetrics('II Stiffness bent 2a.jpg', ...
203                             'II Stiffness bent 2b.jpg', crop3);
204 expII15 = StiffnessMetrics('II Stiffness bent 3a.jpg', ...
205                             'II Stiffness bent 3b.jpg', crop3);
206 expII16 = StiffnessMetrics('II Stiffness bent 4a.jpg', ...
207                             'II Stiffness bent 4b.jpg', crop3);
208 expII17 = StiffnessMetrics('II Stiffness bent 5a.jpg', ...
209                             'II Stiffness bent 5b.jpg', crop3);
210 expII18 = StiffnessMetrics('II Stiffness bent 6a.jpg', ...
211                             'II Stiffness bent 6b.jpg', crop3);
212
213 if saveII

```

```

214     save('expII13.mat', 'expII13')
215     save('expII14.mat', 'expII14')
216     save('expII15.mat', 'expII15')
217     save('expII16.mat', 'expII16')
218     save('expII17.mat', 'expII17')
219     save('expII18.mat', 'expII18')
220 end
221
222 expII.stiffness.bent = [expII13.defl expII14.defl expII15.defl ...
223                       expII16.defl expII17.defl expII18.defl];
224
225 % grasper
226 expII19 = StiffnessMetrics('II Stiffness grasper 1a.jpg', ...
227                            'II Stiffness grasper 1b.jpg', crop2);
228 expII20 = StiffnessMetrics('II Stiffness grasper 2a.jpg', ...
229                            'II Stiffness grasper 2b.jpg', crop2);
230 expII21 = StiffnessMetrics('II Stiffness grasper 3a.jpg', ...
231                            'II Stiffness grasper 3b.jpg', crop2);
232 expII22 = StiffnessMetrics('II Stiffness grasper 4a.jpg', ...
233                            'II Stiffness grasper 4b.jpg', crop2);
234 expII23 = StiffnessMetrics('II Stiffness grasper 5a.jpg', ...
235                            'II Stiffness grasper 5b.jpg', crop2);
236 expII24 = StiffnessMetrics('II Stiffness grasper 6a.jpg', ...
237                            'II Stiffness grasper 6b.jpg', crop2);
238
239 if saveII
240     save('expII19.mat', 'expII19')
241     save('expII20.mat', 'expII20')
242     save('expII21.mat', 'expII21')
243     save('expII22.mat', 'expII22')
244     save('expII23.mat', 'expII23')
245     save('expII24.mat', 'expII24')
246 end
247
248 expII.stiffness.grasper = [expII19.defl expII20.defl expII21.defl ...
249                           expII22.defl expII23.defl expII24.defl];
250
251
252
253 %% Bending category III
254 expIII1 = BendingMetrics('III Bending 1a.jpg', 'III Bending 1b.jpg');
255 expIII2 = BendingMetrics('III Bending 2a.jpg', 'III Bending 2b.jpg');
256 expIII3 = BendingMetrics('III Bending 3a.jpg', 'III Bending 3b.jpg');
257 expIII4 = BendingMetrics('III Bending 4a.jpg', 'III Bending 4b.jpg');
258 expIII5 = BendingMetrics('III Bending 5a.jpg', 'III Bending 5b.jpg');
259 expIII6 = BendingMetrics('III Bending 6a.jpg', 'III Bending 6b.jpg');
260
261 if saveIII
262     save('expIII1.mat', 'expIII1')
263     save('expIII2.mat', 'expIII2')
264     save('expIII3.mat', 'expIII3')
265     save('expIII4.mat', 'expIII4')
266     save('expIII5.mat', 'expIII5')
267     save('expIII6.mat', 'expIII6')
268 end
269
270 expIII.alpha = [expIII1.alpha expIII2.alpha expIII3.alpha ...
271                expIII4.alpha expIII5.alpha expIII6.alpha];
272
273 expIII.disp = [expIII1.disp expIII2.disp expIII3.disp ...
274               expIII4.disp expIII5.disp expIII6.disp];
275
276 expIII.radius = [expIII1.radius expIII2.radius expIII3.radius ...
277                 expIII4.radius expIII5.radius expIII6.radius];
278
279 %% Stiffness category III
280
281 % neutral
282 expIII7 = StiffnessMetrics('III Stiffness neutral 1a.jpg', ...
283                             'III Stiffness neutral 1b.jpg', crop4);
284 expIII8 = StiffnessMetrics('III Stiffness neutral 2a.jpg', ...
285                             'III Stiffness neutral 2b.jpg', crop4);
286 expIII9 = StiffnessMetrics('III Stiffness neutral 3a.jpg', ...

```

```

287     'III Stiffness neutral 3b.jpg', crop4);
288 expIII10 = StiffnessMetrics('III Stiffness neutral 4a.jpg', ...
289     'III Stiffness neutral 4b.jpg', crop4);
290 expIII11 = StiffnessMetrics('III Stiffness neutral 5a.jpg', ...
291     'III Stiffness neutral 5b.jpg', crop4);
292 expIII12 = StiffnessMetrics('III Stiffness neutral 6a.jpg', ...
293     'III Stiffness neutral 6b.jpg', crop4);
294
295 if saveIII
296     save('expIII7.mat', 'expIII7')
297     save('expIII8.mat', 'expIII8')
298     save('expIII9.mat', 'expIII9')
299     save('expIII10.mat', 'expIII10')
300     save('expIII11.mat', 'expIII11')
301     save('expIII12.mat', 'expIII12')
302 end
303
304 expIII.stiffness.neutral = [expIII7.defl expIII8.defl expIII9.defl ...
305     expIII10.defl expIII11.defl expIII12.defl];
306
307 % bent
308 expIII13 = StiffnessMetrics('III Stiffness bent 1a.jpg', ...
309     'III Stiffness bent 1b.jpg', crop4);
310 expIII14 = StiffnessMetrics('III Stiffness bent 2a.jpg', ...
311     'III Stiffness bent 2b.jpg', crop4);
312 expIII15 = StiffnessMetrics('III Stiffness bent 3a.jpg', ...
313     'III Stiffness bent 3b.jpg', crop4);
314 expIII16 = StiffnessMetrics('III Stiffness bent 4a.jpg', ...
315     'III Stiffness bent 4b.jpg', crop4);
316 expIII17 = StiffnessMetrics('III Stiffness bent 5a.jpg', ...
317     'III Stiffness bent 5b.jpg', crop4);
318 expIII18 = StiffnessMetrics('III Stiffness bent 6a.jpg', ...
319     'III Stiffness bent 6b.jpg', crop4);
320
321 if saveIII
322     save('expIII13.mat', 'expIII13')
323     save('expIII14.mat', 'expIII14')
324     save('expIII15.mat', 'expIII15')
325     save('expIII16.mat', 'expIII16')
326     save('expIII17.mat', 'expIII17')
327     save('expIII18.mat', 'expIII18')
328 end
329
330 expIII.stiffness.bent = [expIII13.defl expIII14.defl expIII15.defl ...
331     expIII16.defl expIII17.defl expIII18.defl];
332
333 % grasper
334 expIII19 = StiffnessMetrics('III Stiffness grasper 1a.jpg', ...
335     'III Stiffness grasper 1b.jpg', crop4);
336 expIII20 = StiffnessMetrics('III Stiffness grasper 2a.jpg', ...
337     'III Stiffness grasper 2b.jpg', crop4);
338 expIII21 = StiffnessMetrics('III Stiffness grasper 3a.jpg', ...
339     'III Stiffness grasper 3b.jpg', crop4);
340 expIII22 = StiffnessMetrics('III Stiffness grasper 4a.jpg', ...
341     'III Stiffness grasper 4b.jpg', crop4);
342 expIII23 = StiffnessMetrics('III Stiffness grasper 5a.jpg', ...
343     'III Stiffness grasper 5b.jpg', crop4);
344 expIII24 = StiffnessMetrics('III Stiffness grasper 6a.jpg', ...
345     'III Stiffness grasper 6b.jpg', crop4);
346
347 if saveIII
348     save('expIII19.mat', 'expIII19')
349     save('expIII20.mat', 'expIII20')
350     save('expIII21.mat', 'expIII21')
351     save('expIII22.mat', 'expIII22')
352     save('expIII23.mat', 'expIII23')
353     save('expIII24.mat', 'expIII24')
354 end
355
356 expIII.stiffness.grasper = [expIII19.defl expIII20.defl expIII21.defl ...
357     expIII22.defl expIII23.defl expIII24.defl];

```

Extracting bending metrics

```
1 function exp = BendingMetrics(file1, file2)
2
3 %% Category I
4 imla = imread(file1);
5 imlb = imread(file2);
6
7 % crop images
8 imla_cropped = imcrop(imla,[532, 0, 1110, height(imla)]);
9 imlb_cropped = imcrop(imlb,[532, 0, 1110, height(imlb)]);
10
11 % calibrate images
12 BW=-imbinarize(rgb2gray(imla_cropped));
13
14 row = 1008;    % start looking at row ..
15 col1 = 77;    % start looking at column ..
16 col2 = 997;   % start looking at column ..
17 square1 = find(BW(row,col1:end), 1);
18 square2 = find(BW(row,col2:end), 1);
19
20 scale = 60*.9784/(square2 + col2 - square1 - col1);
21
22 % overlay images
23 tformEstimate = imregcorr(imla_cropped,imlb_cropped);
24 Rfixed = imref2d(size(imlb_cropped));
25 movingReg = imwarp(imla_cropped,tformEstimate,'OutputView',Rfixed);
26 C = imfuse(imlb_cropped, movingReg, 'blend','Scaling','joint');
27 figure; imshow(C); hold on
28
29
30 %% Calculate metrics
31 % manually identify coordinates
32 [coord.x, coord.y] = ginput(4);
33
34 % bending angle
35 alpha = atan2(diff(coord.y(3:4)) / diff(coord.x(3:4)));
36
37 % rod displacement
38 disp = diff(coord.x(1:2));
39
40 % bending radius
41 radius = abs(diff(coord.x([1,3])) / cosd(90-alpha));
42
43 % center of rotation
44 centp = [coord.x(1), coord.y(3) + diff(coord.x([1,3]))*tand(90-alpha)];
45
46 % visualise bending radius and bending angle
47 viscircles(centp, radius);
48 plot(mean(coord.x(3:4)) + diff(coord.x(3:4))*[-3 4], ...
49      mean(coord.y(3:4)) + diff(coord.y(3:4))*[-3 4], 'LineWidth', 2)
50
51
52 %% Store metrics in struct 'exp'
53 exp.coord = coord;
54 exp.alpha = alpha;
55 exp.disp = disp*scale;
56 exp.radius = radius*scale;
57 exp.centp = centp;
```


Extracting stiffness metrics

```
1 function exp = StiffnessMetrics(file1, file2, crop)
2 % for processing of photos (not video frames)
3
4 %% Process images
5 imla = imread(file1);
6 imlb = imread(file2);
7
8 if length(crop.window) == 3
9     crop.window(4) = height(imla);
10 elseif isempty(crop.window)
11     crop.window = [0, 0, width(imla), height(imla)];
12 end
13
14 % crop images
15 imla_cropped = imcrop(imla, crop.window);
16 imlb_cropped = imcrop(imlb, crop.window);
17
18 % calibrate images
19 BW=-imbinarize(rgb2gray(imla_cropped));
20 square1 = find(BW(crop.row,crop.col1:end), 1);
21 square2 = find(BW(crop.row,crop.col2:end), 1);
22
23 % multiply with #mm and paper error
24 scale = crop.squares*5*.9784/(square2 + crop.col2 - square1 - crop.col1);
25
26 % overlay images
27 tformEstimate = imregcorr(imla_cropped,imlb_cropped);
28 Rfixed = imref2d(size(imlb_cropped));
29 movingReg = imwarp(imla_cropped,tformEstimate,'OutputView',Rfixed);
30 C = imfuse(imlb_cropped, movingReg, 'blend','Scaling','joint');
31 figure; imshow(C); hold on
32
33 % check if scaling points in black square
34 scatter([crop.col1 crop.col2],[crop.row crop.row])
35
36
37 %% Calculate metrics
38 % manually identify coordinates
39 [coord.x, coord.y] = ginput(2);
40
41 % deflection
42 defl = diff(coord.y(1:2));
43
44
45 %% Store metrics in struct 'exp'
46 exp.coord = coord;
47 exp.defl = defl*scale;
```